GEOLOGICAL SURVEY OF NAMIBIA

MINISTRY OF MINES AND ENERGY

GEOLOGY, MINERALOGY, GEOCHEMISTRY AND HYDROTHERMAL ALTERATION OF THE BRANDBERG ALKALINE COMPLEX, NAMIBIA.

by

M. DIEHL

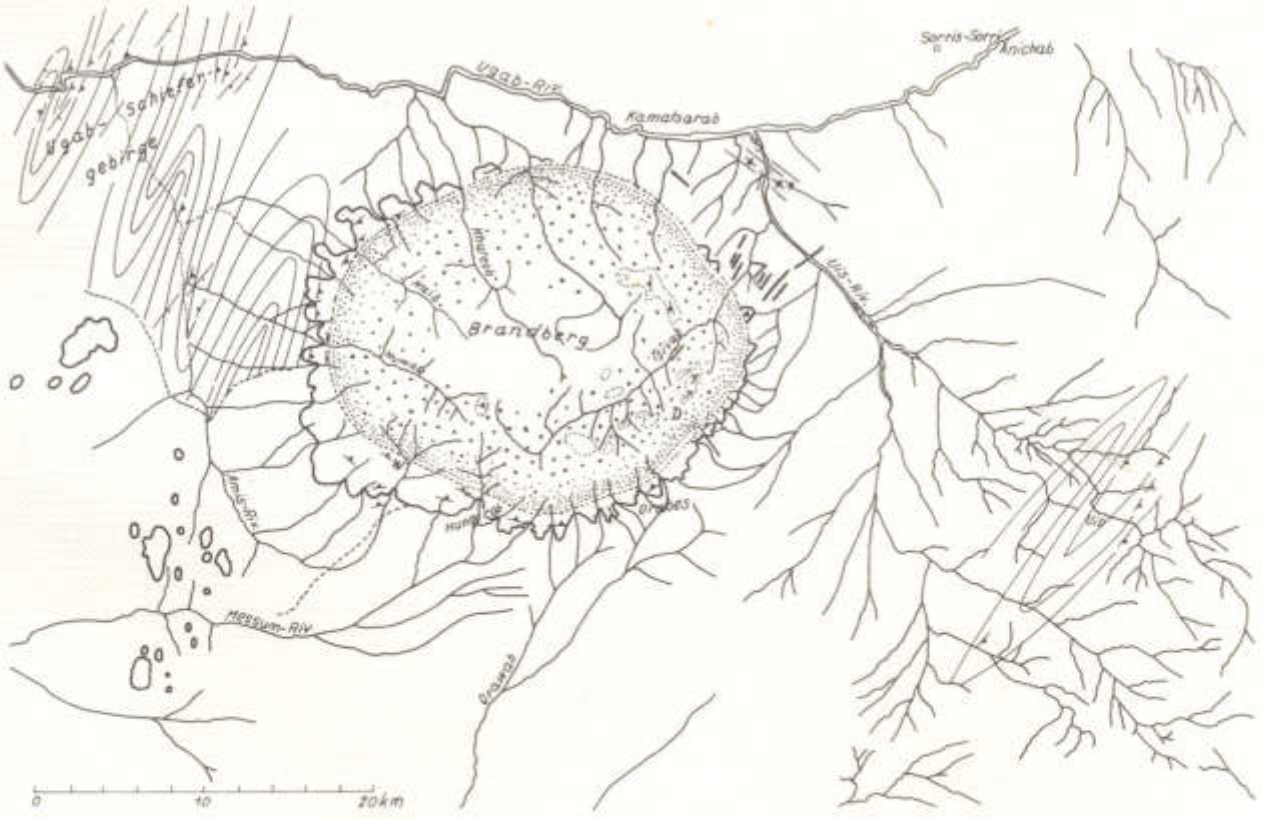

MEMOIR 10
1990

MINISTRY OF MINES AND ENERGY

GEOLOGICAL SURVEY OF NAMIBIA

Director: R. McG. Miller

MEMOIR 10

Geology, mineralogy, geochemistry and hydrothermal alteration of the Brandberg Alkaline Complex, Namibia

by

M. Diehl

Typesetting and layout: J. Angermund

Obtainable from the Geological Survey
P.O. Box 2168, Windhoek, 9000, Namibia

Price	
Local (+ GST)	R 20.00
Abroad Post Free	R 25.00

ISBN 0 86976 232 X

The text of this publication is from a dissertation submitted to the Institut für Geowissenschaften, Johannes Gutenberg Universität Mainz, for the Degree of Doctor rerum naturalium.

CONTENTS

ABSTRACT

The Brandberg Complex represents an anorogenic ring complex of the intra-plate type emplaced during Jurassic-Cretaceous times at a high level in the crust. At the present level of erosion the complex exhibits a number of subvolcanic, magmatic centres which are entirely granitic in composition. Metaluminous granites and quartz-monzonitic rocks were emplaced as cone-sheets outside the later caldera or as thick, ring-shaped sheets. Peraluminous granites occupy the central part of the complex and are followed by peripheral peralkaline granites. All rock types associated with the Brandberg Complex carry significant mineralogical and geochemical features of HHP, A-type granites with anomalous high levels for HFS- and LIL-elements. Several types of post-magmatic, hydrothermal alteration processes were recognised which are similar to those associated with anorogenic complexes in Nigeria. Depending on the initial chemical composition of the crystallising granite and its metasomatising hydrothermal fluids, processes of potassium metasomatism, sodium metasomatism, greisen-type alteration, tourmalinisation and chloritisation have been recognised. Cationic exchange processes led to the breakdown of the primary mineral assemblages in the granite and the generation of hydrothermal mineral parageneses, locally associated with deposition of Zn, Sn, Nb, Y and REE ore minerals. The spectrum of subsolidus minerals in these assemblages is characterised by the occurrence of albite (An 0.6-3.2), reddened maximum microcline, the destabilisation of early crystallising biotite to micas of the siderophyllite-zinnwaldite series and locally concentrations of tourmaline. Fenitised granites carry hydrothermal zincian fluor-arfvedsonite and stanniferous aegirine as newly generated minerals and occur in layered, agpaitic rock series of the Amis Complex, a mineral stratified satellite intrusion in the southwestern periphery of Brandberg. The following types and styles of mineralisation were identified: Dispersed Nb, Ta, REE-mineralisation; Disseminated Sn-mineralisation; Fissure and vein controlled sulphide/oxide (Zn/Sn-mineralisation). Mineralisation in the Brandberg Complex is generally limited to zones where post-magmatic rock-fluid interaction processes acted long and were intense enough to allow the generation of ore minerals. Alteration zones occur in the roof zones of the complex, along the contacts and margins of individual intrusions, and in adjacent country rock.

1. Introduction

The Brandberg Complex belongs to the Damaraland Alkaline Province in Namibia consisting of over twenty Jurassic-Cretaceous, anorogenic complexes of the intraplate type. They represent high level, subvolcanic ring complexes exposed in a northeast-trending zone, approximately 350 km long and 130 km wide (Fig. 1). The complexes have intruded into Damaran metasedimentary rocks and granites of late Pan African age (600 - 460 Ma), Karoo sediments and volcanic rocks. Cloos (1911, 1919, 1929) was the first to recognise that some of the granitic complexes (Erongo, Spitzkoppie and Brandberg) are "young granite plutons" and postulated a Mesozoic emplacement age. The complexes are aligned along three major, northeast -trending zones (Fig. 1), representing basement lineaments which to some extent have controlled the emplacement of the ring complexes. The northern line includes Messum, Brandberg, Okonjeje, Kwaggaspan, Otjihorongo, Paresis and Okorusu (Fig. 1). Among these Brandberg forms a dominant granite massif rising 2000 m above the plains of the Namib desert, with Konigstein peak (2573 m), the highest mountain in Namibia. The oval shaped complex covers an area of -420 km^2 and has approximate dimensions of 26 x 21 km (Fig. 2). Due to the inaccessibility of the mountain and the lack of water only limited work has been carried out in the past. It originally was described by Cloos and Chudoba (1931) and Hodgson (1972, 1973), followed by two short communications of Von Knorring (1985) and Schlag and Willgallis (1988).

The aim of the present study was to carry out geological mapping (sheet 2114 AB and BA, open file maps 1 :50000 -Geological Survey Windhoek, Namibia), petrological, mineralogical and geochemical investigations and to evaluate the potential for oxide/sulphide mineralisation in Mesozoic alkaline granites in Namibia.

Compared with other complexes of the Damaraland Alkaline Province the Brandberg Massif is almost entirely composed of granitic rocks. Outcrops of syenitic, gabbroic and carbonatitic rocks, commonly associated with other alkaline complexes of the province are not known from Brandberg. The dominant granitic composition and the presence of hydrothermal alteration is comparable to Mesozoic ring complexes in Nigeria which are known to contain economic potential for disseminated and vein controlled Sn, Zn, Pb, Nb and REE mineralisation.

2. Emplacement and Structural Control of the Damaraland Alkaline Complexes

The Brandberg belongs to the group of Mesozoic alkaline ring complexes of the Damaraland Alkaline Province (Fig. 1) which are dominantly composed of oversaturated rock types, in contrast to the undersaturated complexes (Etaneno), basic complexes (Messum, Doros, Wolfsgrund), mixed acid/basic types (Cape Cross, Paresis) and centres including carbonatites (Ondumakorume, Osongombe, Kalkfeld, Okorusu). The complexes are aligned along a northeast-trending, 130 km wide and 350 km long zone which coincidences with the dominant north-easterly strike direction of Precambrian lineament zones. Marsh (1973) and Prins (1981) suggested that the northeast-striking direction of Mesozoic ring complexes correlates with the direction of transform faults which developed during the rifting of Gondwanaland. Black *et al*. (1985) has pointed out that the distribution pattern of anorogenic, intra-plate complexes may be linked with anorogenic magmatism associated with distention processes, which resulted in rifting and the formation of ridges. In this model the complexes are either aligned along the future ridge (Black *et al*. 1972), or along continental extensions of transform faults (Marsh, 1973). In contrast, Bowden and Turner (1974) and

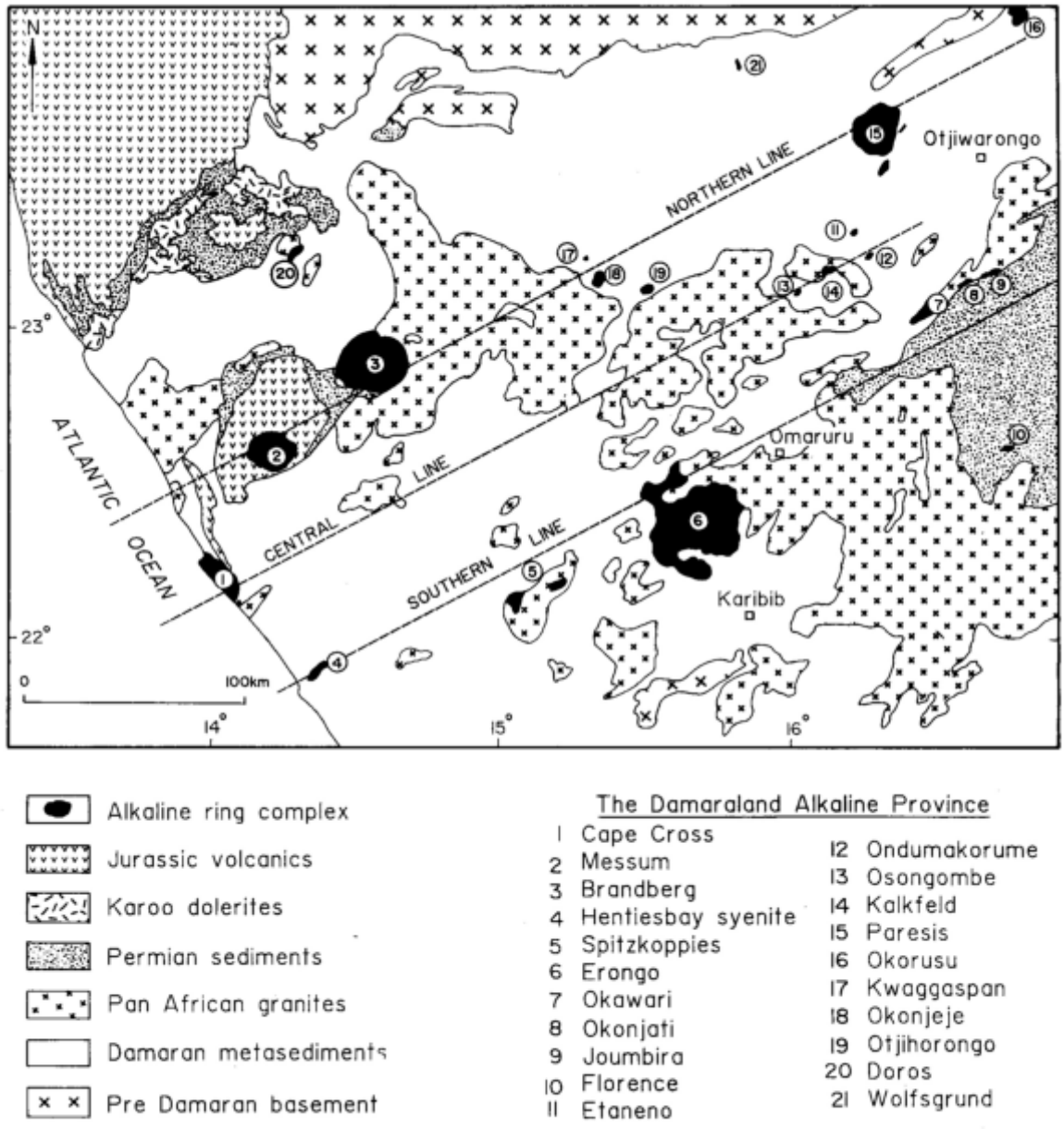

Fig. 1: Generalised geological map of the Damaraland Alkaline Province and the distribution of Mesozoic ring complexes.

Van Breemen and Bowden (1973) have interpreted the linear nature of the Niger-Nigeria line of complexes, and the fact that the emplacement ages for these complexes are getting younger towards the coast, in terms of a northward moving African plate over a stationary mantle plume ("hot spot"). Giret and Lameyre (1985) pointed out that it is generally accepted that continental rifting starts with an uplift which is followed by alkaline magmatic activity and postulated that uplift and alkaline magmatism is controlled by a system of "lithospheric shear openings" (mega-gashes) and not by a rising mantle plume (Giret et Lameyre, 1985).

Northeast-trending zones of crustal weakness, along which the complexes are aligned, date back to early Pre-Damaran times at a stage of initial graben formation. Reactivation of these lineaments has occurred at several stages in the history of the Damara Orogen and the latest activity is believed to be associated with the break-up of Gondwanaland, which in the southern part of the province resulted in the reactivation of the Cape Cross - Uis graben (Northern Tin Belt) immediately south of Brandberg and Messum (Diehl, 1986). The Brandberg complex is sited at the northern shoulder of this old half-graben system and mainly has intruded into post-tectonic, orogenic two-mica granite of late Pan African age and overlaying Permian-Jurassic sediments and volcanics. In addition to these old basement lineaments which mainly have controlled the emplacement of the ring complexes, a number of Mesozoic, northwest-southeast and north-south striking faults have been recognised in the south-western portion of the province (Diehl, 1986). Prins (1981) has interpreted the north-south trending lineaments as a series of up and downwarps, parallel to the coastline during early opening of the Atlantic Ocean. On the other hand, it is obvious that the northwest-southeast direction, parallel to the recent coastline has to some extent contributed to the emplacement

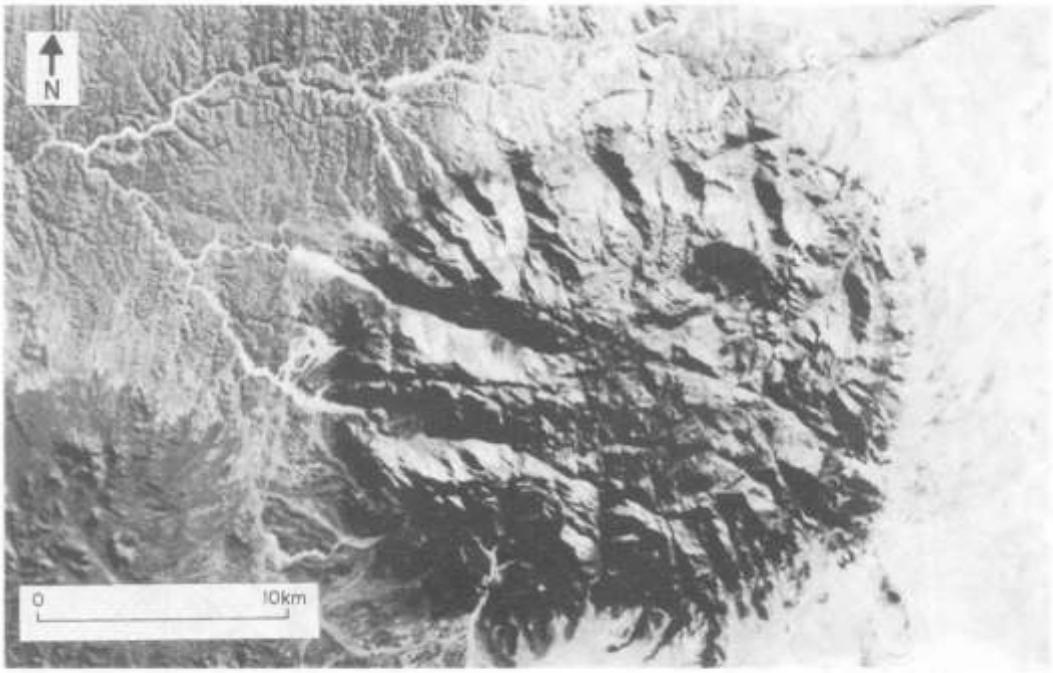

Fig. 2: Satellite image of the Brandberg Complex (Produced and permission for publication granted by the Satellite Application Centre, MIKOMTEK, CSIR).

mechanism (Cloos and Chudoba, 1931, p. 60). Early quartz-monzonitic centres towards the north of the Brandberg Complex are aligned along this trend (Fig. 5).

3. Age of the Damaraland Complexes

Limited isotopic investigations have been carried out but the K/Ar isotope work of Siedner and Miller (1968) and Siedner and Mitchell (1976) indicates a range in ages for Okonjeje (164 Ma, gabbro), Paresis (136 Ma, basalt), Doros (125 Ma, gabbro) and Messum (123 Ma, basalt). Burger *et al.* (1965) reported a K/Ar-age for a biotite (190 18) Ma from a vug in Klein Spitskop granite containing aquamarine.

If comprehensive isotopic dating should proof that emplacement ages of the complexes are getting younger towards the coast, like in Nigeria (Bowden *et al.* 1976), which would fit the "hot spot" model of Bowden and Karche (1984) proposed for the Niger-Nigeria Anorogenic Province, it would cast some doubt on the alternative "transform fault" model of Marsh (1973) and Prins (1981).

4. Geological setting and magmatic evolution

4.1 General

The Brandberg ring complex represents an eroded, continental volcano emplaced into late Precambrian granites and metasedimentary rocks of the Damara Sequence, unconformably overlain by sediments and volcanics of the Karoo Sequence (Fig. 3). Along the southern and western margins of the complex remnants of the Karoo strata consisting of hornfelsed mud- and siltstones of the Prince Albert Formation and conglomerates of the Hungurob Formation are affected by contact metamorphism and to a lesser extent by contact metasomatism. The sediments are conformably overlain by basaltic lava flows and ignimbritic quartz latites forming a dark-coloured peripheral rim. Sediments and volcanics generally dip 2-50 towards the complex with a sudden increase to 2-500 in the vicinity of the contact (Fig. 4).

Pelitic metasediments of the Amis River Formation (upper Khomas Group, Damara Sequence) composed of biotite-schist, calc silicate and quartzite occur along the north-western and western margins (Figs 2 and 3). The country rock to the north, east and south of Brandberg consists of syn- to post-tectonic granites which dominantly have intruded at the close of the Pan African event about 500 Ma ago.

4.2 Magmatic evolution

The Brandberg is believed to have a magmatic evolution similar to that of other granitic alkaline ring complexes described by Lameyre and Bonin (1985) and Bowden (1985). The formation of the Brandberg Alkaline Complex classically began with initial doming of the crust which resulted in the formation of cone fractures and was followed by the emplacement of cone sheets and dykes. Earliest volcanic activity presumably started with predominantly pyroclastic products and flows of rhyo-dacitic composition. According to Bonin's (1982) emplacement model for alkaline ring complexes, the *pre-caldera stage* of a complex is followed by the *volcanic*

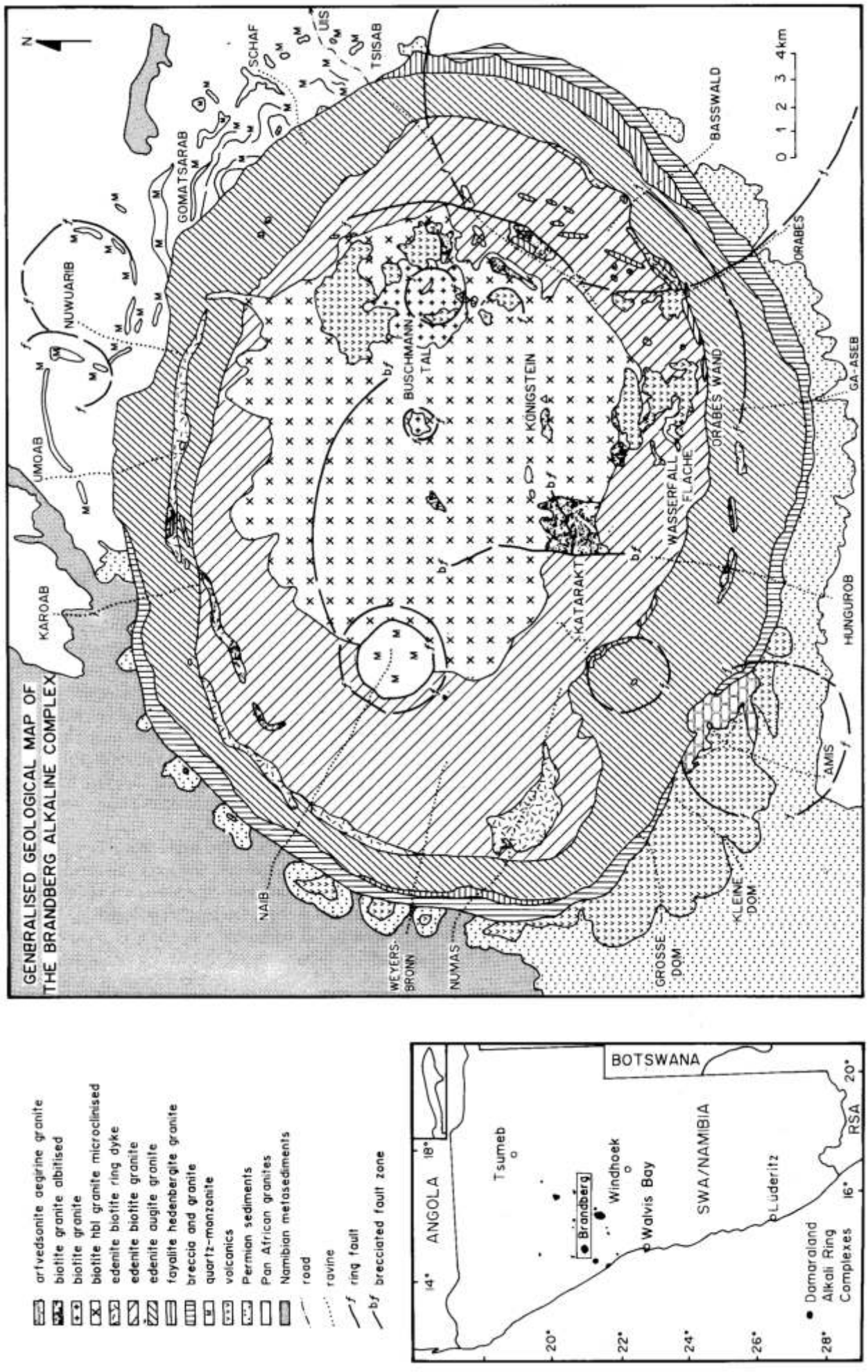

Fig. 3: Generalised geological map of the Brandberg Alkaline Complex.

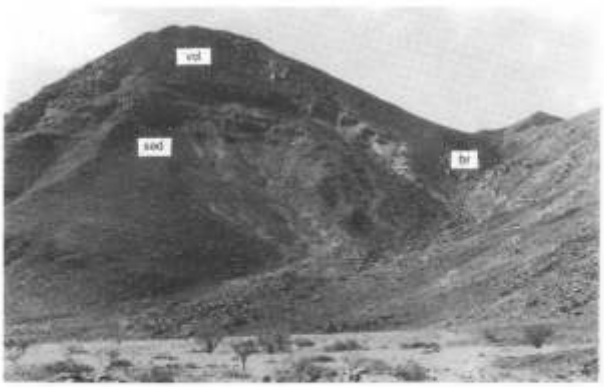

Fig. 4: Karoo sediments (sed) and volcanics (vol) dipping towards the complex (Numas Ravine). Note the increase in dip in the vicinity of the breccia zone (br) associated with cauldron subsidence along the major caldera fault.

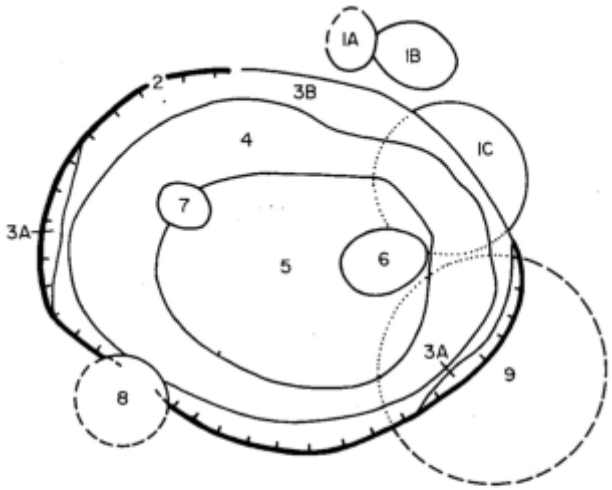

Fig. 5: Evolution of subvolcanic and magmatic centres commencing with the emplacement of quartz monzonitic rocks of the pre-caldera stage (centres 1A, B, C) and subsequent caldera formation (2), followed by granitic centres (3-6) of the plutonic stage and a later circular centre (7) of quartz monzonitic rocks. Centre 8 dominantly consists of agpaitic granites and metasomatites.

stage which generally initiates violently with eruptions of pyroclastic material and ignimbrites (Bonin, 1982 ; Bowden 1985). The emptying of the magma chamber resulted in surface cauldron subsidence and the extrusion of intra caldera ignimbrite flows (*caldera-stage*). At the *plutonic stage*, granitic magma was channelled upwards and emplaced as thick sheets at higher levels. This stage was followed by successive subsidence and intrusion of the next granitic magma pulse from the same magma chamber. Renewal of doming resulted in the formation of a new centre expressed by early cone sheets of monzonitic or monzo-granitic composition and ended with the emplacement of a central dome or plug-like intrusion. The emplacement of alkaline granites was followed by a peripheral intrusion of a laccolithic, perfectly layered, peralkaline granite and associated dykes. Finally, late radial fractures were filled by olivine- and quartz-dolerites.

4.3 Magmatic centres

In the Brandberg Complex eight major cycles of subvolcanic/magmatic activity are recognised which are expressed by magmatic centres.

The *pre-caldera stage* with the formation of circular dykes outside the later caldera is represented by three subvolcanic centres (1A, 1B, 1C, Fig. 5). They occur towards the north-east of the massif as distinctive cone sheets which have been largely obliterated by post-caldera intrusions (Fig. 3). The individual sheets dip 30-50° towards their centre and consist of porphyritic quartz monzonite partly transitional to monzo-granite porphyry and have intruded into Pan African granite. The quartz monzonite porphyries are believed to represent subvolcanic equivalents of quartz-latitic ignimbrite (rhyodacite) flows initiating the early volcanic, *pre-caldera stage* of the Brandberg Complex.

Sinking of the updomed area and subsequent updoming led to the development of a master caldera fault (2 in Fig. 5) which resulted in the formation of surface cauldron subsidence. Intensive brecciation associated with the master caldera fault is most intense in the southern and eastern part, but absent along the north-eastern contact with Pan African granite. Due to the level of erosion, the *intra-caldera volcanic stage* is not preserved at Brandberg but indicated by the presence of ignimbrite feeder-dykes.

The system entered the *plutonic stage* with the emplacement of acid magma as a cupola sheet underlying the volcanics. Centre 3A (Fig. 5) started with the intrusion of hypersolvus fayalite-hedenbergite granite preserved as outer ring-dyke towards the east and west of the complex. The hypersolvus stage was followed by the intrusion of the edenite-augite granite ring-dyke (3B). Caused by updoming and subsequent subsidence, the granites were emplaced as voluminous ring-shaped sheets of slightly different composition, texture and grain size. The next evolutionary stage in the history of the complex is expressed in the generation of centre 4. Magmatic activity started again with the formation of cone fractures which are partly occupied by dykes of hypersolvus fayalite-hedenbergite granite and followed subsequently by the emplacement of horizontal sheets of hornblende-biotite granite and a hornblende-biotite granite ring dyke (Fig. 2). The next magmatic cycle (centre 5) initiated with the development of ring fractures in the central part of the complex and the intrusion of cupola-like sheets of originally hornblende-bearing biotite granite which have been transformed to biotite granite under the influence of late-stage fluidising processes.

The cupola sheets of slightly peraluminous granite are intruded by stocks of peraluminous biotite granite in the central areas of the complex (centre 6).

A circular stock of alkali quartz monzonite in the Naib Ravine (centre 7) possibly marks the beginning of a new volcanic stage in the history of the complex.

A perfectly layered, laccolithic body (centre 8), intrusive into alkali granite and country rock occurs in the Amis Valley towards the south-western periphery of the massif. It is composed of a perfectly layered series of predominantly peralkaline arfvedsonite- and aegirine-arfvedsonite granites with subordinated alkali granite layers. In the vicinity of the Amis

Complex the granites and country rock are highly altered to peralkaline metasomatites displaying the characteristic features of fenite, often found in carbonatite complexes.

Towards the east of the Brandberg massif a ring fracture, 13.5 km in diameter and clearly visible on the landsat image (Fig. 2), overlaps the complex (9).

5. Petrography and mineralogy of the principal rock types

5.1 Quartz-monzonitic rocks

5.1.1 Quartz monzonite porphyry

The quartz monzonite porphyries of the pre-caldera stage occur towards the north and northeast of the massif (Fig. 6). The cone sheets have intruded into late Pan African granite and vary in thickness from 1.5-45 m and dip at angles between 30 - 50° towards their centre. The smaller centres (1A and 1B in Fig. 5) are up to 4 km in diameter and consist of a single 4 - 6 m wide, bluish-grey, fine grained dyke of quartz monzonite porphyry, often irregular and discontinuous along a cone fracture (Fig. 3).

Fig. 6: Cone sheets of quartz monzonitic composition, northeast of the Brandberg massif, partly obliterated by post caldera stage granites.

The Gomatsarab centre (1C in Fig. 5) occurs towards the northeast of the massif and is 50 per cent obliterated by later post-caldera intrusions (Fig. 3). The outermost of five single cone sheets is up to 45 m thick and consists of dark grey, fine to medium grained, porphyritic quartz monzonite transitional towards monzo-granite. Petrographically the rock is composed of glomerophyric aggregates of strongly zoned phenocrysts of andesine, (Figs 7 and 8) andesine-labradorite and oligoclase phenocrysts, up to 3 cm in length, together with phenocrystic hornblende of edenitic composition, rimmed by ferro-actinolite, often with a ferro-hedenbergite core. The groundmass consists of granophyric intergrown quartz and alkali feldspar, biotite, partly replaced by chlorite, and occasionally tiny flakes of brown hornblende. Apatite is a common accessory together with minor zircon and magnetite. Towards their centre the individual cone sheets are thinner (3-6 m wide) and exhibit some textural and mineralogical changes caused by devitrification processes.

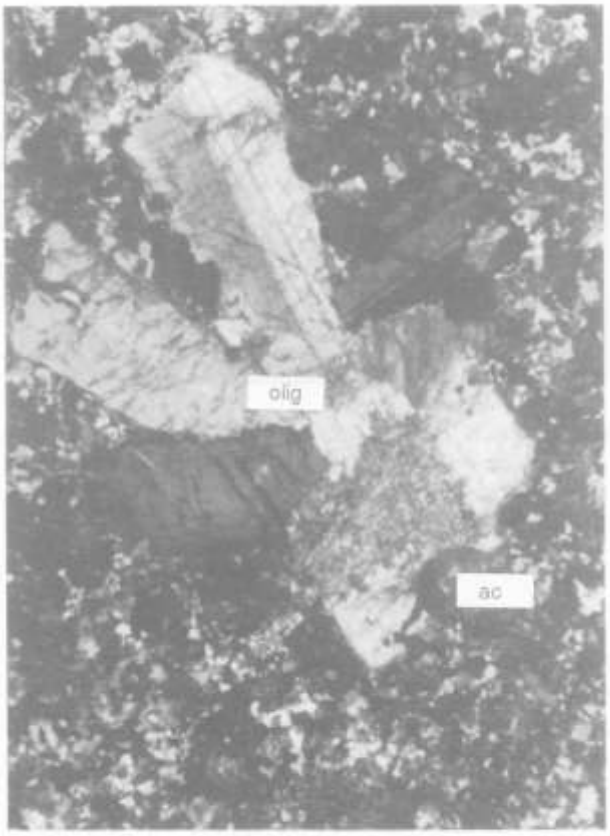

Fig. 7: Photomicrograph of altered, porphyritic quartz monzonite (magnification x 20, XPL). Glomerophyric aggregate of oligoclase-andesine (An_{25-31}) (olig) and actinolitic hornblende (ac) in a granophyric quartz/alkali feldspar matrix.

Some of the dykes contain phenocrysts of oligoclase and andesine-labradorite and decomposed clinopyroxene which is partly replaced by ferro-actinolite and aggregates of biotite, set in a devitrified, spherulitic matrix. The spherulites consist of fibrous, radially arranged K -feldspar crystals and extremely fine, fibrous needles, probably of pyroxene and magnetite, forming curved and radiating needles, resembling spinifex texture. The matrix between the spherulites is composed of quartz, alkali feldspar and biotite.

A medium grained, greyish-red, porphyritic hornblende-biotite monzogranite forms the innermost cone sheet. Highly embayed and resorbed plagioclase phenocrysts, occasionally up to 5 cm in length, range in composition from andesine to oligoclase. Reverse zoning is prevalent in the larger crystals. The mafic assemblage invariably include phenocrystic or poikilitic, edenitic hornblende and biotite partly replaced by chlorite. The groundmass is felsic, chiefly composed of quartz and turbid K-feldspar. Accessory minerals in addition to the usual apatite, are iron oxides and calcite.

The *pre-caldera stage* quartz monzonite porphyries comprise a general trend from quartz monzonitic at the periphery (SiO_2 ~65 wt per cent) transitional to monzogra¬nite (SiOF 68-70 wt per cent) towards the centre. Based on mineralogical and geochemical data, the porphyries are interpreted as

Fig. 8: Photomicrograph of porphyritic quartz monzonite (magnification x 20, XPL). Zoned andesine-oligoclase (olig) in a granophyric quartz/alkali feldspar matrix.

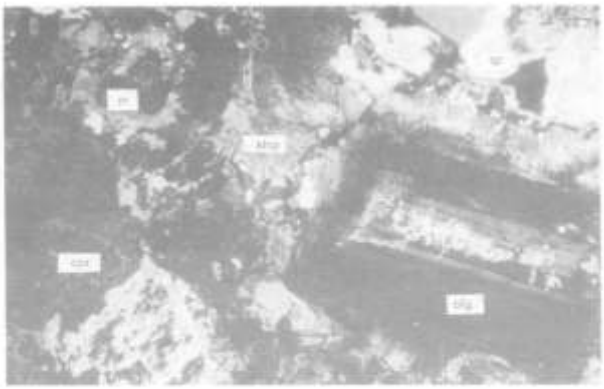

Fig. 9: Photomicrograph of quartz monzonite from the Naib centre (magnification x 14, XPL). Rhombic oligoclase (olig), alkali feldspar (kfsp), quartz (qz), pyroxene (cpx) partly replaced by ferro-actinolite and magnetite (m).

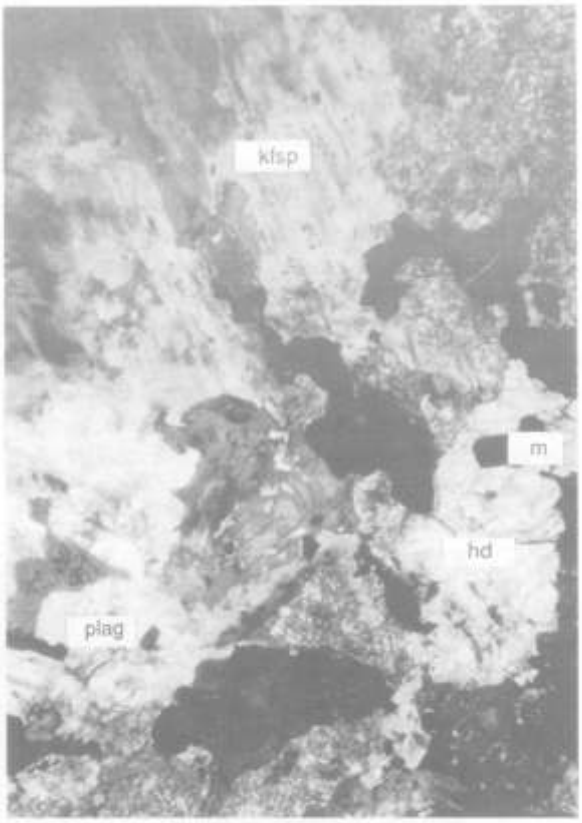

Fig. 10: Photomicrograph of quartz monzonite from the Naib centre (magnification x 20, XPL). Plagioclase (plag), alkali feldspar (kfsp), diopsidic hedenbergite (hd) and magnetite (m).

subvolcanic equivalents of quartz latitic flows which form the remnant roof rocks of the Brandberg massif.

Quartz-monzonitic rocks generally occupy early cone fractures which have been developed at the pre-caldera volcanic stage of the Brandberg Complex. So far, the Gomatsarab, Nuwuarib and Umoab quartz monzonites are the only known occurrences of subvolcanic rocks which show compositional similarities with ignimbritic quartz-latite flows of the Etendeka Formation described by Milner (1988). It can be speculated that at least some of the Etendeka quartz-latite flows, northwest of the Brandberg Complex are associated with pre-caldera and caldera-stage volcanism in connection with intra-plate, Mesozoic alkaline ring complexes of the Damaraland Province.

5.1.2 Quartz Monzonite

A 2,5 km wide, circular centre, entirely composed of alkali quartz monzonite occurs in the Naib Ravine towards the west of the complex and has intruded into edenite-augite and hornblende- biotite granite (Fig. 3). The melanocratic rock is medium grained with finer grained margins and consists of plagioclase, alkali feldspar, hornblende, pyroxene, biotite and quartz. Perfectly zoned plagioclases ranging from andesine to oligoclase occur together with K-feldspar of a compositional range from orthoclase-perthite to microcline-perthite (Fig. 9).

Both feldspars show a rhombic shape resembling that of phenocrysts in equivalent effusive quartz latites from the top of Brandberg. Relatively fresh pyroxene of the diopsite-hedenbergite series, rimmed by ferro-actinolite occurs in patches together with iron ore, apatite and biotite which replaces a greenish-brown, highly altered hornblende (Fig. 10). The feldspars are typically myrmekitic overgrown from the rim towards the core. Patches of granophyric and wormlike

intergrown quartz and alkali feldspar occasionally contain quartz phenocrysts. Apatite is an abundant accessory reaching concentrations up to 1.5 wt per cent.

The Naib quartz monzonite was formed at a relatively late stage in the history of the Brandberg Complex and possibly marks the beginning of a new volcanic period which presumably commenced with the eruption of chemical equivalent quartz-latitic material.

5.2 Granite

5.2.1 Introduction

Alkali granite is the most abundant and characteristic rock type of the Brandberg Complex previously described as a "homogeneous, main mass of undifferentiated granite" (Hodgson, 1973). Ninety per cent of the massif is formed by ring-shaped and sheet-like intrusions of fayalite- hedenbergite granite, hornblende-pyroxene granite, hornblende biotite granite and biotite granite. They comprise a series of alkali granites with variable texture, mineralogy, chemical composition and differences in the proportions and composition of their amphiboles and micas. Perthitic alkali feldspars generally dominate over plagioclase. All categories of Shand's classification have been recognised including peraluminous, metaluminous and peralkaline alkali granites (see Fig. 35). The peraluminous types are characterised by the presence of mica, topaz and/or tourmaline. Metaluminous granites typically contain hornblende/clinopyroxene assemblages whereas in peralkaline granites sodic amphibole (arfvedsonite), sodic pyroxene (aegirine) and zirconium- and titanium silicate minerals are dominant.

Using the nomenclature of Bonin (1982), based on the classification of Tuttle and Bowen (1958), the granites can be subdivided into three main groups according to the content and composition of their feldspars:

hypersolvus granite (one feldspar)
- metaluminous (fayalite, pyroxene)
- hyperaluminous (biotite)

subsolvus granite (two feldspars)
- hyperaluminous (biotite)
- hyperalkaline (arfvedsonite, aegirine)

transolvus granite (ternary feldspar, sodic plus potassium feldspar)
- hyperaluminous (biotite)

5.2.2 Fayalite hedenbergite granite

Fayalite bearing granite outcrops towards the southeast and west of the massif as remnants of an early outermost ring intrusion and occurs as ring dykes around the biotite bearing granites of the central area (Fig. 3). Enclaves of fayalite bearing granite were recognised in hornblende-pyroxene granite along the northern contact zone of the complex. When relatively fresh, fayalite granite has a distinct bluish-green colour and weathers brownish-black, in contrast to the more reddish-yellow weathering biotite granites. The fayalite granites are characterised by their typical granophyric texture and their metaluminous nature. Quartz and alkali feldspar show radiate intergrowths about oligoclase. In equigranular types orthoclase crystals are up to 1 cm long and commonly overgrown by bluish-green, micro-perthitic alkali feldspar. The composition of clino-pyroxene is variable from grey, augitic cores to sodic or ferro-hedenbergitic rims of yellowish to green colour. Fayalite crystals are heavily fragmented and altered to yellowish-red iddingsite (Fig. 11). In highly altered types the original

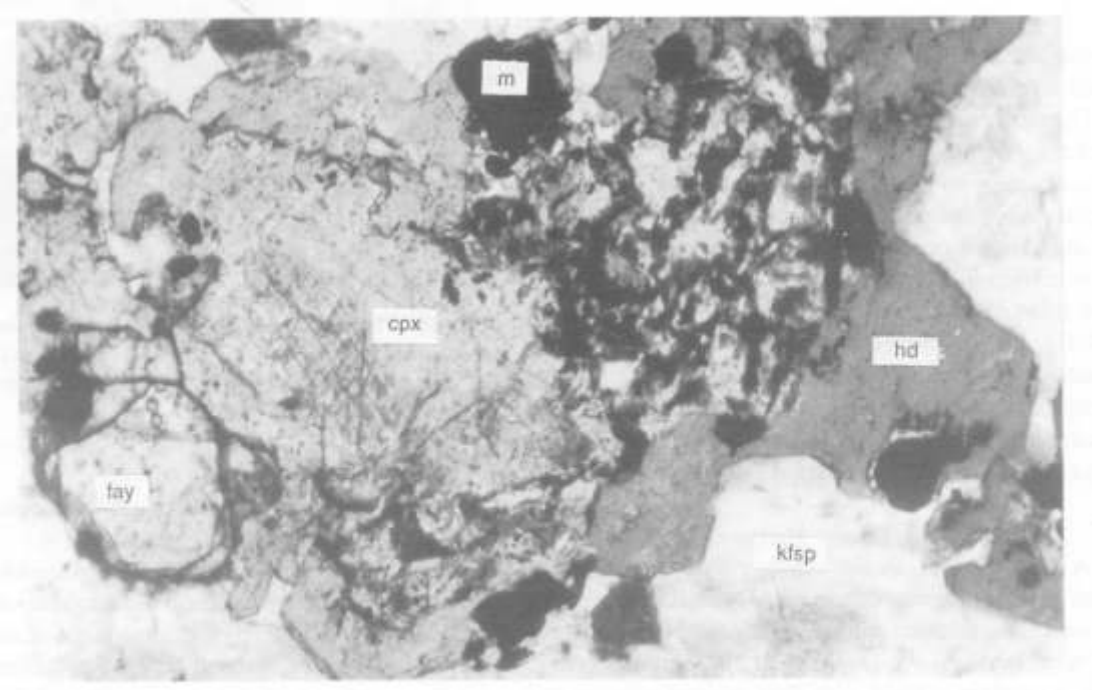

Fig. 11: Photomicrograph of equigranular fayalite-hedenbergite granite (magnification x 41, PPL). Diopsitic augite (cpx) rimmed by sodic hedenbergite (hd), fayalite phenocryst (fay), alkali feldspar (kfsp) and magnetite (m).

Fig. 12: Ring dyke of fayalite-hedenbergite porphyry (dark weathering material towards the left side of photograph), upper Tsisab Ravine/Basswaldrinne.

Fig. 13: View towards the western side of the Brandberg showing Karoo sediments and volcanics (foreground), the breccia zone along the outer caldera fault (br), fayalite granite of the first ring intrusion (fay gr) and hornblende granite (hbl gr) in the background.

fayalite is partly replaced by greenish-brown ferro-edenite/ferro-actinolite aggregates occasionally with small flakes of biotite. The conversion of the mafic mineral assemblages to amphibole under subsolidus conditions is most intense in areas where the fayalite granites have been subjected to late-stage metasomatic processes, indicated by the presence of abundant fluorite (up to 0.2 wt per cent).

A yellowish-brown, fine to medium grained, highly altered hornblende alkali granite occurs as a ring dyke in the upper Tsisab Ravine (Figs 3 and 12) and has intruded between the ferroedenite biotite granite and the central biotite granite. It consists of euhedral quartz, turbid microcline, microcline-perthite, perthite, orthoclase and plagioclase. Aggregates of edenitic hornblende occasionally preserve a highly altered core of fayalite which is decomposed to a yellowish red, isotropic, earthy mass surrounded by fine grained aggregates of aegirine-augite, clustered biotite and magnetite. Secondary, green, ferroedenitic hornblende has replaced pyroxene which often forms the turbid core of edenite crystals. Remnants of iddingsite pseudomorph after fayalite, are partly replaced by magnetite and rimmed by aegirine-augite, which itself is occasionally replaced by ferro-actinolite, giving the rock a slightly peralkaline character. Accessory minerals include fluorite, apatite, zircon, monazite, chevkinite, calcite and haematite. In general it can be stated that fayalite-hedenbergite granites have been intensely altered by post-magmatic fluids, rich in alkalis, which have modified the original mineralogical composition. Similar fayalite bearing granites and alterations are described from Nigeria (Bowden and Kinnaird, 1984).

5.2.3 Hornblende bearing granites

5.2.3.1 Introduction

The group of alkaline granites containing hornblende is the most abundant type of granite forming 60 per cent of the Brandberg Complex. They occur as ring dykes and sheet-like intrusions which form the outer rings of the massif (Fig. 13). The hornblende bearing granites comprise a variety of magmatic and subsolidus mineralogical changes expressed in compositional changes of the amphibole and biotite and can be subdivided into ferroedenite-pyroxene granites and ferroedenite-biotite granites. Post-magmatic alteration processes locally have transferred clinopyroxene into biotite bearing types. Often it is difficult to distinguish transitional types in the field.

5.2.3.2 Ferroedenite augite granite

The hornblende-clinopyroxene granites of the Brandberg Complex comprise a series of subparallel sheets of metaluminous hornblende-pyroxene granite previously described as "main granite" (Hodgson, 1973) or as "Kerngranit" = core granite (Cloos and Chudoba, 1931).

In the northern part of the complex where fayalite-hedenbergite granite is absent or only occurs as enclaves, ferroedenite-augite granite forms the outermost ring-intrusion. The individual sheets of ferroedenite-pyroxene granite are fine to medium grained. When relatively unaltered, the granite is greyish-green in color with reddish-brown weathering crusts and is composed of greenish feldspar, green hornblende-ferroaugite aggregates, quartz and biotite. Anhedral, green hornblende of ferro-edenitic composition replaces pyroxene of the diopsite-hedenbergite series, which forms the highly altered core of the aggregates (Fig. 14). The hornblende itself is partly replaced by fine aggregates of ferro-actinolite and occasionally by yellowish-green, pleochroic biotite of annitic composition. Turbid feldspars are composed of orthoclase, microcline-perthite, perthite and zoned plagioclase. Myrmekitic intergrowth of quartz and alkali feldspar is common and frequently grano-phyric patches have been recognised. Interstitial quartz and small laths of euhedral albite form the latest components accompanied by rare tourmaline microlites between quartz crystals. Other accessory minerals include locally abundant sphene, zircon, allanite, monazite, fluorite and haematite.

5.2.3.3 Ferroedenite-biotite granite

The next concentric ring intrusion towards the centre of the complex is composed of sheets of peraluminous hornblende-biotite granite. Ferroedenite-biotite granites from Brandberg show variable textures from equigranular to granophyric

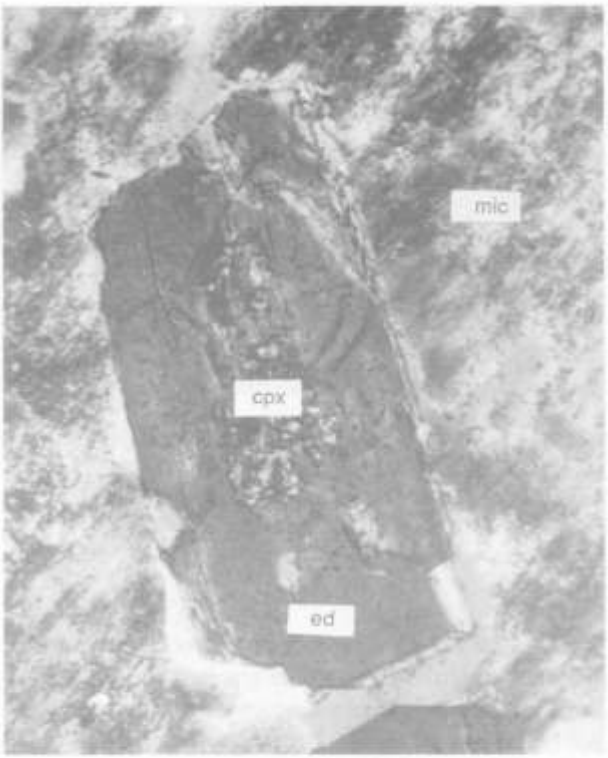

Fig. 14: Photomicrograph of a ferro-edenite (ed) crystal with a core of augitic clinopyroxene (cpx) surrounded by turbid microcline microperthite (mic), (magnification x 20, XPL).

Fig. 15: Photomicrograph of granophyric hornblende biotite granite (magnification x 41, XPL), consisting of granophyric intergrown quartz (qz) and turbid perthite and microcline-microperthite (kfsp) partly replaced by albite (alb), plagioclase (plag) and a large flake of annitic biotite (b).

and comprise some characteristic sub solidus mineralogical changes. The rock is reddish-grey in colour and, depending on the thickness of the individual sheets, is fine to medium grained.

The spectrum of ferromagnesian minerals includes greenish-brown, poikilitic ferroedenite which is often replaced by aggregates of greenish-brown, annitic biotite and magnetite. Big flakes of dark-brown, strongly pleochroic biotite of annitic composition are rimmed by light-green to colourless siderophyllite. Equigranular types contain feldspars including orthoclase, turbid microperthite, microcline-perthite and plagioclase. Quartz crystals are unaltered, anhedral, interstitial and contain needles of rutile in the neighbourhood of altered biotite. Accessory minerals always present in the rock include magnetite, apatite, zircon and monazite.

Deuterically altered types, lacking hornblende, occur towards the contacts of the sheets additionally containing fluorite, allanite, epidote, chlorite, rare tourmaline and occasionally topaz. Individual sheets of hornblende biotite granite often grade into micrographic and granophyric variants (Fig. 15). Intergrowth of quartz and alkali feldspar is dominantly of the micrographic type but radial arrangements around plagioclase are not uncommon. Granophyric patches and micrographic, sheet-like types are highly altered and occasionally mineralised containing chloride, epidote, fluorite, tourmaline, topaz and locally small grains of light coloured, non-pleochroic cassiterite. Metasomatised granites of this type show a characteristic, pinkish-red colour caused by tiny inclusions of haematite in alkali feldspar of the compositional range from microcline - perthite to maximum microcline. The facies occurs more or less irregularly along the contact between the ferroedenite-biotite granite and the biotite granites. Fine grained, marginal zones of some of the sheets show the greatest effect of subsolidus alteration and in places grade into biotite granites with locally relict hornblende. The Numas Ravine ring-dyke is medium to coarse grained mainly consisting of plagioclase, orthoclase and micro-perthite. The dominant mafic mineral is a yellowish-red biotite randomly replacing edenitic hornblende. Towards the finer grained chilled margins the hornblende is replaced by deep-green aegirine-augite and the rock contains patches of granophyric intergrown quartz and perthite. In addition to zircon, ilmenite and rutile, fluorite is the most common accessory.

5.2.4 Biotite granite

5.2.4.1 General

Peraluminous biotite granites occur as cupola sheets and circular plutons in the central part of the massif or as ring dykes between the ferroedenite-pyroxene and ferroedenite-biotite granites of the outer ring intrusions (Fig. 3). Similar to the hornblende granites they comprise a variety of subsolidus alterations and textures, ranging from fine grained, porphyritic to coarse grained, equigranular, and are greyish, reddish pink, flesh red or white in colour.

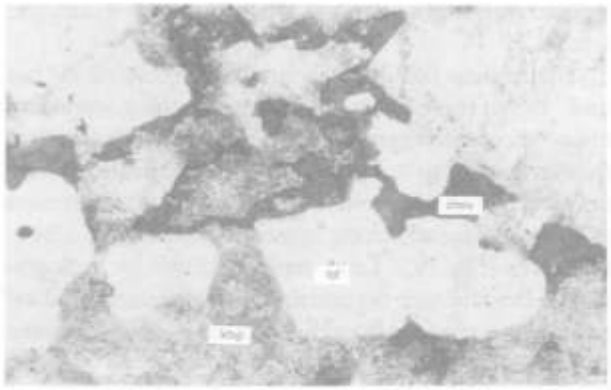

Fig. 16: Photomicrograph of interstitial chevkinite (chev), quartz (qz) and turbid alkali feldspar (kfsp) in transolvus biotite granite (magnification x 43, XPL + helplense).

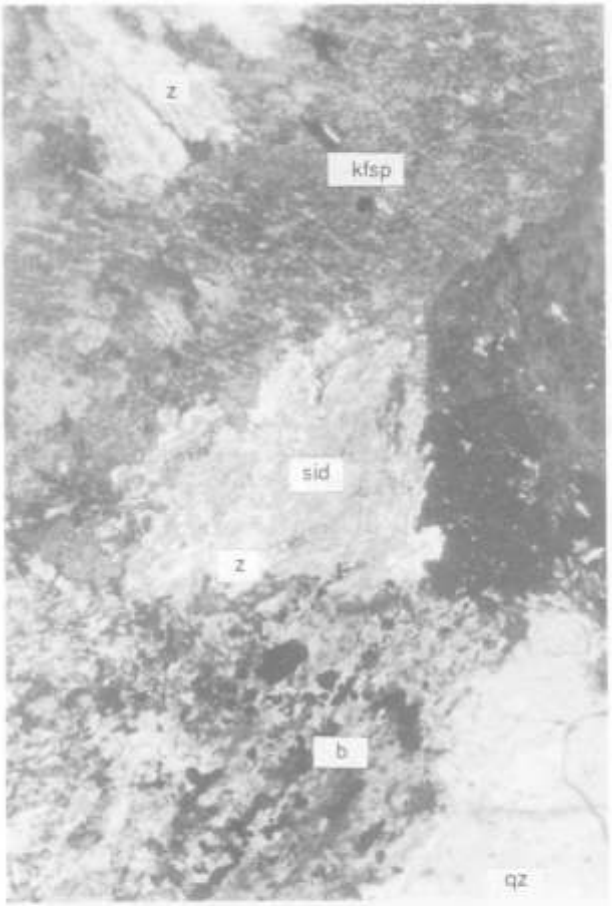

Fig. 17: Photomicrograph of the Buschman Valley biotite granite (magnification x 41, XPL). Remnant, annitic biotite (b) partly replaced by siderophyllite (sid) and colorless zinnwalditic mica (z), alkali feldspar (kfsp) and quartz (qz).

5.2.4.2 Transolvus biotite granite

Pinkish-red, fine grained transolvus biotite granite occurs along the contact with the hornblende biotite granite in a zone, up to 150 m wide. Transolvus types contain albite, turbid orthoclase, mesoperthite, microcline-perthite and irregular shaped quartz, often interstitial to feldspar. Ragged crystals of biotite compositionally range from Ti/Mg-rich, annitic biotite to yellowish-green siderophyllite. Remnants of a former amphibole are replaced by haematite. Chlorite locally forms aggregates together with irregular crystals of sphene. Locally abundant zircon and chevkinite, gadolinite, monazite and rare baddelyite are characteristic accessory minerals in the transolvus biotite granites (Fig. 16).

5.2.4.3 Subsolvus biotite granites

5.2.4.3.1 Central biotite-hornblende granite

The central subsolidus biotite-hornblende granite is medium grained, greyish-pink in colour and contains dark-brown to red, clustered annitic biotite often rimmed by greenish-brown annite. Depending on the intensity of metasomatic processes in the cupola, hornblende may only be present as relicts. Unaffected portions of the intrusion indicate that the primary rock was originally composed of hornblende-biotite granite which has been deuterically transformed into biotite granite and albite granite by intense rock-fluid interaction processes. The feldspars consist of greenish-grey perthite, orthoclase and albite. Accessories include zircon, forming radioactive halos in biotite, iron ore, fluorite, allanite and monazite.

5.2.4.3.2 Bushman Valley biotite granite

The Bushman Valley subsolidus biotite granite (Fig. 2) forms a stock-like plug with outward dipping contacts and has intruded into the central cupola sheets of subsolidus hornblende-biotite granite. The medium to coarse grained granite is greenish-red in colour and consists of quartz, greenish-grey orthoclase to albite-orthoclase, flesh-red, turbid, intermediate to maximum microcline and biotite. The biotite is either partly replaced by iron ore and has reddish brown, Ti-rich cores rimmed by greenish-brown siderophyllite or is entirely replaced by colourless mica (Fig. 17).

Argillic alteration often led to the breakdown of the feldspars and the formation of clay minerals and sericite accompanied by the breakdown of biotite to chlorite-haematite aggregates. Enclaves of fine grained biotite granite (chilled margin) and hornblende granite, up to 1 m in diameter, have been observed along the contact.

5.2.4.4 Microclinised biotite granite

Potassic altered, peraluminous biotite granite is found in the central cupola and along contacts between the central biotite granite and hornblende bearing biotite granite. The irregularly distributed zones of altered biotite granite are characterised by a flesh-red colour and contain turbid microcline-perthite, red microcline, albite and greenish-brown to colourless, pleochroic mica. Fine disseminated cassiterite, with associated topaz, chlorite and more rarely tourmaline and turbid microperthite partly replaced by mica, may occur along fractures and in miarolitic, potassium-feldspar rich zones (Fig. 18). Vugs are either filled by quartz or contain euhedral crystals of microcline together with quartz, light coloured mica and occasionally topaz. Accessory minerals include zircon, monazite, haematite and locally abundant fluorite.

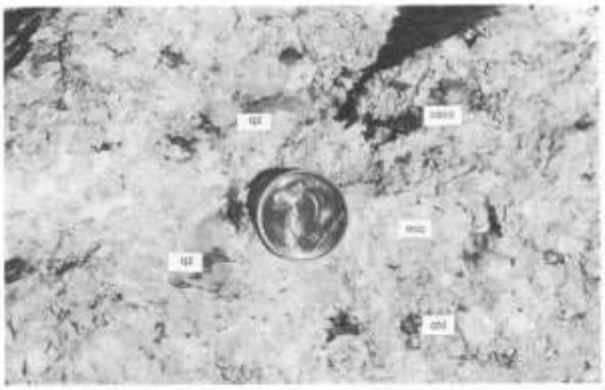

Fig. 18: Microclinised, vuggy biotite granite from the cental cupola with fine disseminated cassiterite mineralisation (cass), chlorite (chl), quartz (qz) and reddened microcline (mic).

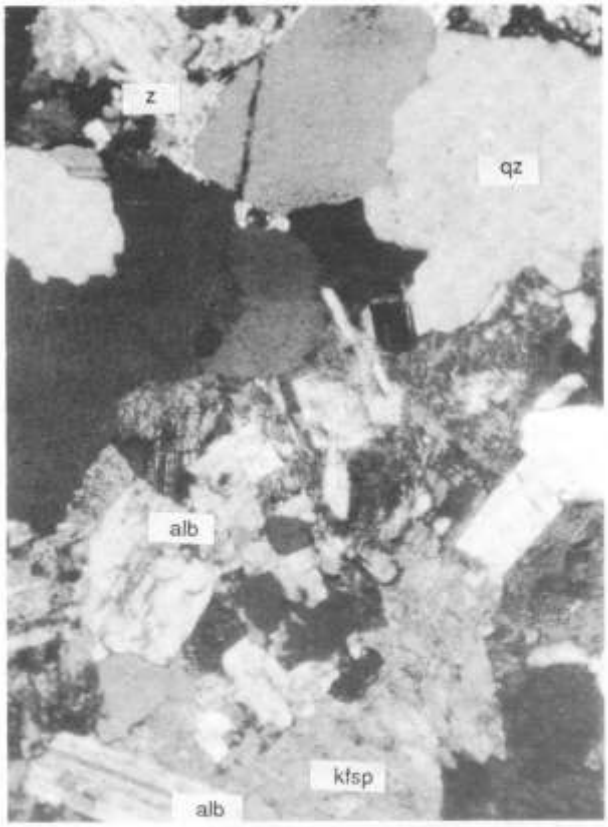

Fig. 19: Photomicrograph of albite-rich biotite granite from the central ring-dyke (magnification x 41, XPL). Quartz (qz), alkali feldspar (kfsp) partly replaced by albite (alb) and colourless, zinnwalditic mica (z).

5.2.4.5 Albitised biotite granite

Fine grained, greyish-white albite-rich biotite granite occurs as irregular bodies in the cupola, as ring dykes in the central biotite granite and between the hornblende bearing granites (Fig. 3). Textural variations ranging from sugary and equigranular to granophyric may occur in a single intrusion. Albitised biotite granite is mainly composed of quartz, turbid perthite to microcline-perthite and euhedral laths of albite, often enclosing anhedral quartz and alkali feldspar, or replacing perthite. Both, granophyric and radiate intergrowth of quartz and alkali feldspar is a common feature.

Biotite is the dominant ferromagnesian mineral and has dark brown cores rimmed by yellowish-green, secondary mica. Micaceous aggregates occur together with abundant fluorite (locally up to 1 wt per cent). Increasing rock-fluid interaction locally has resulted in the complete replacement of alkali feldspar and biotite to produce zinnwaldite- albite-rich rocks (Fig. 19). Leucocratic, peraluminous aplogranites in Brandberg do not contain any columbite mineralisation which is reported from Nigerian counterparts (Bowden and Kinnaird, 1984).

5.2.4.6 Tourmalinised biotite granite

Albitised biotite granite of the Hungurob ring-dyke locally carry abundant tourmaline specks and nodules ranging from 0.5 to 12 cm in diameter (Fig. 20). They consist of bluish-black, interstitial schorl with characteristic bluish-green ple-

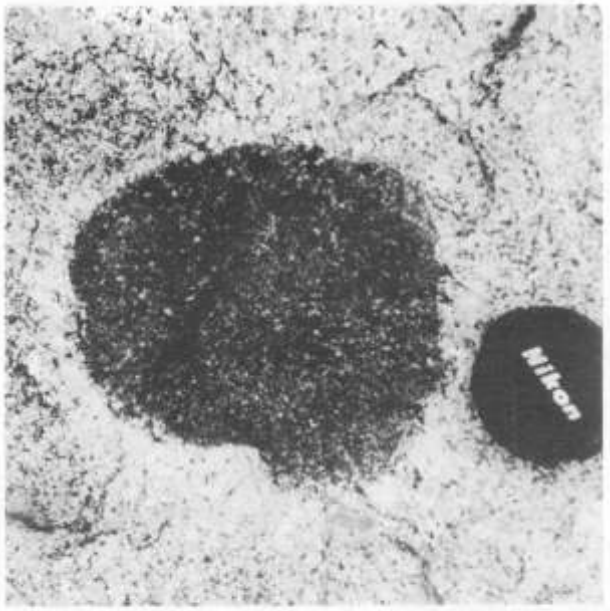

Fig. 20: Tourmaline nodule in albitised granite from the Hungurob ring-dyke with the characteristic white halo.

ochroism, quartz, alkali feldspar, plagioclase, fluorite minor topaz, greenish-brown siderophyllite partly replaced by tourmaline and accessory monazite and zircon. The feldspars are composed of microcline-perthite, orthoclase and euhedral albite. Development of white halos around the tourmaline nodules is a common feature (Fig. 20). The light coloured zones are lacking ferromagnesian minerals but otherwise show the same mineralogy as the host. (Detailed descriptions and genetic implications are given in chapter 8.5 on boron metasomatism). It is interesting to note that similar tourmaline nodules have been reported from the Erongo Complex Haughton *et al.* (1939).

A quartz-rich, tourmalinised zone in the Katarakt area (Fig. 3) is well developed along a ring fracture in potassium altered, red biotite granite. Feldspar and mafics are almost completely replaced by radial arranged tourmaline suns, up to 0.5 cm in diameter, similar to those known from luxullianites (Lister, 1978). The tourmaline is strongly pleochroic

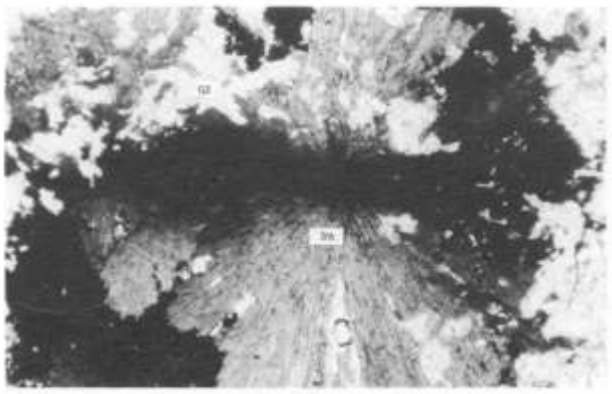

Fig. 21: Photomicrograph of tourmalinised granite (luxullianite) from the Katarakt (magnification x 8, XPL). Rosettes of tourmaline (tm) and quartz (qz).

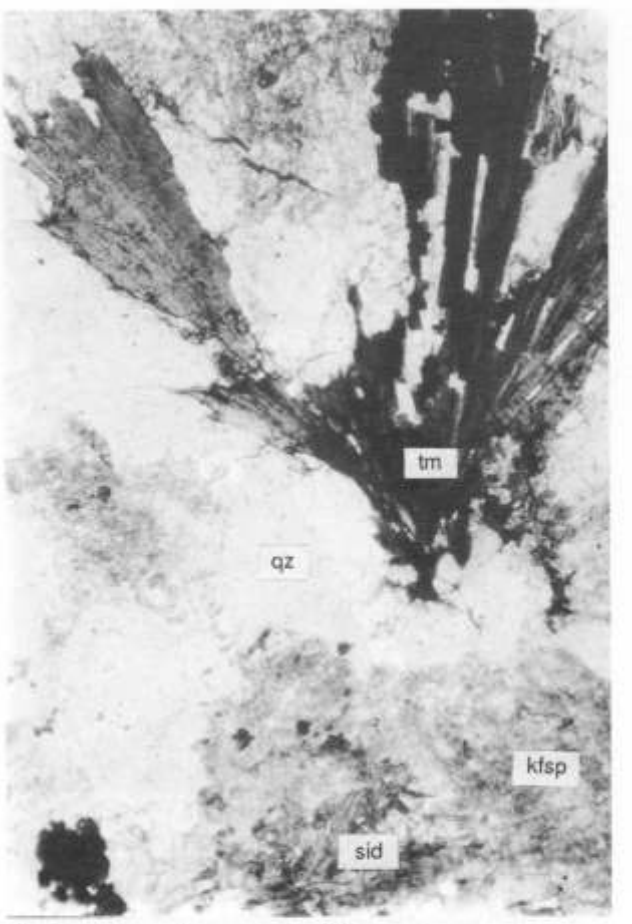

Fig. 22: Photomicrograph of radial growing tourmaline (tm), quartz (qz), alkali feldspar (kfsp) and siderophyllite (sid) in altered biotite granite, Bushman Valley (magnification x 48, PPL).

from deep blue through yellowish-green to pale violet, showing typical extinction crosses which are caused by strong colour absorption parallel to the c-axis. Tourmaline has also replaced graphic intergrown alkali feldspar of the matrix which locally has produced a "graphic intergrown quartz-tourmaline rock" (Fig. 21). Beside accessory zircon and intensely reddened relicts of feldspar, quartz has recrystallised and contains primary and secondary fluid inclusions.

Perfect, deep bluish to black tourmaline rosettes occur along fractures in potassium altered biotite granite in the Bushman Valley. The granite is composed of quartz, turbid alkali feldspar, partly replaced by micaceous aggregates of yellowish-green siderophyllite, topaz and fluorite. Radial growing, deep blue tourmaline replaces alkali feldspar and siderophyllite (Fig. 22).

2.5 Arfvedsonite-aegirine granite

Peralkaline granitic rocks dominantly occur as marginal intrusions in the south-western and western parts of the massif intrusive into country rock, the marginal breccia zone and hornblende granite.

The Amis Layered Complex (see chapter 9) forms the volumetrically largest occurrence of peralkaline rocks in the south-western periphery of the massif (Fig. 3). The granites are characterised by Na-Fe silicates like arfvedsonite, aegirine and astrophyllite, accompanied by microcline, microcline-perthite, albite and quartz. The accessory mineral assemblage includes pyrochlore, zircon, cryolite, colorless mica and REE-minerals. The peralkaline rocks exhibit a wide range in colour, texture and chemical composition caused by intense rock-fluid interaction processes under hydrothermal conditions. (Geological and petrological descriptions of the Amis Layered Complex are given in chapter 9).

5.2.6 Dyke rocks

5.2.6.1 Fayalite hedenbergite porphyry

The occurrence of fayalite-hedenbergite porphyry seems to be restricted to the upper Hungurob Ravine although boulders of this rock type have been found in the upper Tsisab Ravine.

In outcrop the greenish-blue, fine grained rock forms 20-30 cm wide dykes in ferroedenite-augite granite. The primary mineral assemblage includes phenocrysts of red fayalite, hedenbergitic clinopyroxene, orthoclase, microperthite and zoned oligoclase-andesine in a quartzo-feldspathic matrix. Mineralogical changes under subsolidus conditions led to development of annitic biotite and deep-green ferro-actinolite overgrowing hedenbergitic pyroxene. In places of intense rock-fluid interaction fayalite is fragmented and altered to iddingsite whereas primary hedenbergite is entirely replaced by actinolitic hornblende witch itself is overgrown by ferrorichterite (Fig. 23). Accessory minerals include Fe- Ti oxides, monazite, zircon and apatite.

5.2.6.2 Granite porphyry

In the Hungurob Ravine, dark-grey dykes of granite porphyry, up to 1 m wide and 200 m long, have intruded into ferroedenite-biotite granite. The porphyry contains phenocrysts of corroded quartz and perthite, set in a quartzo-feldspathic groundmass with late crystallising, annitic biotite. The matrix shows patches of granophyric or myrmekitic quartz/feldspar intergrowths. Zircon, fluorite and magnetite are accessories.

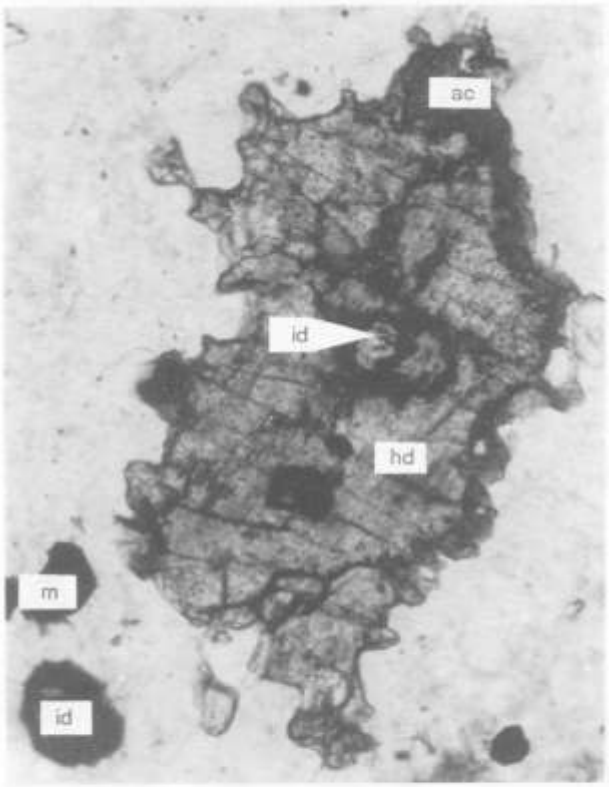

Fig. 23: Photomicrograph of fayalite-hedenbergite porphyry, upper Hungurob Ravine (magnification x 41, PPL). Fragmented, yellowish-red iddingsite (id), hedenbergite phenocryst (hd) rimmed by green actinolite (ac) and magnetite (m), set in a quartzo-feldspathic matrix.

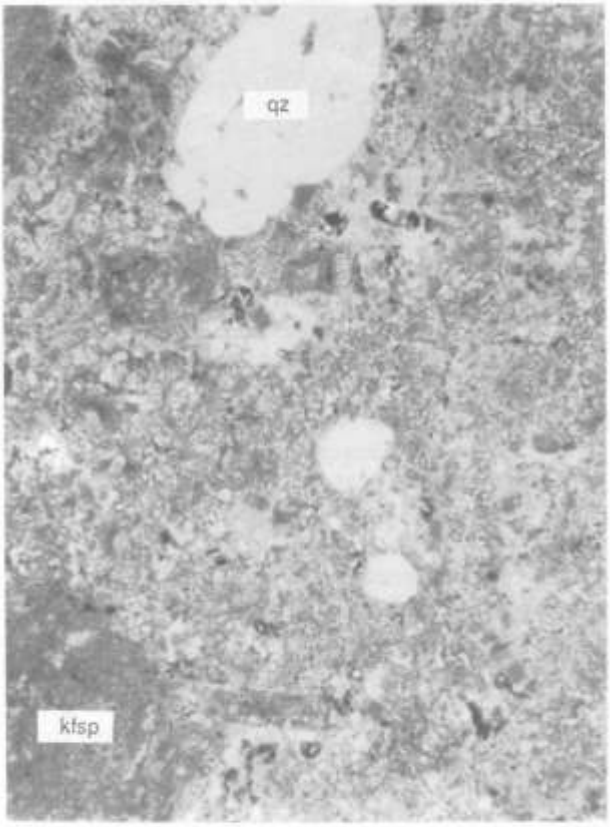

Fig. 24: Photomicrograph of granophyric quartz porphyry, Tsisab Ravine (magnification x 20, PPL). Embayed quartz (qz) and highly altered, turbid feldspar phenocrysts (kfsp) in a granophyric quartz-alkali feldspar matrix.

A negative weathering, pink granite porphyry has intruded into ferroedenite-biotite granite in the Tsisab Ravine. The north-northeast-striking dyke is 4-6 m wide, consisting of flesh-red alkali feldspar, up to I cm in size, rounded, deeply embayed, subhedral quartz and highly altered plagioclase in a light pink coloured, granophyric intergrown quartz/alkali feldspar matrix. Perthite and microcline-perthite are rounded and enveloped by granophyric intergrown reaction rims (Fig. 24).

5.2.6.3 Granophyre

Late peraluminous dykes occur along the south-western margin of the Brandberg Complex and have mainly intruded into the marginal breccia zone and edenite-augite granite. The steeply dipping dykes are 0.2-3 m wide, up to 30 m long and strike parallel to the outline of the complex. Generally they can be described as leucocratic, equigranular, granophyric biotite granites showing different stages of post -magmatic alteration. Relatively unaltered, equigranular, granophyric types are composed of alkali feldspar, plagioclase, quartz and annitic biotite. The granophyres consist of graphic intergrown quartz and alkali feldspar, plagioclase, yellowish-brown, needle-shaped biotite and secondary, greenish-brown siderophyllite. Quartz has preferentially grown along cleavage fractures and lamellae in perthite and microcline-perthite, strongly indicating a post-magmatic origin for the granophyric texture. At a more advanced stage of alteration the biotite breaks down to chloritic aggregates, locally ac-

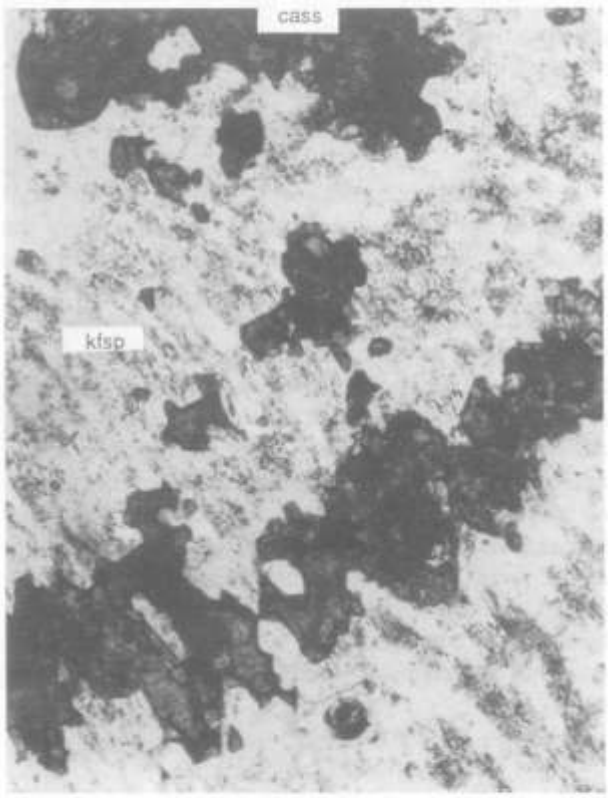

Fig. 25: Photomicrograph of unzoned, pleochroic cassiterite (cass), with graphic intergrown quartz and turbid alkali feldspar (kfsp) in altered granophyre dyke (magnification x 20, PPL).

companied by pleochroic, unzoned cassiterite (Fig. 25). Other accessory minerals include zircon, apatite, monazite, Ti-oxide and magnetite.

5.2.6.4 Ignimbritic quartz porphyry

Quartz porphyry intrusive into hornblende granite and fine grained, pink biotite-bearing quartz porphyry occur in the Weyersbrunn- and Tsisab Ravine and in the Bushman Valley. The dykes are 20-30 cm wide, of light, bluish-grey colour and consist of corroded and embayed quartz fragments, alkali feldspar phenocrysts, plagioclase and fragments of granophyric granite set in a micro-crystalline, quartzo-feldspathic groundmass with late biotite microcrysts and fluorite (Fig. 26). The crystal-rich porphyries have ignimbritic textures

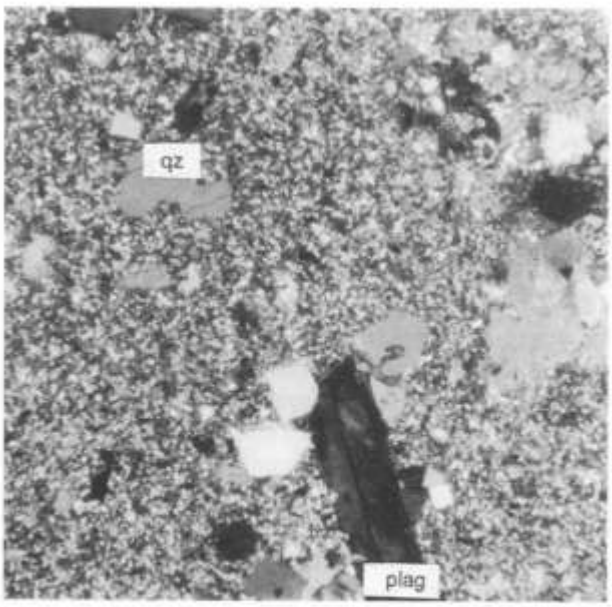

Fig. 26: Photomicrograph of a crystal-rich, ignimbritic porphyry, Buschman Valley consisting of highly fragmented crystals of quartz (qz) and feldspar (plag) in a devitrified, glassy matrix (magnification x 40, XPL).

and are believed to represent feeder channels for late intra caldera ignimbrites. Highly altered relicts of such ignimbritic flows have been found in the Bushman Valley (Fig. 27).

5.2.6.5 Microgranite

Fracture-filling, aplitic microgranite occurs dominantly as fine grained, slightly phenocrystic, greyish or pinkish dykes. They cross-cut hornblende and fayalite bearing alkali granite and are regarded as fine grained equivalents of the central biotite granite and associated ring dykes. The greyish type consists of phenocrystic quartz and perthite, randomly myrmekitic intergrown with quartz or partly replaced by small albite laths, set in a quartzo-feldspathic matrix. The groundmass consists of quartz, orthoclase, perthite and albite with small flakes of biotite and accessory fluorite. Frequently highly granophyric micro granite-dykes have been found in which perthite is partly replaced by granophyric quartz-feldspar aggregates. Biotite is randomly replaced by green annite-siderophyllite. Potassium-rich microgranite dykes and veins

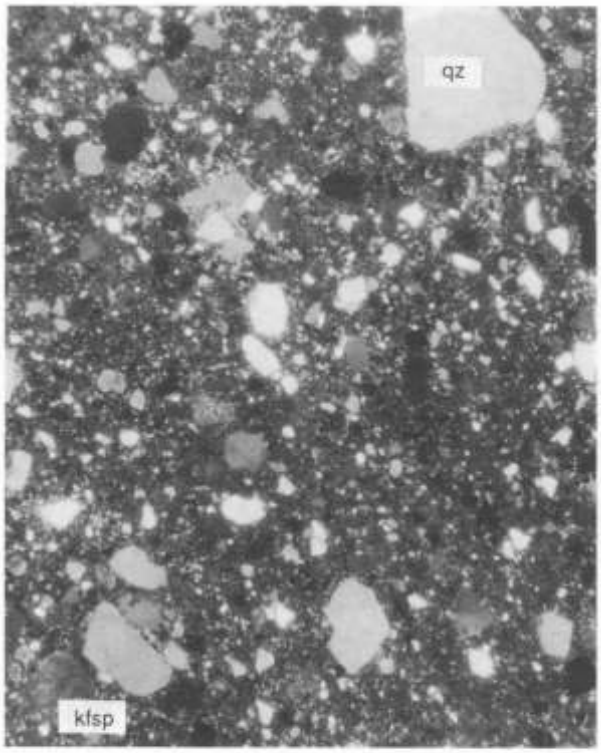

Fig. 27: Photomicrograph of a crystal-rich ignimbrite flow consisting of quartz (qz) and feldspar fragments (kfsp) set in a glassy matrix (magnification x 40, XPL).

have a distinct, pinkish-red colour and consists of quartz, orthoclase and perthite, partly replaced by turbid microcline-perthite, giving the rock a reddish colour. Accessory minerals are magnetite, fluorite, zircon and rare biotite.

5.2.6.6 Arfvedsonite porphyry

Isolated exposures of steeply dipping, peralkaline dykes, parallel to the outline of the massif, form part of a late ring-dyke system in the south-western, marginal part of the massif. Outcrops are limited to the Kleine- and Grosse Domschlucht and the Amis Valley where the dykes have intruded into volcanics and peralkaline granites (Fig. 28). The rock consists of vertically orientated zones of arfvedsonite granite, ranging from fine grained through medium grained to coarse grained/ pegmatitic. Arfvedsonite occurs as ragged, often skeletal crystals, 1 mm up to 5 cm across, set in a network of albitised perthite, microcline and late, interstitial quartz. Accessory, unzoned zircon in the pegmatitic zones is occasionally up to 0.5 cm in diameter.

5.2.6.7 Pegmatite

Apart from pegmatitic patches, located within their parent granite, pegmatites are rare in alkaline rocks of the Brandberg Complex and limited to the peralkaline rock series of the Amis Complex. The pegmatite bodies are 20-80 cm wide, up to 4 m long and have intruded the arfvedsonite-aegirine granite and volcanics and sediments in the periphery of the layered series (Fig. 29). The internally zoned, mica free pegmatites belong to the shallow depths pegmatite group (Ginsburg *et al.* 1979; Cerny, 1982) and genetically belong

Fig. 28: Ring dyke of arfvedsonite porphyry (arfv) cross cutting Karoo volcanics and peralkaline granite, Amis West.

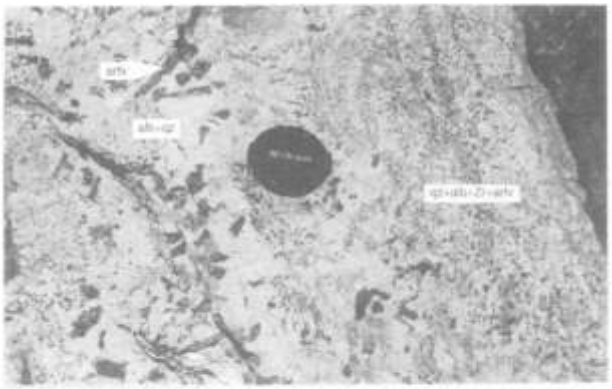

Fig. 29: Rare metal pegmatite of agpaitic composition, Amis Complex, showing a fine grained marginal zone composed of quartz, albite, zircon and arvfedsonite (qz+alb+Zr+arfv), and a coarse grained core zone of arfvedsonite (arfv), partly replaced by aegirine, set in a matrix of quartz and albite (qz+alb).

to the rare-element association of agpaitic magma series. The fine grained border zone consists of quartz, microcline and arfvedsonite, partly replaced by aegirine, followed by an intermediate zone of microcline, quartz and arfvedsonite, up to 3 cm in length, partly replaced by aegirine. The core zone is composed of quartz, microcline and up to 8 cm long, dark, greyish-green, niobium-rich aegirine. Accessory minerals include zircon, xenotime, pyrochlore, bastnaesite, monazite, fergusonite and REE-fluorite.

A miarolic pegmatite type forms an irregular body, up to 1 m wide, emplaced into arfvedsonite granite. The pegmatite is entirely composed of microcline and quartz with abundant fluorite and zircon, up to 1 cm in diameter. Miarolic cavities are filled with quartz or calcedony.

5.2.6.8 Dolerite

Dolerite dykes which have been postulated to be absent in Mesozoic granites of the Brandberg massif (Hodgson, 1973) occur in the Tsisab Ravine and more frequently in the biotite granite of the Bushman Valley (Fig. 3). Olivine bearing, intersertal to subophitic dolerites have intruded into hornblende bearing granites and consist of labradorite and subhedral grains of diopsidic augite, partly altered to ferro-actinolite. Olivine generally is decomposed to iddingsite-chlorite aggregates.

Late dolerites, intrusive into the Bushman Valley biotite granite are mainly olivine free with a pronounced alkaline character. Many of them are highly altered along fractures and the contacts. They carry subophitic to intergranular arranged clinopyroxene and labradorite, accessory magnetite and abundant needles of apatite. Along fractures the rock is cataclastic and highly altered to a fine grained mass of plagioclase, actinolitic hornblende and biotite.

6. Contact relationships, enclaves and xenoliths

Contact relationships between alkali granite of the complex and country rock in the south and southeast differ from those in the north and northeast and generally are controlled by the presence or absence of brecciation along the early major caldera-fault. The contact is relatively sharp in the north and northeast where brecciation is absent, and it is interesting to note that this zone is associated with the area occupied by early quartz-monzonite subvolcanic centres (Fig. 3).

Along the contact of the Mesozoic alkali hornblende granite with the Pan African granite, a distinct, 2-6 cm wide, dark coloured reaction zone is developed. Petrographically the fine grained rock consists of micro-fragments of alkali hornblende granite and Pan African biotite granite set in fine grained matrix of quartz, alkali feldspar and abundant interstitial, brown, annitic biotite. Along schlieren-like zones the brown biotite is overgrown or replaced by light-green to colourless siderophyllite accompanied by scattered grains of deep-green Fe-spinel (Fig. 30). XRD and microprobe analysis revealed that the microscopic crystals, which has been found in Pan African granite up to 8 m from the contact, belong to the hercynite-gahnite series. Mineralogical changes in the Pan African granite include overgrowths and replacement of brown biotite by green annite-siderophyllite and secondary growth of perthite. Generation of myrmekitic and granophyric textures has been observed up to 3 m from the contact.

The contact relations in the south and southeast are controlled by the presence of brecciation along the caldera master-fault. The magma has passively penetrated the space between the network of brecciated blocks of country rock which mainly consists of Karoo volcanics and sediments (Fig. 31). No signs of a late collapse of the entire complex have been recognised, as postulated by Hodgson (1973). Instead, it is obvious that brecciation along the major fault occurred at the early *caldera-stage* of the complex, long before the granitic magma passively entered the fault-zone. Apophyses of fine grained alkali granite often interfinger

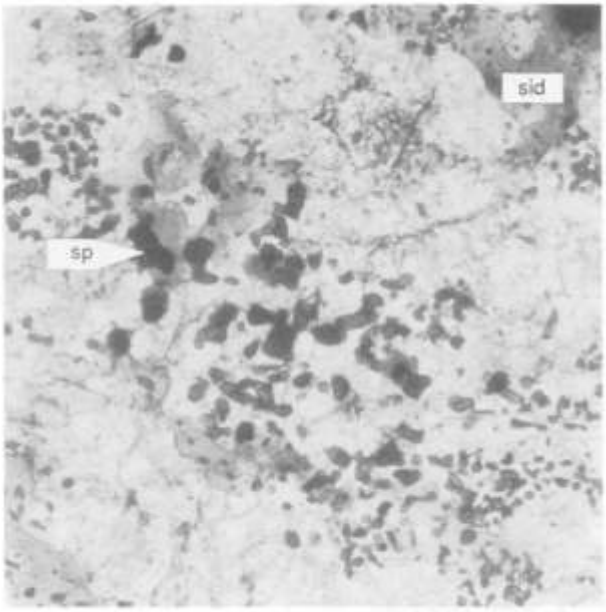

Fig. 30: Photomicrograph of green spinel (sp) and siderophyllite (sid) from the contact zone between edenite-augite granite and Pan African granite, Umoab Ravine (magnification x 240, PPL).

Fig. 31: Brecciated zone along the major caldera fault with xenoliths of volcanic material in edenite-augite granite, Numas Ravine.

Fig. 32: Enclaves of chilled margin in edenite-biotite granite, south of the Katarakt.

of individual sheets of alkali granite. Two types can be distinguished:

A synmorphic type occurs as rounded enclaves of chilled margin, up to 50 cm in diameter, showing identical composition and texture as the host. Their distribution is limited to roof facies of the biotite granites or to the intimate contact zone between the individual intrusions (Fig. 32).

Allomorphic enclaves have a different texture and composition than the host and are distributed more regularly in the marginal facies of the individual intrusions occasionally together with synmorphic types. Enclaves of altered fayalite granite have frequently been found in the marginal facies of ferroedenite-augite granite along the northern contact zone of country rock and the outer ring dyke. Fayalite commonly has been destabilised to magnetite- iddingsite aggregates, and pyroxene has broken down to clusters of Ca-Na amphibole with flakes of deep-brown biotite. Porphyritic to glomerophyric textures characterise this type of enclave resembling that of marginal transolvus granites. Allomorphic fragments and blocks range from 10 cm to 10m in size. The bigger blocks generally are located only a short distance from their source.

Xenoliths of country rock are commonly found in the brecciated contact zone of the complex in the southern periphery which has been passively penetrated by the magma and in the roof facies of the cupola. All types of country rock fragments with the volcanics and to a lesser extent have intruded along bedding planes of the pelitic sediments which have been converted into andalusite hornfelses. Low grade contact metamorphic changes in the sediments and volcanics can be recognised up to 1300 m from the contact.

Mineralogical changes associated with metasomatic processes in the sediments have been observed along the southern contact and described as altered by a "pneumatolitic phase" (Cloos and Chudoba, 1931). Metasomatic changes are most intense in the south-eastern periphery of the complex (see chapters 8.5 and 8.6).

Xenoliths (enallogenious [foreign] rock fragments) are common only along the wall and roof zones of the complex. Enclaves (rounded rock fragments genetically linked with their host) are more limited and occur in the roof zone of the biotite granites or locally along the outermost contact zone

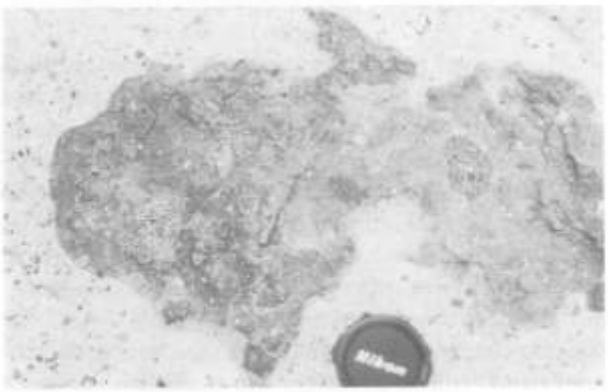

Fig. 33: Xenolith of volcanic material in edenite-augite granite showing assimilation and resorption features, Hungurob Ravine.

are present but xenoliths of volcanic rock are by far the most common (Fig. 31).

At greater distances from the contact, features of assimilation, resorption and growth of new feldspar have been recognised, indicating disequilibrium conditions with their environment (Fig. 33).

Despite the occurrence of lindinosite nodules (arfvedsonite- albite-quartz "enclaves", Lacroix, 1923), which are believed to be of metasomatic origin (see chapter 9.6), peralkaline granites generally lack enclaves.

7. Geochemistry

7.1 Whole rock chemistry

7.1.1 Major element chemistry

Alkaline rocks from the Brandberg Complex, like similar non-orogenic suites, have geochemical characteristics of A-type granitoids. Compared with I- and S-type granites they are relatively depleted in MgO, CaO, TiO_2 and P_2O_5. A striking feature in all these rocks are the varying levels of Na_2O, K_2O and Al_2O_3. Slight differences in the molecular ratio of Na+K to Al may result in significant changes of the mineralogical composition (Bowden and Kinnaird, 1984; Bowden 1985). Therefore, the agpaitic index (Na+K/Al) successfully has been applied to classify A-type granitoids into metaluminous (Na+K<Al<Na+K+2Ca), peraluminous (Al>Na+K+2Ca) and peralkaline (Al>Na+K), (Bonin, 1982; Bowden and Kinnaird, 1984). Each group is characterised by the presence of distinctive mineral assemblages. Metaluminous granites contain altered fayalite, pyroxene and/or edenite; peraluminous granites are characterised by the presence of trioctahedral micas, ranging in composition from annite to zinnwaldite, and peralkaline granites contain arfvedsonite and/or aegirine.

The distribution of the three groups is illustrated in the ternary plot of CaO - (Na_2O+K_2O) - Al_2O_3 (in mol per cent), (Fig. 34). Bonin's classification (Bonin, 1982) of Corsican anorogenic granites based on the classical nomenclature of Tuttle and Bowen (1958) subdivides in:

hypersolvus granite	(single feldspar)
subsolvus granite	(two feldspars)
transolvus granite	(mesoperthite plus two subsolvus feldspars)

Hypersolvus granites are characterised by assemblages of fayalite-pyroxene or hornblende-pyroxene; subsolvus granites contain biotite or arfvedsonite, whereas transolvus hornblende-biotite granite occupies an intermediate position. In the molar diagram CaO - Na_2O+K_2O - Al_2O_3 Brandberg granites separate into three normative domains (Fig. 34). Peralkaline rocks with normative Di + Ac, metaluminous rock types with normative Di + An and peraluminous granites characterised by normative Cor + An. The diagram clearly shows that slightest variations in the proportions of sodium, potassium and aluminium can cause distinct chemical and mineralogical changes in rocks ranging from peralkaline to peraluminous in composition (Bonin, 1982).

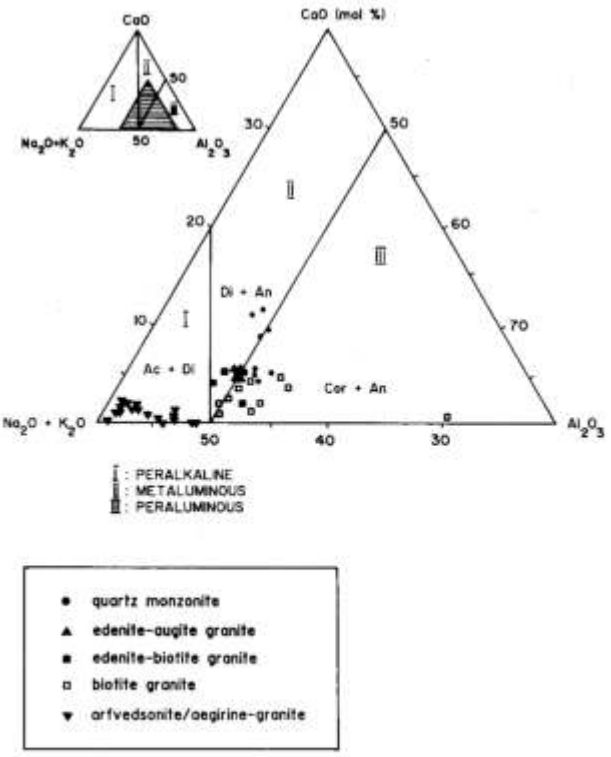

Fig. 34: Molar plot of CaO - (Na_2O + K_2O) - Al_2O_3 showing the fields for peralkaline- (normative Ac + Di), metaluminous- (normative Di + An) and peraluminous granites (normative Cor + An).

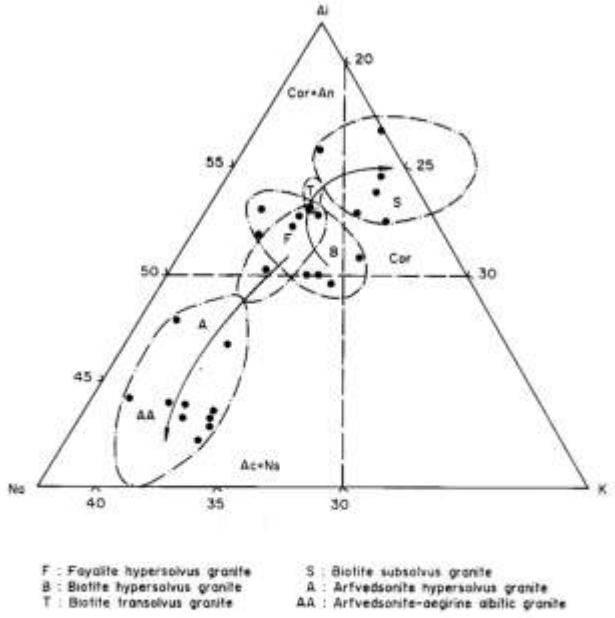

Fig. 35: Ternary plot of Al - Na - K separating Brandberg granites into the fields of sodic feldspar rich and potassium feldspar rich granites, subdivided by the line of aluminium saturation (Al_{50}) into Cor- and Ac-normative granites. Two main evolutionary lines indicate a trend from early metaluminous hypersolvus granites (F, B) to late peraluminous (S) and peralkaline arfvedsonite granites (A, AA).

The ternary plot of Na - K - Al (Fig. 35) allows separation into Al-undersaturated peralkaline granites, characterised by normative Ac + Ns, and Al-saturated granites (Al>50),

which subdivide into Cor and Cor + An normative granites. The peralkaline line leading to arlvedsonite granite illustrates the significant role of sodium. With decreasing Al and K during Na for K exchange processes, arlvedsonite granites grade into albite-rich varieties. The peraluminous line, similar to the trend for Corsican acid rocks (Bonin, 1982), is characterised by an increase in Al while the K/Na-ratio remains constant. Highly differentiated biotite granites plot in the field of subsolvus granites with constant Al-content but growing K/Na-ratio. For Al-saturated rocks there is a general progression from hypersolvus/transolvus granite towards subsolvus types.

The variation of the major oxides as a function of silica (Harker diagrams) confirms the strongly alkaline nature of Brandberg granitoids (Figs 36 and 37). Negative correlation of TiO_2, Al_2O_3, Fe_2O_3 (total iron), MnO, MgO, CaO and P_2O_5

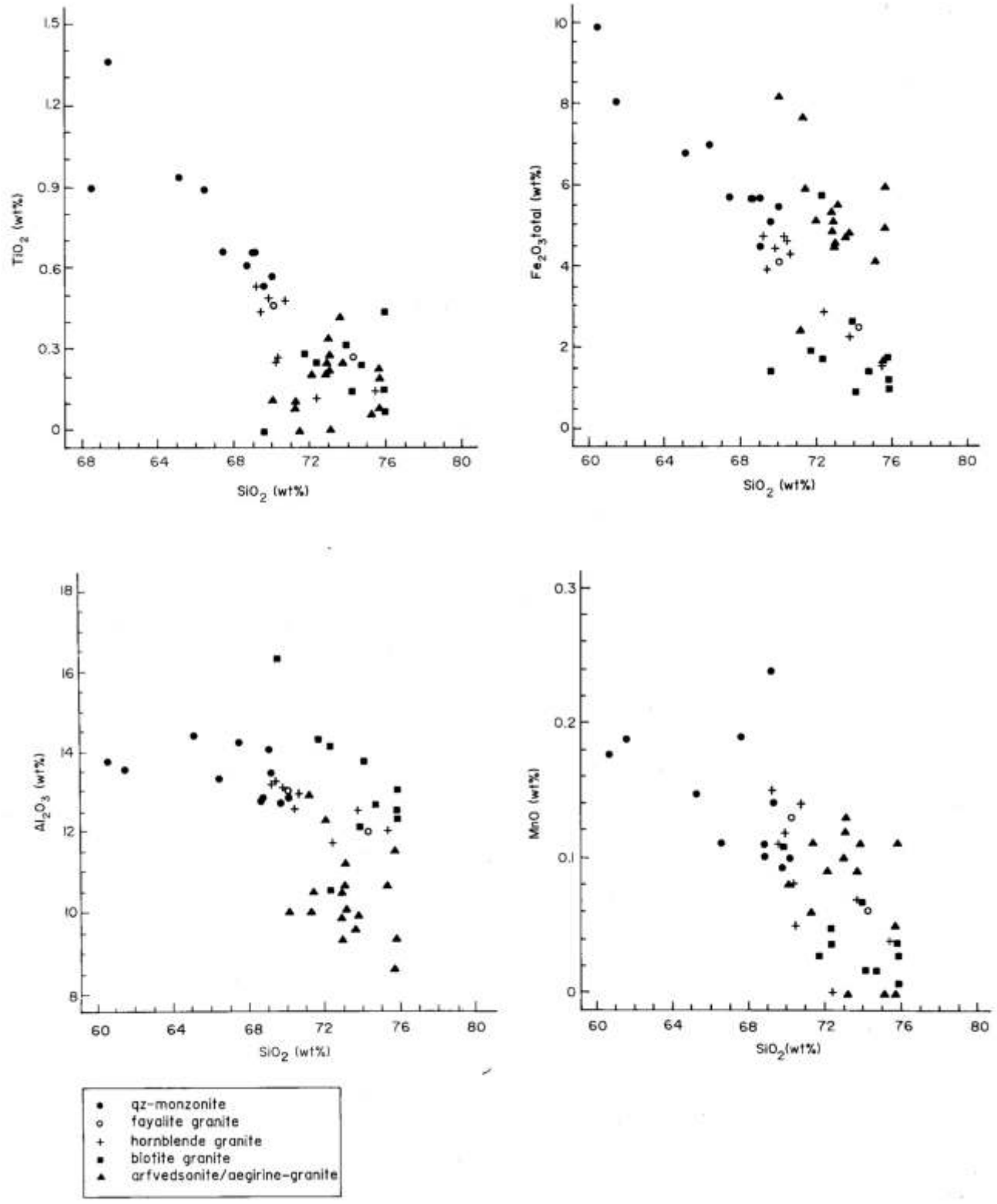

Fig. 36: Harker diagrams of Brandberg granitoids.

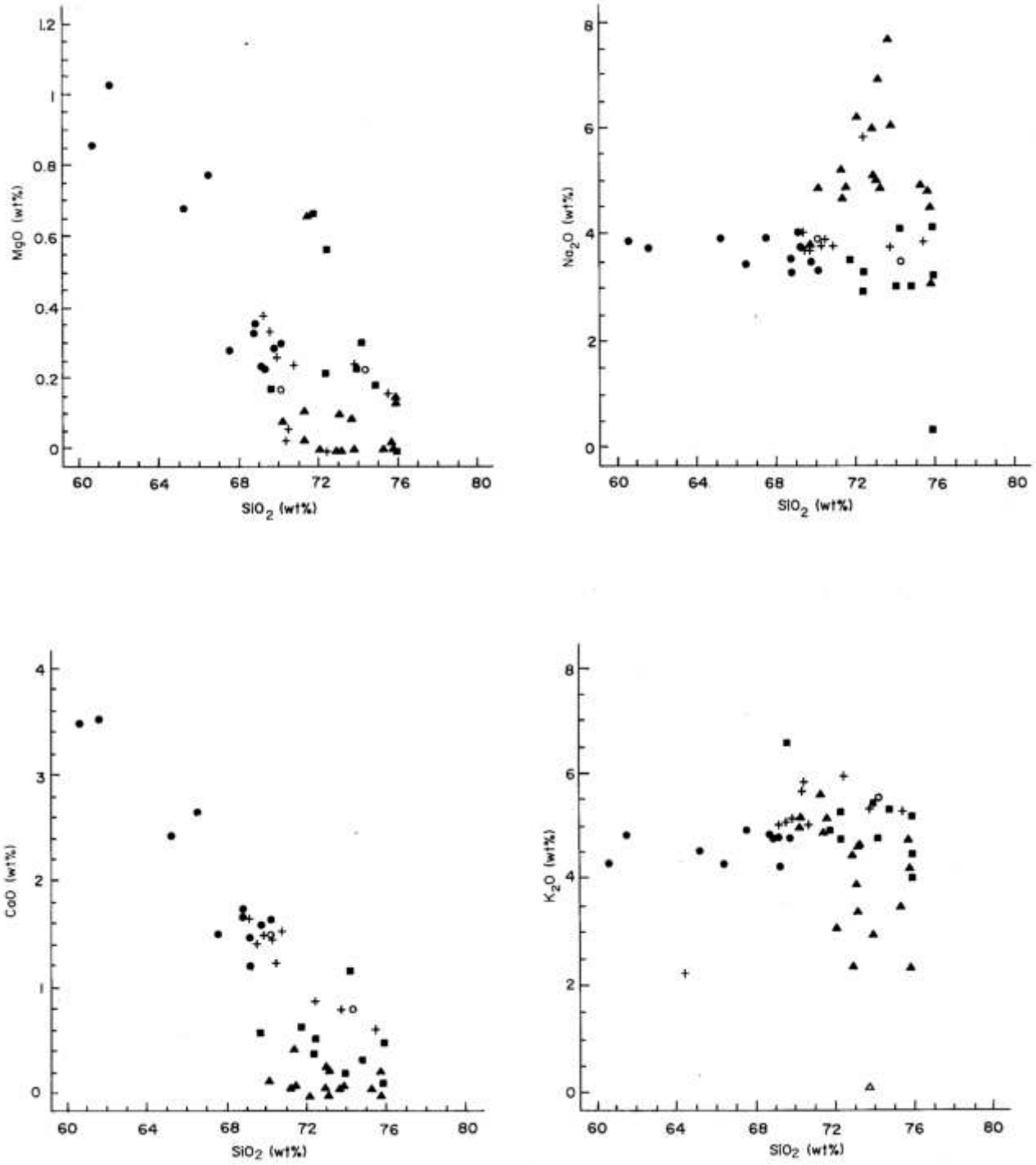

Fig. 37: Harker diagrams of Brandberg granitoids; (same legend as figure 36).

against SiO_2 but positive correlation in the plots of Na_2O and K_2O versus SiO_2 characterises rocks from alkaline, anorogenic environments described as "A-type" by Loiselle and Wones (1979). With fractionation, expressed by increasing SiO_2, the Brandberg data show a progression from quartz monzonites through mica-free granites to biotite and arlvedsonite granites. The scattered nature of the latter is indicative of hydrothermal alteration effects like desilication and loss of CaO, MgO, MnO and Al_2O_3 during late-stage magmatic and hydrothermal alteration. TiO_2, Fe_2O_3 (total iron), MgO and CaO contents decrease with increasing silica reflecting the concentration of these oxides in the coloured minerals of mesocratic rock types. The concentrations of total iron show a more or less linear decline from metaluminous to peraluminous types, whereas the upward-shift in peralkaline granites reflects the high concentration of iron in sodic amphibole and Na-Fe-pyroxene. Discrimination trends for the alkalis in Harker diagrams are more problematic. The generally positive trend for Na_2O and K_2O is masked by both increasing and decreasing tendencies in more differentiated granites. As shown by Bowden and Kinnaird (1978) fractional crystallisation alone cannot be responsible for the removal or con-

centration of Na_2O and K_2O. From their study of Nigerian anorogenic granites they concluded that hydrothermal alteration processes and fluid-phase transfer have modified the chemical composition of the original rock type. Al_2O_3 stays relatively constant in intermediate rock types ranging from 60 to 70 wt per cent SiO_2 and decreases rapidly in high-silica granitic rocks.

The plot of Al_2O_3 versus the Larsen Index (Fig. 38) illustrates the effect of aluminium loss and alkali fractionation.

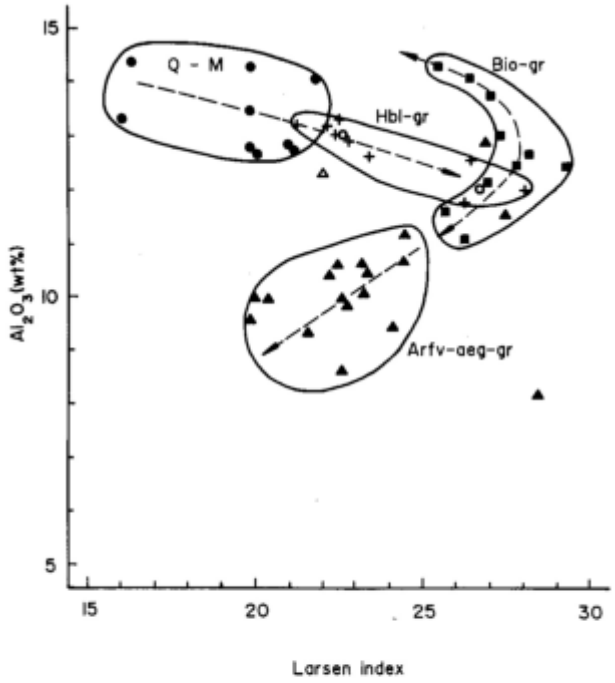

Fig. 38: Plot of Al_2O_3 versus the Larsen Index (1/3 SiO_2 + K_2O - (FeO + MgO + CaO); Larsen, 1938) illustrating the role of aluminium and alkali fractionation in early quartz-monzonitic, fayalite and hornblende granites, in contrast to Al-saturated and undersaturated granites affected by hydrothermal fluid systems; (same legend as figure 36).

Early metaluminous rocks like quartz monzonites and mica-free granites follow a trend of aluminium loss with higher Larsen indices caused by low MgO, MnO, CaO and total Fe (Fe_2O_3). In contrast, the fractionation trend for late-stage peraluminous biotite granite and peralkaline granites illustrates significant losses of Al, Mn, Mg, Ca, K and Si during sodic metasomatism expressed in lower Larsen indices for the post- solidification altered granites (Fig. 38).

Compared with granitic suites from other provinces in Africa, Brandberg granites show distinct similarities with granites associated with dominantly oversaturated Mesozoic ring complexes. The plot of log $CaO/(Na_2O+K_2O)$ versus SiO_2 (Fig. 39) illustrates similarities in the chemical composition of the Brandberg suite with counterparts from Nigeria.

The multicationic diagram of De La Roche (1964) and De La Roche *et al.* (1980) has been successfully applied to rocks from the Nigerian anorogenic province by Bowden and Kinnaird (1984) and Batchelor and Bowden (1985), not only to define magmatic trends but also to display major element

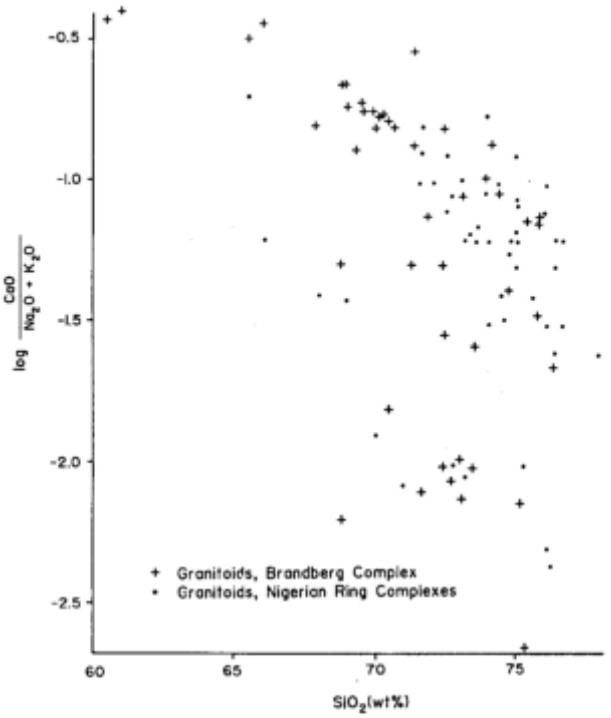

Fig. 39: Plot of log $CaO/(Na_2O + K_2O)$ versus SiO_2 illustrating similarities in the chemical composition of alkaline granites from the Nigerian Younger Granite Province and the Brandberg Alkaline Complex, Namibia.

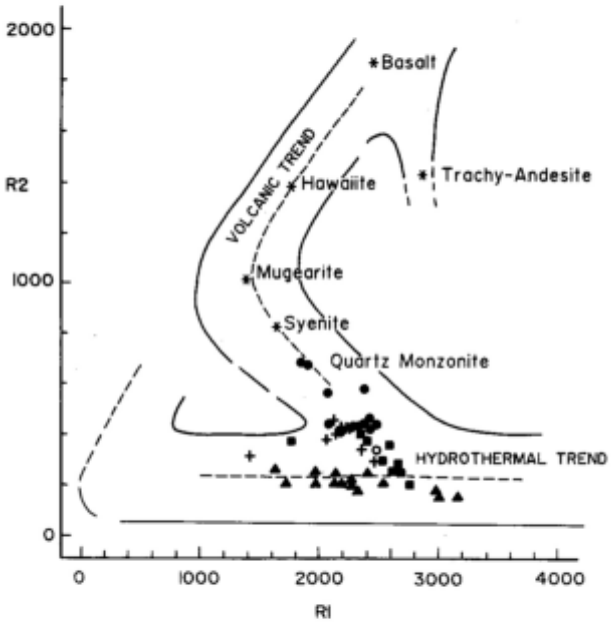

Fig. 40: Brandberg granitoids in the multi-cationic diagram of De la Roche.
R_1: 4Si- 11(Na+K) - 2(Fe+Ti) R_2: 6Ca + 2Mg + Al (all data in millications).
Note that early quartz monzonitic rocks, fayalite-hedenbergite- and ferroedenite-augite granites plot towards the end of the volcanic trend, whereas hydrothermally altered granites follow a horizontal trend with a small range for R_2; (same legend as figure 36).

variations in post-magmatic altered granites. Volcanic rocks from anorogenic complexes define an alkaline fractionation trend ranging from basalt and hawaiite through mugearite and

trachyte to alkali rhyolite. A second "andesitic trend" leading from basalt to rhyolite has been interpreted as mixing of both magma types (Bowden and Kinnaird, 1984)

When plotted in the De La Roche diagram (Fig. 40), subvolcanic rocks of quartz monzonitic composition from Brandberg follow the volcanic trend, and subsequently subvolcanic fayalite granite and mica-free, hornblende bearing types plot towards the end of the volcanic line. In contrast, most of the biotite and arfvedsonite granites plot in groups along a horizontal trend with decreasing R1-values reflecting apparent desilication of peralkaline and peraluminous granites during albitisation and microclinisation processes. Mineralogically these granites are characterised by mineral assemblages which generated under sub solidus conditions, reflecting intensive changes in major oxide ratios during metasomatism.

The plot of K_2O versus Na_2O (Fig. 41) illustrates the chemical variation of sodium and potassium which is most prominent in peraluminous and peralkaline granites. Highest concentrations of sodium occur in desilicated, albitised arfvedsonite/aegirine granites, whereas K-rich/Na-poor granites mainly belong to the group of microclinised peraluminous biotite granite.

The overall presence of a hydrothermal overprint in rocks of the Brandberg complex is masking the magmatic fractionation trend. Most of the variation diagrams and chemical parameters existing in the literature often fail to display magmatic fractionation trends when the rocks are affected by hydrothermal fluids and ion-exchange processes during metasomatism.

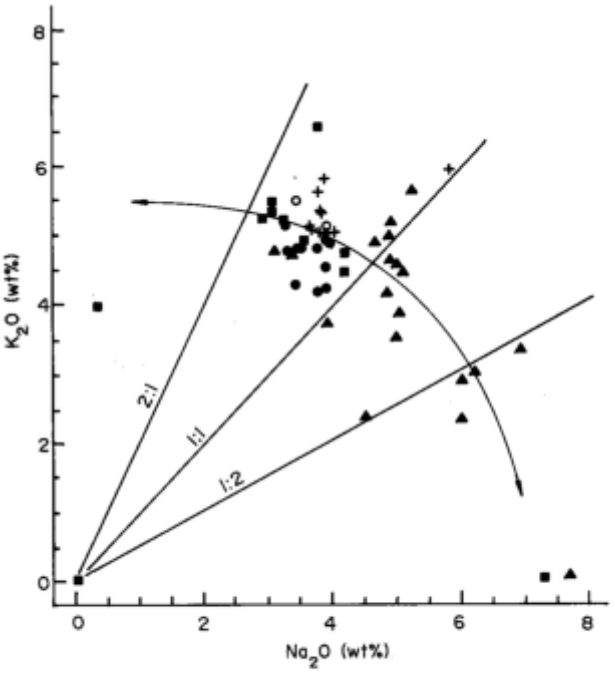

Fig. 41: Plot of K_2O versus Na_2O illustrating K-Na and Na-K exchange processes in Brandberg granites; (same legend as figure 36).

The multicationic classification diagrams of Debon and Lefort (1988) for plutonic rocks and their associations (Figs 42 and 43) turned out to be most useful in displaying not only the evolutionary trend for alkali-saturated granitic rocks associated with Brandberg, but also clearly discriminate the

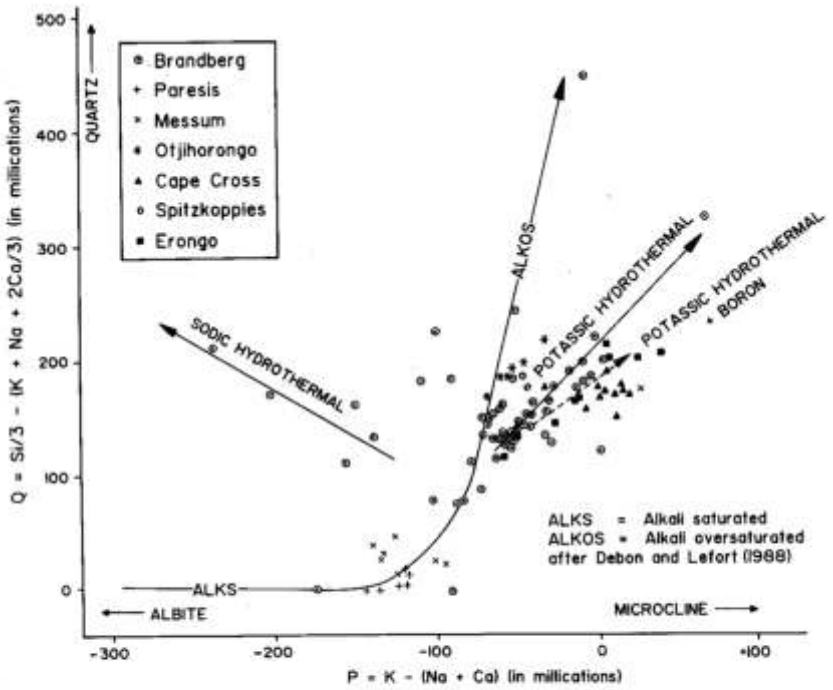

Fig. 42: Evolutionary trends of rocks from Brandberg, Paresis, Messum, Otjihorongo, Cape Cross, Spitzkoppie and Erongo in the Q-P diagram (after Debon and Lefort, 1988) showing an evolutionary path from early alkali saturated towards alkali oversaturated rocks (magmatic trend) and prominent hydrothermal trends for granites affected by sodic and potassic metasomatism.

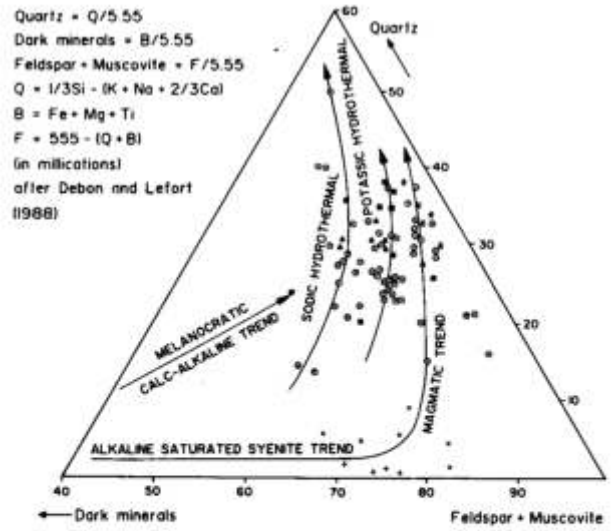

Fig. 43: Ternary QBF-diagram (after Debon and Lefort, 1988) illustrating the evolutionary trend for alkaline rocks of the Damaraland Alkaline Province. Depending on the composition of the hydrothermal fluids associated with the granitic centres, the data plot along a sodic and a potassic hydrothermal trend, tending away from the magmatic line; (same legend as figure 42).

different metasomatic overprints. In order to understand evolutionary trends of granitic rocks from ring complexes of the Damaraland Alkaline Province, the available data (Linning, 1968; Zuleger, 1987; Schlag and Willgallis, 1988; Von Knorring (open file data, Geol. Survey of Namibia) and Bowden and Kinnaird (unpublished data) was incorporated into the diagram.

When plotted into the Q- P diagram of Debon and Lefort (1988) (Fig. 42), granitic rocks associated with Mesozoic alkaline ring-complexes in Namibia plot along a trend of early alkali-saturated composition (ALKS), which continuously grades into an alkali-oversaturated trend for early granites. Syenitic rocks from Paresis, Messum and the Naib quartz monzonite from Brandberg are believed to represent the most primitive rocks associated with the granitic centres. The Naib quartz monzonite which forms a late, circular intrusion in the western part of Brandberg is interpreted to represent the beginning of a new volcanic centre. Hence, its relative primitive syeno-monzonitic composition chemically plots together with syenites from Paresis and Messum. Pre-caldera stage quartz monzonitic rocks of the Gomatsarab-Umoab centres (Fig. 3), which are affected by post-magmatic hydrothermal processes, reveal higher Q-values caused by silicification and loss of sodium/potassium. This trend is marked by a slight shift towards the albite or microcline pole. In coincidence with petrological results, fayalite- and pyroxene-bearing, mica-free granites plot along the magmatic trend (ALKOS). Rocks affected by hydrothermal fluid phases plot distinctively away from the magmatic, alkali-oversaturated trend, reflecting intense ion-exchange processes during chemically variable rock - fluid interaction processes. Peralkaline granites of the Amis Layered Complex (chapter 9), which most intensely are affected by sodic metasomatism (Na for K exchange), plot along a trend proposed for albitised granite of the pyrochlore-REE type (Fig. 42). Potash metasomatised granites (K for Na exchange) plot along a trend characterised by increasing P-(low Na+Ca) and Q-values (high Si). The proposed trend for boron metasomatised granites combined with potash alteration and the development of microcline is indicated by a dotted line (Fig. 42).

When plotted in the ternary QBF-diagram (Fig. 43) of Debon and Lefort (1988) a similar pattern is demonstrated. Distinct sodic and potassic-hydrothermal trends plot away from the magmatic trend for alkali-saturated syenite and alkali-oversaturated quartz monzonite, fayalite- pyroxene - and mica-bearing granites.

7.1.2 Trace element chemistry

7.1.2.1 Introduction

According to their alkaline nature Brandberg granites follow the overall trace element pattern of A-type granites. Variations in trace and major element distribution are characteristic for the metaluminous, peraluminous or peralkaline compositional trends and therefore show continuous variation from early to late-stage intrusives. The most characteristic feature of all the analysed rocks is the marked increase in Rb, Zr, Zn, Nb, Y, Li and Sn with increasing silica content. Late-stage, peralkaline rocks of the Amis layered complex show the most anomalous enrichment of Rb (600¬1480 ppm), Zr (600-11400 ppm), Zn (300-1860 ppm), Nb (150-2000 ppm), Y (100-2000 ppm), Li (180-700 ppm) Sn (50-1300 ppm), Ta (10-100 ppm), U (3-300 ppm), Th (20-400 ppm) and Ce (up to 2000 ppm). Parallel with the increase of lithophile elements the concentration of Sr and Ba decreases together with

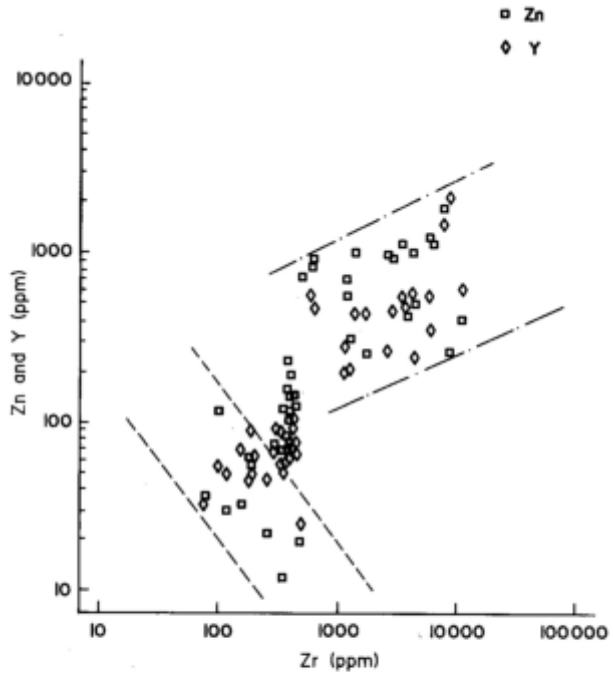

Fig. 44: Plot of Zn and Y versus Zr. Note the contrasting behaviour of the trace elements Zn and Y during metasomatic exchange processes. Depending on the chemical composition of the granites and the hydrothermal fluids, Zr-rich rocks (Zr > 600 ppm = peralkaline) show a positive correlation, in contrast to peraluminous environments (Zr < 600 ppm).

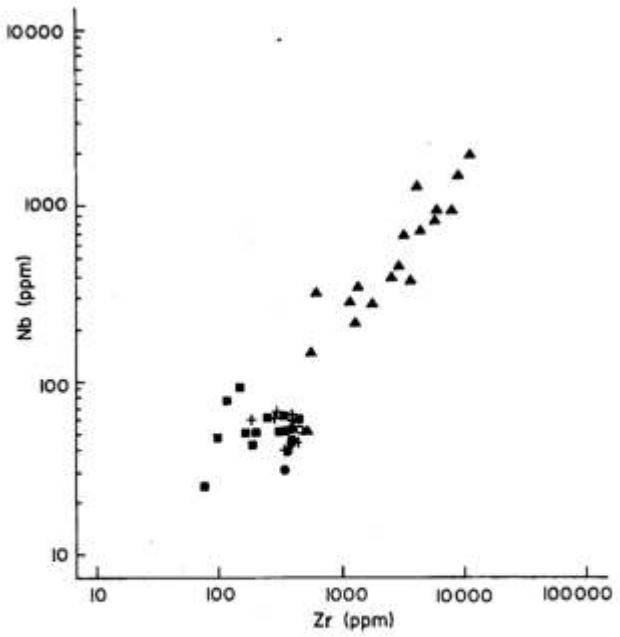

Fig. 45: Plot of Nb versus Zr. There is a good positive correlation of Nb and Zr in Brandberg granites. Highest concentrations of Zr and Nb are found in peralkaline environments (fenites), reaching Zr-levels of 1 wt per cent and Nb concentrations up to 0.2 wt per cent; (same legend as figure 36).

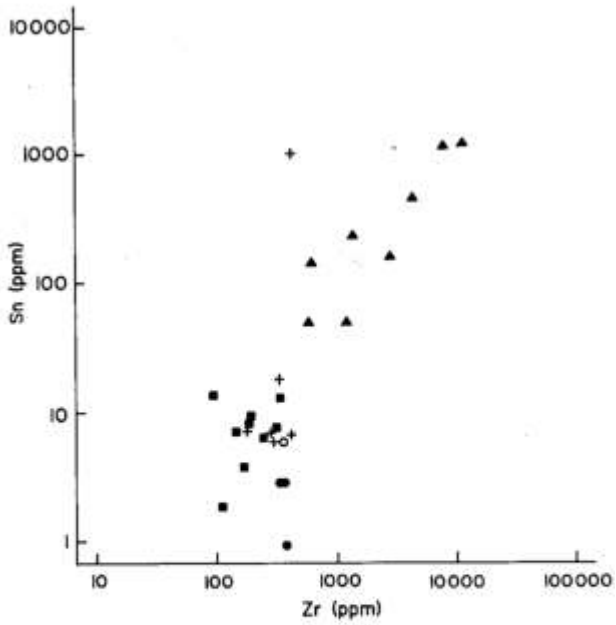

Fig. 46: Plot of Sn versus Zr. Sn generally plays a dual role and enrichment trends are found in both, peralkaline and peraluminous granites. Highest concentrations of Sn, together with other LIL-elements, are found in agpaitic environments, indicating the important role of the peralkaline phase to leach and to transport these trace elements; (same legend as figure 36).

the transition metals Co, Ni, V and Cr.

7.1.2.2 Zr, Nb, Sn, Y and Zn

The studies of Dietrich (1968), Bowden (1966), Bowden and Turner (1974), Radain *et al.* (1981) have shown that Zr-levels are significantly higher in peralkaline environments than in associated peraluminous rock types. The different trends in peraluminous and peralkaline rocks are best displayed when the lithophile elements are plotted as function of Zr (Figs 44, 45 and 46). The plot of Y and Zn versus Zr (Fig. 44) clearly shows a positive correlation for peralkaline granites and a negative correlation trend for peraluminous granites. Metaluminous granitoids occupy an intermediate position with relatively constant levels of Zr (300-450 ppm), Y (60-100 ppm) and Zn (60-200 ppm), depending on the stage and intensity of post-magmatic alteration processes which partly have affected metaluminous rocks as well.

Rb, Nb, Sn and Li (Figs 45 and 46) playa dual role, and enrichments of these elements are present in both peralkaline and peraluminous granites but highest concentrations have been found in agpaitic metasomatites of the Amis Complex.

7.1.2.3 Rb/Sr, K/Rb

Enrichment of Rb combined with an impoverishment of Sr and Ba is described from many oversaturated complexes and alkaline provinces worldwide (Bowden and Whitley, 1974; Bonin, 1982; Imeokparia, 1983; Bowden, 1985; Teale and Lottermoser, 1987). The Rb/Sr-ratios in the different granitic rocks from the Brandberg Complex range from:

0.6-1 in quartz-monzonites
1.5-7 in fayalite and hornblende granites
1.6-11 in unaltered biotite granites
16-214 in altered biotite granites
78-253 in arfvedsonite granites

Bonin (1982) interpreted the negative correlation trend and the shifting tendency towards higher Rb-values as magmatic fractionation between residual liquid and cumulates. The concentration of Rb can be explained by early precipitation of Ba and Sr with Ca in plagioclases without the influence of a fluid phase (Bonin 1982). Authors like Bowden (1985), Imeokparia (1986) and Teale and Lottermoser (1987) have suggested that high Rb- and Rb/Sr-ratios together with low K/Rb-ratios in anorogenic granites invoke alkali metasomatism and recrystallisation processes under subsolidus conditions.

The shift to higher Rb values in the plot of Sr versus Rb (Fig. 47) may therefore be used as a parameter for the intensity of alkali metasomatism. In the Sr-Rb diagram the data from Brandberg show a linear progression from quartz monzonite towards clinopyroxene-bearing fayalite- and hornblende-granites which is believed to display the magmatic differentiation trend for more primitive quartz-monzonitic rocks and mica-free granites. With increasing differentiation and feldspar fractionation Rb is enriched in residual liquids, resulting in the formation of true magmatic biotite granite. Biotite and arfvedsonite granites, with typical sub solidus textures and characteristic mineral assemblages, are shifted towards higher Rb-values, away from the proposed magmatic fractionation trend.

All these granites show alkali metasomatic changes such as albitisation or microclinisation reflecting the presence of a fluid phase which has reacted with the rock under subsolidus conditions.

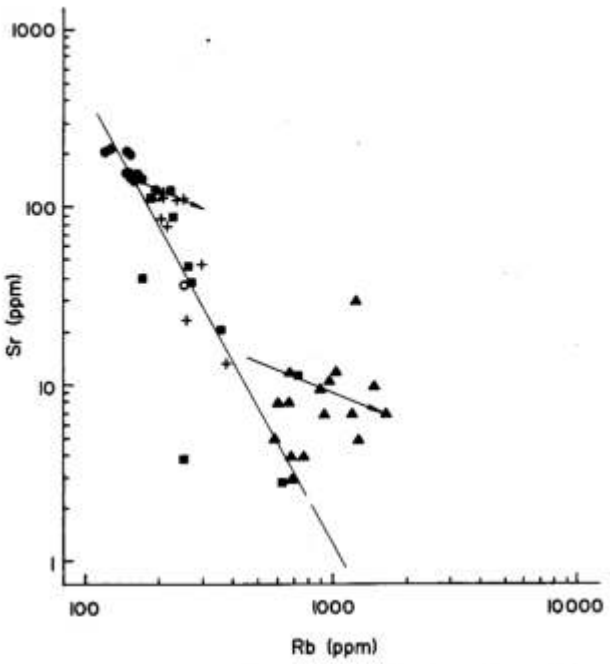

Fig. 47: Rb/Sr diagram. The correlation indicates that enrichment of Rb is coupled to an impoverishment in Sr during magmatic fractionation. The shift towards higher Rb-values may be used as a parameter for the intensity and duration of alkali metasomatism; (same legend as figure 36).

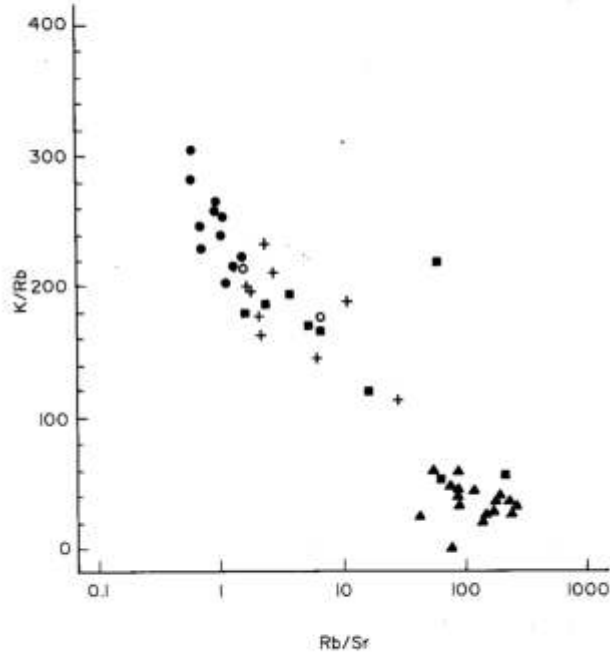

Fig. 48: Plot of K/Rb versus Rb/Sr reflecting the intensity of alkali metasomatism and the increase of Rb during cationic exchange processes under hydrothermal conditions, combined with an impoverishment of Sr; (same legend as figure 36).

A similar distribution of the data is recognised when the K_2OlRb-ratio is plotted against the RbjSr-ratio (Fig. 48).

7.1.2.4 Ba/Rb

The overprint of a hydrothermal fluid-phase on the magmatic fractionation trend is displayed in the plot of Ba versus Rb (Fig. 49). Ba constantly decreases from metaluminous- towards peraluminous granite while the Rb-Ievel stays constant between 200 and 300 ppm. The sudden increase of Rb combined with complete depletion of Ba in peraluminous biotite and especially in agpaitic arfvedsonite-aegirine granites can only be attributed to the influence of hydrothermal fluid-phases.

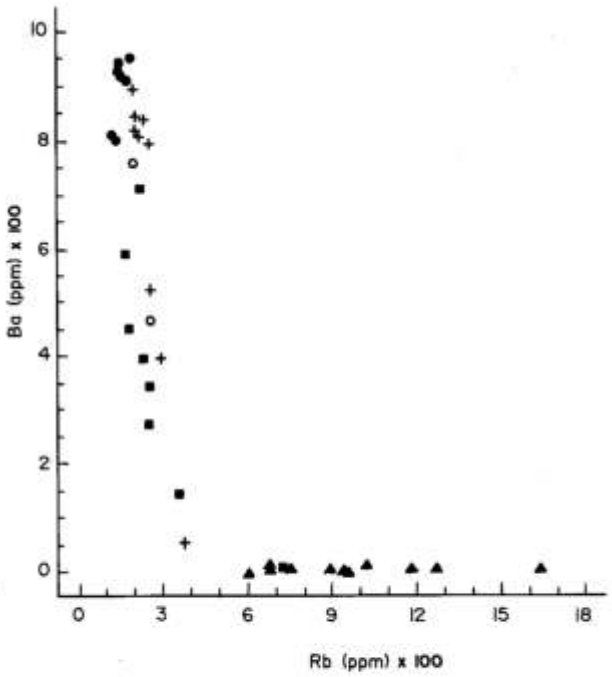

Fig. 49: Ba/Rb diagram illustrating the constant decrease of Ba during magmatic fractionation and the influence of hydrothermal fluid phases in peraluminous and peralkaline environments; (same legend as figure 36).

7.1.2.5. Rb - Ba - Sr

El Bouseily and Sokkary (1975) used the ternary plot of Rb-Ba-Sr to trace differentiation trends in granitic rocks and to distinguish between granites of magmatic and metasomatic origin (Fig. 50). The field of "normal granite" is mainly occupied by quartz monzonites with high Ba/Rb-ratios, metaluminous, mica-free and slightly peraluminous, mica-bearing granites with increasing Ba/Rb-ratios. Some of the transitional quartz monzonites plot in the field of "anomalous granite" displaying low Rb-concentrations which are attributed to Rb-fractionation during metasomatism (El Bouseily and El Sokkary, 1975). The group of "strongly differentiated granites" with highest enrichment in Rb and depletion in Ba and Sr (due to feldspar fractionation and hydrothermal processes) plot towards the Rb-corner. The group of highly specialised granites includes subsolidus altered, mineralised peraluminous and peralkaline granites with characteristic low-temperature mineral assemblages.

7.1.2.6 U/Th

High heat productive elements like U and Th generally show a positive correlation in anorogenic granites. Elevated levels have been recognised in albitised, peralkaline and peraluminous granites but highest concentration are found in

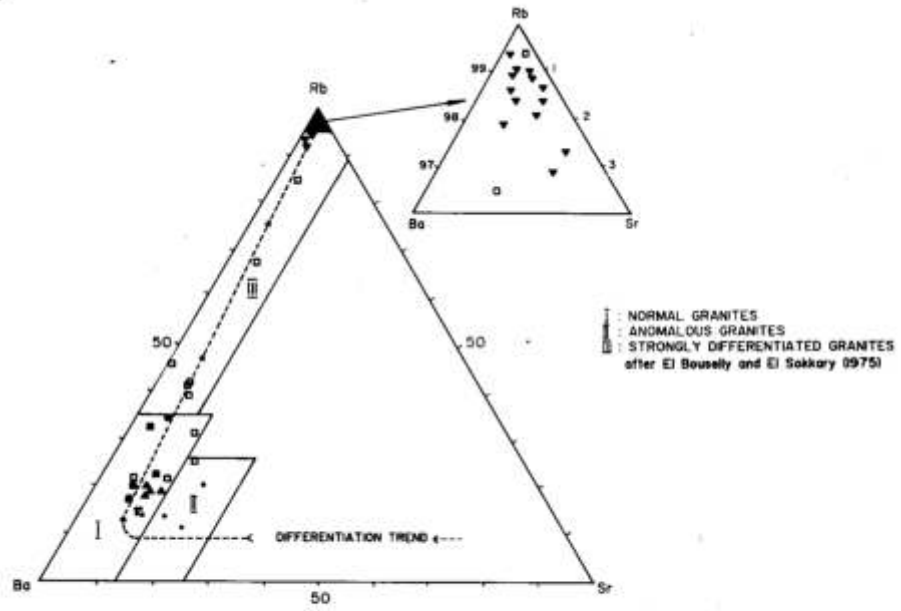

Fig. 50: Ternary plot of Rb - Ba - Sr illustrating the differentiation trend in Brandberg granites and Rb-fractionation in specialised granites; (same legend as figure 34).

the agpaitic rocks (U up to 300 ppm, Th up to 700 ppm). When uranium is plotted as function of zirconium (Fig. 51), which allows discrimination between peralkaline (>550 ppm Zr) and peraluminous granites «550 ppm Zr), the uranium enrichment trend in AI-saturated and undersaturated granites is displayed. In both types the concentration of Th is higher than that of U indicating a substantial loss of uranium relative to thorium. High uranium mobility and remobilisation processes in anorogenic granites during sodic, potassic and H^+-metasomatism have been documented (Kinnaird *et al.* 1985).

In his study of Th and U in the St Austell granite Allman Ward (1985) could show that the "true" uranium content of a granite is difficult to obtain, due to the fact that uranium forms highly soluble and mobile uranyl complexes under oxidising conditions (surface weathering, alteration effects) whilst thorium levels remained unchanged. Despite the problem of uranium-loss in granites the enriched levels of radioactive elements in metasomatised Brandberg granites indicate the important role of the high heat producing capacity to provide the energy to drive hydrothermal convection cells when meteoric water is added to the system. Highly saline fluid systems could have leached significant amounts of uranium during boiling. In the presence of boron (tin) new silicates and oxides may form as proposed by Simpson *et al.* (1979) and Stone and Exley (1985).

The plot of U versus Th/U (Fig. 52) illustrates the contrasting behaviour of the two radiogenic elements during the different alteration processes. In peralkaline granites which dominantly have been affected by sodic metasomatism, both uranium and thorium levels increase dramatically, which causes a significant decrease of the Th/U-ratio from 10 towards 0.3 in pyrochlore-/REE-mineralised types. Peraluminous granites affected by microclinisation processes are uranium depleted, while the thorium concentration stays unchanged, reflecting increasing Th/U ratios. Early K for Na

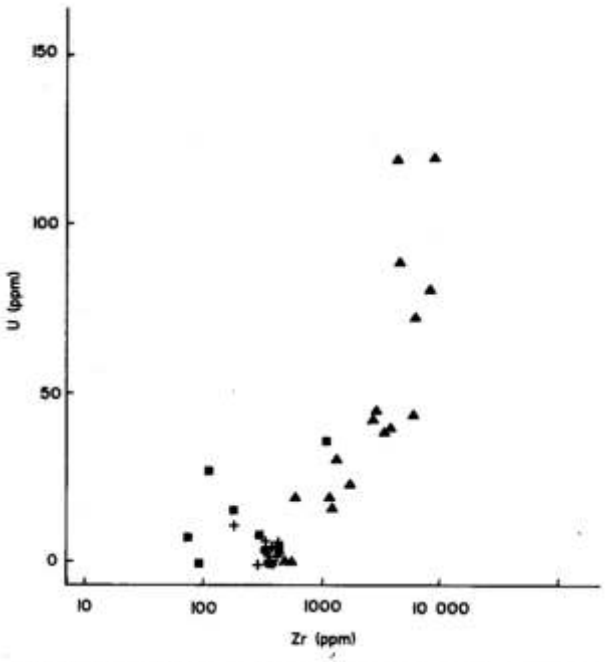

Fig. 51: Plot of U versus Zr. There is a good positive correlation between U and Zr indicating a high mobility of U in peralkaline (Na for K exchanged) environments with Zr-concentrations >600 ppm; (same legend as figure 36).

exchange processes in Brandberg granites are therefore responsible for the leaching of uranium which was possibly introduced into the system during rock-fluid interaction processes in late-stage, peralkaline environments.

The immobile nature of thorium, which is located in resistant minerals like monazite, is in contrast with extremely high Th-values in arfvedsonite and aegirine-astrophyllite granites. The intense enrichment of Th, U, Y, Nb, Rb, Zn and Sn in these granites is believed to be the result of an infiltrated per-

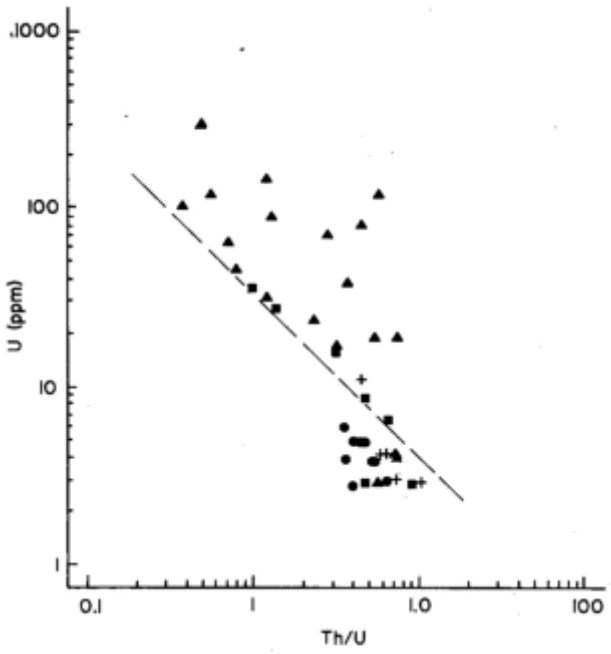

Fig. 52: Plot of U versus U/Th demonstrating the contrasting behaviour of U and Th in peralkaline and peraluminous granites. In agpaitic rocks affected by sodium metasomatism, there is significant increase in both radiogenic elements, in contrast to microclinised biotite granites from which Th and U have been leached during K for Na exchange processes; (same legend as figure 36).

alkaline fluid-phase. The new mineral assemblages which developed in adjacent granite and country rock are almost identical to those of fenites, which are known to be associated with undersaturated syenite complexes and carbonatites, but with the characteristic difference that the granitic Brandberg fenites are depleted in Sr, Ba and Ca. Fenitisation associated with Si-oversaturated ring complexes has been reported from only a few complexes in the world (Bowden 1985). Therefore the Amis Valley granites in Brandberg represent an unique example of fenitisation associated with peralkaline infiltration metasomatism (see chapter 9).

7.2 Mineralogy and mineral chemistry

7.2.1 Introduction

To interpret the chemistry of granitic rocks affected by post-magmatic alteration processes it essential to study the chemistry of the various mineral components and their compositional changes. In order to understand mineral replacement processes in rocks of the Brandberg Complex, information on mineral compositions has been obtained using electron microprobe and XRD techniques. Since whole rock data from Brandberg rocks have been very limited, virtually no data on mineral compositions have been published, and this study is the first of its kind for anorogenic granites belonging to the Damaraland Alkaline Province. A selection of microprobe analyses of the various minerals are given in the appendix (table 2).

7.2.2 Mica

The various types of micas which were recognised in Brandberg granites, using optical methods, belong to a series of annitic biotites which, depending on the intensity of hydrothermal fluids, have been partly or entirely replaced by micas of the siderophyllite-lithionite-zinnwaldite series. Microprobe data clearly indicate that trioctahedral Brandberg micas generated under subsolidus conditions in the presence of fluorine-rich fluid phases. Changes in colour, from reddish-brown through green to colourless combined with changes in the optical properties are controlled by chemical exchange processes under the influence of a fluid-phase. Affected by metasomatising fluids, the original granitic biotite becomes randomly or entirely replaced by subsolidus mica-types. Microprobe analyses demonstrate that early granitic biotites are generally Fe-rich with high Ti-, Mg- and low AI-, Si- and F-concentrations (appendix, table 2.1). Green-yellowish, pleochroic siderophyllite often rimming and enclosing annite is chemically characterised by increasing Si, Fe and Al while Ti and Mg are decreasing (see appendix, table 2.1). This trend continues with increasing ion-exchange processes to generate colourless mica with chemical characteristics of zinnwaldite from greisen environments. Micas of endmember composition in mineralised granite are enriched AI, Si and F and strongly depleted in Fe, Mg and Ti. Alkali saturation in peralkaline rocks is reflected in the pronounced Fe-rich and AI-poor composition of annite and lepidomelane from brandbergites (chapter 9.5). Biotites from fenitised country rock and highly altered contact metamorphosed alkali granite containing green spinel (hercynite-hoegbomite) have Mg-contents up to 8.6 wt per cent and intermediate FeO concentrations (20 wt per cent). Their "phlogopitic" nature furthermore is reflected in the substitution of Al^{IV} for Si and Mg:Fe-ratios 2:1. This is in contrast with the fox-red colour and small axial angles (2V=0-20°). As shown by Deer *et al*. (1962), the usage of the term phlogopite is somewhat arbitrary for phlogopite of end-member composition which forms a solid solution series with annite.

When plotted in the Al^{VI}/Fe diagram (Fig. 53), micas from Brandberg granites plot along three distinct trends reflecting the primary composition (Al-saturation/-undersaturation) of the host rock and the chemical composition of the fluid phase. Peraluminous granites have developed tri-octahedral mica in the compositional range annite-siderophyllite-zinnwaldite (Figs 54 and 55). Al-undersaturated, peralkaline granites have developed a series ranging from annite - lepidomelane to lithionite-zinnwaldite (Fig. 53). Metaluminous fayalite granites contain granitic biotite with highest TiO_2 (up to 4.7 wt per cent) and MgO (up to 13.5 wt per cent). Partly chloritised biotites from hypersolvus and transolvus hornblende-biotite granites plot along a compositional trend ranging from annite to siderophyllite. They coexist with ferroedenite, magnetite and late alkali feldspar and show unusual high MgO concentrations (up to 10 per cent) for biotites from alkaline environments. According to the experimental work of Wones and Eugster (1965) biotite which is coexistent with magnetite and al-

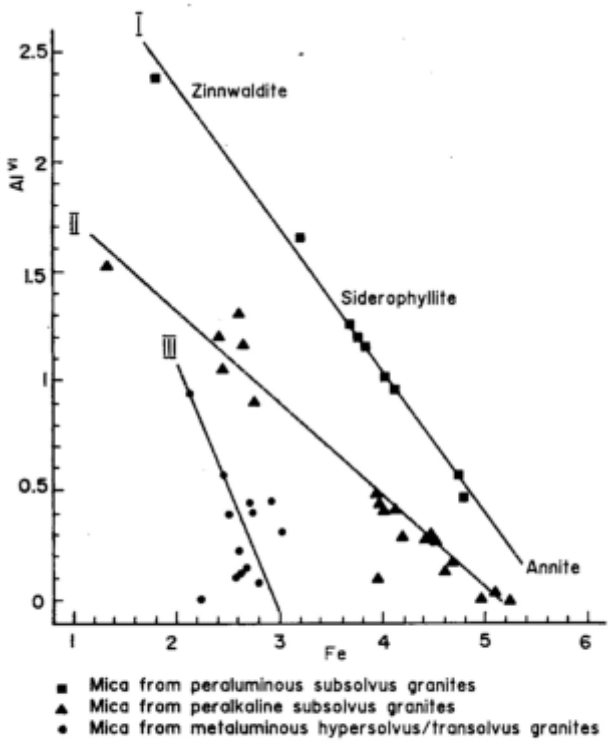

Fig. 53: Compositional trend of micas from peraluminous granite (I), peralkaline granite (II) and metaluminous granite (II) in the Al^{VI}/Fe - diagram.

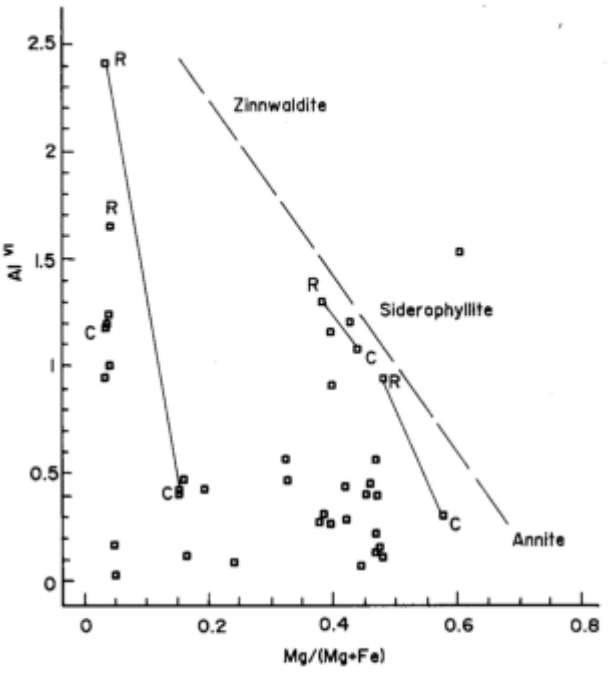

Fig. 54: Compositional differences of micas in the plot of Al^{VI} versus Mg/(Mg+Fe). C, R, = core and rim of the same crystal.

kali feldspar will decompose by the reaction: biotite = more magnesian biotite + alkali feldspar + magnetite, under unstable oxygen fungacity with decreasing temperatures. This would explain the observation that with increasing iron in the host rock the biotites become more magnesian (Speer, 1984). Such conditions apply to chilled margins of plug-like intrusions or rapidly cooling ring dykes which in Brandberg have preferentially developed characteristic transolvus textures (chapter 5.2.4.2). Bowden and Jones (1978), Imeokparia (1982) and Bennet *et al.* (1984) have reported similar compositional trends (annite-siderophyllite-zinnwaldite) for micas from peraluminous granites of the Banke, Shira, Tibchi and Afu complexes in Nigeria.

The plot of Al^{VI} against the Mg/(Mg+Fe) ratio (Fig. 54) illustrates that both annite and zinnwaldite may be present in one and the same rock type or even in one single crystal. The core of a crystal has often preserved the primary granitic or annitic composition whereas, under the influence of fluid-phases, the outer zones of the crystal have been first transformed into siderophyllite and subsequently into colourless zinnwaldite along the outermost rim. Biotites from albitised biotite granites show the most intense Fe-Mg and Al-substitution expressed in low Mg/(Mg+Fe)-ratios (<0.1) while phlogopite-biotites are characterised by ratios up to 0.6 (see appendix, table 2.1).

The $Fe_t(Fe_t+Mg)$-ratio of the analysed micas range from 0.4 (magmatic biotite) to 0.98 (zinnwaldite). In his work on biotites from the Afu complex, Nigeria, Imeokparia (1982) showed that biotites associated with rare metal-mineralisation have the highest Fe/(Fe+Mg)-ratios(0.95-0.99). Discrimination of the different groups of micas are best

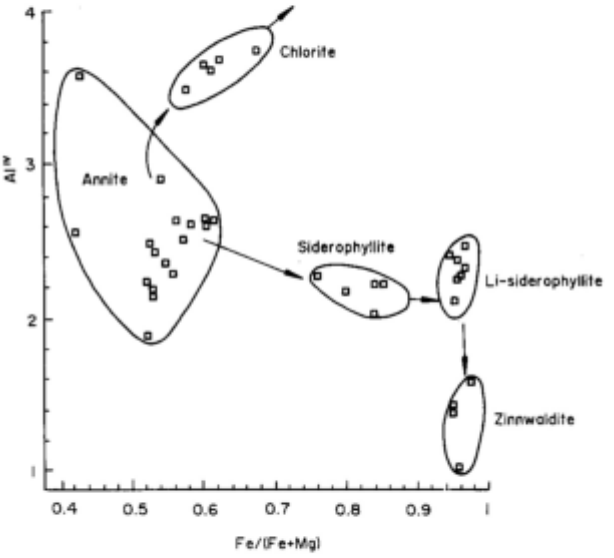

Fig. 55: Subsolidus alteration trend of micas from Brandberg granites in the plot of Al^{VI} versus Fe/(Fe+Mg) showing significant compositional changes of the original annitic biotite under the influence of hydrothermal fluid-phases, which led to the development of chlorite or trioctahedral micas of the siderophyllite-zinnwaldite series.

displayed in the plot of tetrahedral aluminium versus Fe/(Fe+Mg) (Fig. 55).

7.2.3 Chlorite

Alteration of biotite to chlorite is a common feature in hydrothermally altered and mineralised granite. In Brandberg, the chlorites differ from their parental biotites in being more oxidised with higher Mg-values and are iron-rich (33-37wt

per cent FeO_t) combined with a depletion in Ti and K and F. The loss of titanium is commonly recognised in thin section by the development of secondary rutile needles whereas leaching of potassium generally resulted in the growth of alkali feldspar according the reaction: biotite + quartz + water = chlorite + alkali feldspar (Chayes, 1955). Disseminated chloritisation in Brandberg granites and country rock is commonly accompanied by albitisation and late epidotisation processes, in contrast to vein controlled alterations in potassium-rich environments, displaying characteristic mineral assemblages of the paragenesis: quartz-microcline-chlorite-epidote-siderite-sphalerite-casiterite. According to the classification of Foster (1962) the analysed chlorites are mainly ripiolites.

7.2.4 Pyrophyllite

Pyrophyllite is regarded as a hydrothermal mineral which occurs through the alteration of feldspar (Deer *et al.* 1962; Frey, 1987). In Brandberg, occurrences of the mineral are limited to low-grade metamorphosed and acid metasomatised Karoo-pelites forming an alteration killas adjacent to the peralkaline granites of the Amis Layered Complex. The mineral was identified using XRD and is seemingly related to metasomatic processes during low temperature rock-fluid interaction processes (see chapter 8.6 for more detailed descriptions).

7.2.5 Pyroxene

In the Brandberg Complex, pyroxene occurs in subvolcanic quartz monzonite, ferro-edenite granite, fayalite granite and -porphyries and in arfvedsonite granite. According to their chemical composition the analysed pyroxenes fall broadly in a calcic and a sodic group. Ca-pyroxene is the characteristic mafic mineral of metaluminous rocks where it dominantly occurs as phenocrysts. In quartz monzonites, the crystals show distinct zoning with a greyish to yellowish-grey core of ferro-augite grading continuously into green to bluish-green rims of ferroaugite/hedenbergite and sodic ferro-augite. Individual grains are occasionally randomly replaced by deep-green aegirine-augite. Clinopyroxenes from ferro-edenite granites occur as highly altered and fragmented crystals of ferro-augitic composition. Relict crystals often form the core of edenic hornblende and ferro-actinolite aggregates or have been almost completely replaced by the latter. In fayalite bearing granites and porphyries the composition of pyroxene varies from ferro-augite to ferro-hedenbergite. Zoned phenocrysts from granite ring-dykes consist of a yellowish-grey core of ferro-augite/hedenbergite rimmed by sodic augite, whereas phenocrysts from fayalite porphyries are composed of ferro-hedenbergite often rimmed by bluish-green aegirine-augite.

Sodic pyroxene is dominantly developed in late-stage agpaitic rocks containing arfvedsonite and forms interstitial, poikilitic crystals. Deep-green aegirine trends chemically towards endmember composition and is either coexistent with sodic amphibole or successively replacing it. Some selected microprobe analyses of aegirine from the Amis Complex are given in the appendix. Characteristic high concentrations of Na_2O and total iron as FeO, accompanied by complete depletion in CaO and MgO, indicate a main substitution of $NaFe^{3+} \leftrightarrow Ca(Mg,Fe^{2+})$. The most striking feature in aegirine from metasomatites (fenite) are high TiO_2-values (up to 2 wt per cent) (chapter 9). In crystals with high TiO_2 concentrations, surprisingly high Sn-accumulations (up to 0.5 wt per cent SnO_2) have been recognised. The occurrence of stanniferous aegirine together with zincian fluor-arfvedsonite indicates that post-magmatic fluid-phases, similar to fenitising fluids associated with carbonatites, had infiltrated sufficient quantities of trace elements that Sn and Zn could enter the lattice of subsolidus crystallising pyroxene and amphibole in a highly peralkaline environment. Crystallisation of sodic pyroxene and hornblende at low pressure and shallow depths is reflected in total lack of Al in octahedral positions (Leake, 1965; Neumann, 1976).

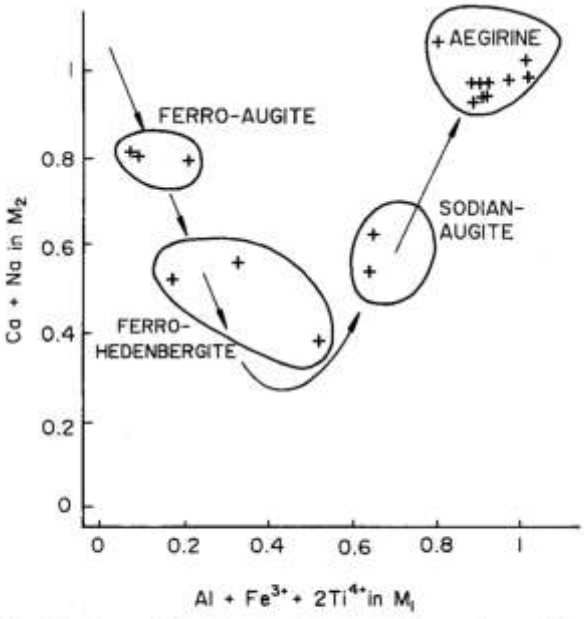

Fig. 56: Compositional range of pyroxene from early metaluminous- to late peralkaline granite in the plot of Ca + Na versus $Al + Fe^{3+} 2Ti^{4+}$. The sharp turn in the evolutionary trend marks the stage where the composition of the host rock became agpaitic.

The different compositional trends towards clinopyroxene in acid metaluminous rocks and sodic pyroxene in peralkaline granites is illustrated in the plot of Ca+Na in the M2-site versus $Al + Fe^{3+} + 2Ti^{4+}$ in the M1-site (after Robinson 1980) (Fig. 56). The data plot along a trend which is controlled by Mg-Fe and Ca-Na substitutions starting with ferro-augite in early subvolcanic rocks. With increasing fractionation hedenbergitic pyroxene is formed which dominates in fayalite porphyries. The sharp turn in the trend towards sodic pyroxene marks a stage where the composition of the host-rock becomes agpaitic. Bonin and Giret (1985) found that in metaluminous series, sodic clinopyroxene follows calcic clinopyroxene in rocks with an agpaitic index 0.85, which correspond with the value of 0.9 for the occurrence of sodic amphibole (Giret *et al.* 1980). At Brandberg sodic clinopyroxene may occur in metaluminous rocks with agpaitic coefficients >0.83 which coincide with the value found by Bonin and Giret (1985). Pyroxene analyses from peralkaline rocks

(agpaitic index >1) plot in the field for Na- and Fe-rich aegirine of endmember composition. The general trend towards more sodic clinopyroxene with increasing fractionation has been described by Neumann (1976) from alkaline rocks of the Oslo region. She concluded that the trend is the result of fractional crystallisation of plagioclase and augite, suggesting that Bowen's (1945) "plagioclase effect" is the most likely mechanism leading from alkaline magmas to peralkaline residual liquids.

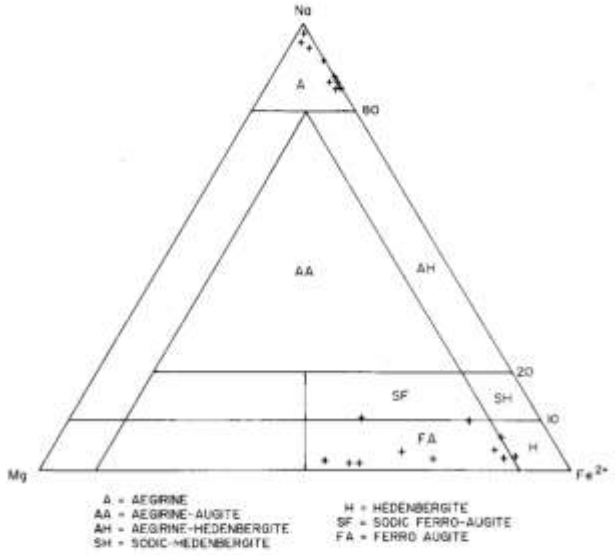

Fig. 57: Compositional trend for pyroxenes from quartz monzonite and alkali/peralkali-granites in the Na-Mg-Fe diagram (in cations per 6 oxygens).

7.2.6 Astrophyllite

The titanium silicate astrophyllite (Fig. 73) is a rare constituent of agpaitic, dominantly Si-undersaturated rocks of the alkali series and commonly occurs in mineral parageneses of alkali feldspar, aegirine, sodalite, cancrinite and apatite (Tröger, 1969). It was first described from Brandberg in a short note by Von Knorring (1985) and generally occurs in zirconium rich, albitised peralkaline granite and associated dyke-rocks (brandbergite) of the Amis Complex together with aegirine, arfvedsonite, zirconium-minerals, pyrochlore and occasionally lepidomelane, as a typical mineral of the pegmatitic-hydrothermal phase (Tröger, 1969). The occurrence of astrophyllite in Brandberg is limited to metasomatites (fenites). Coexisting aegirine occurs as distinct radial arranged rosettes or 'fiamme shaped' aggregates (Figs 72 and 80) indicating a post-magmatic origin. Microprobe analyses reveal that astrophyllite is a mineral with a high holding-capacity for lithophile trace elements like Sn (0.3 per cent), Nb (1 per cent) and Zn (5 per cent) (see appendix, table 2.2).

7.2.7 Pyrochlore

Pyrochlore is the most characteristic Nb/Ta ore-mineral in metasomatic, peralkaline granites and dyke-rocks associated with the Amis Complex (chapter 9). It generally occurs in the same mineral-paragenesis as astrophyllite but is limited to albitised portions in arfvedsonite-aegirine granites. Pyrochlore generally forms yellowish-brown octahedra from 0.1-1 mm in diameter but is often metamict exhibiting a dirty-brown colour (Fig. 58)

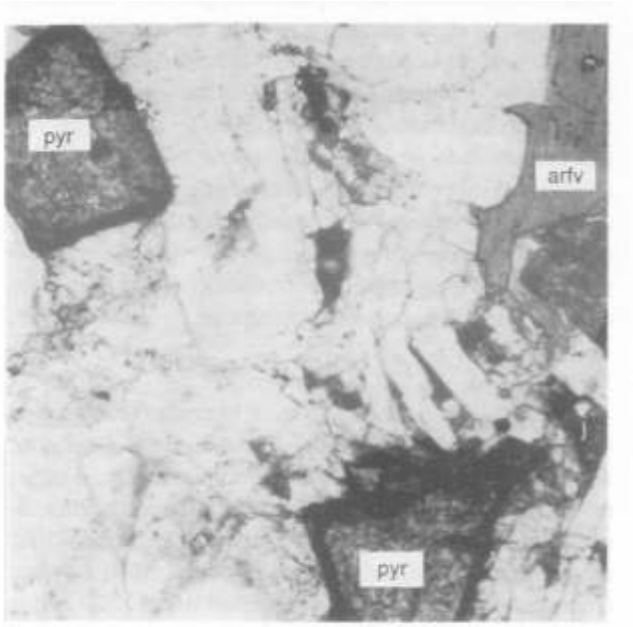

Fig. 58: Octahedra of yellowish pyrochlore (pyr) and arfvedsonite (arfv) in altered peralkaline-granite from the Amis Valley (magnification x 120, PPL).

The mineral is known to be sporadically associated with miaskitic syenites, carbonatites and associated fenites and highly alkalic granites containing sodic amphibole and Na-pyroxene (Parker and Fleischer, 1968; Bowden and Turner, 1974). Partial analysis of pyrochlore from Brandberg (see appendix, table 2.6) shows an average $(Nb,Ta)_2O_5$ content of 51. 78 wt per cent with a relatively low Nb_2O_5/Ta_2O_5 ratio of 13, characteristic for pyrochlore from syenitic fenites (Deans, 1966; Parker and Fleischer, 1968; Hogarth, 1977). The TiO_2 content (7-10 wt per cent) is relatively high compared with data from other localities but compares well with uranian-pyrochlore from Ilomba Hill, Malawi (Deans, 1966) containing 10.10 wt per cent TiO_2. Pyrochlore seems to be the latest crystallisation product in these assemblages of metasomatic origin (Parker and Fleischer, 1968). It is interesting to note that Nb and Ta do not enter the lattice of arfvedsonite or aegirine, which was interpreted by Parker and Fleischer (1968) as an example of the accumulation and late crystallisation of Nb and Ta in pyrochlore. On the other hand, the highly interstitial nature of coexistent astrophyllite with high concentration of Zn, Sn and Nb indicates that astrophyllite has crystallised as one of the latest minerals in the paragenesis when appreciable amounts of lithophile trace elements were concentrated in the fluid-phase.

7.2.8 Amphibole

Amphibole is the dominant mafic constituent in metaluminous and peralkaline granites. Based on petrographic observations, amphiboles from Brandberg granites fall into a calcic and a sodic group. Euhedral hornblende occurs as early phenocrysts in subvolcanic quartz-monzonitic rocks and has often crystallised before feldspar and quartz. In metalumi-

nous granites, the most common rock type in Brandberg, the amphibole consists of euhedral to subhedral greenish-brown hornblende of edenitic composition which has obviously grown at the expense of early clinopyroxene, which occasionally is preserved in the core of edenite crystals. Rims of dark-green to bluish-green, iron-rich amphibole of richteritic composition have often been developed at the expense of hedenbergite or edenitic hornblende in fayalite and quartz porphyries. Interstitial and poikilitic, dark-blue arfvedsonite is the characteristic sodic amphibole of the peralkaline granites and slightly agpaitic (agpaitic index >0.9) rocks and has crystallised later than feldspar and quartz, indicating a non-magmatic origin. Chemical analysis of Fe-rich amphibole is somewhat critical using microprobe analytical methods because the main drawback of this technique lies in the fact that the discrimination of Fe^{2+} and Fe^{3+} is impossible (which is important to calculate the structural formula), especially for sodic-iron rich end members. The different methods of estimating the Fe^{2+}/Fe^{3+} -ratio and calculating the structural formula of amphiboles are discussed in Neumann (1976), Leake (1978) and Robinson *et al.* (1982). The structural formula for arfvedsonite of endmember composition was calculated on the basis of 15.20 cations to obtain a stoichiometric structural formula with full charge balance. For Ca-amphiboles the formula has been calculated on the basis of 22 oxygens to avoid an overestimation of Fe^{3+}.

The chemical composition of amphiboles from Brandberg depends strongly on the chemistry of the host rock. Two distinct compositional trends have been recognised (Figs 59 and 60):

1. A Ca-Al^{IV} -rich (Si-Na-K)-poor trend in persolvus and transolvus granites and quartz monzonites with agpaitic ratios <0.9.

2. A Ca-Al^{IV}-poor and (Si+Na+K)-rich trend in high alkali-granites (Al=0.90-1.00) and peralkaline granites with agpaitic ratios >1.

The existence of calcic- and sodic-calcic- to sodic trends for amphiboles in Si-oversaturated rocks from alkaline ring complexes have been recognised and investigated by Giret *et al.* (1980), Bonin (1982), Ike *et al.* (1985) and Hogarth *et al.* (1987). In early subvolcanic quartz monzonites the composition of calcic amphiboles ranges from ferro-actinolite to ferro-edenite. High Mg-Ca-ferro-actinolites have been apparently developed at the expense of Ca-rich pyroxene and successively became replaced by hornblende of ferro-edenitic composition.

In places where late aegirine-augite is present, ferro-edenite is rimmed by bluish sodic-calcic amphibole. Ferro-edenite from persolvus granites tends to be slightly more enriched in Si due to Na/Al^{IV} - Si substitutions and often occurs together with secondary aggregates of annitic biotite (Bonin, 1982). Hydrothermally altered rocks in the vicinity of ring fractures contain ferro-edenite with characteristic deep-green to bluish rims of richteritic/arfvedsonitic composition with parallel, increasing agpaitic coefficients towards 1.

Sodic amphiboles from peralkaline Brandberg granites have previously been described as "pneumatolytic arfvedsonite" (Cloos and Chudoba, 1931) and as "riebeckite" (Von Knorring, 1985). The optical and chemical results of this study clearly show that most of the blue amphiboles associated with the 'peralkaline facies are in fact fluor-arfvedsonites of endmember composition according to the nomenclature of Leake (1978). With increasing peralkalinity of their host rock, arfvedsonites become more depleted in Ca and

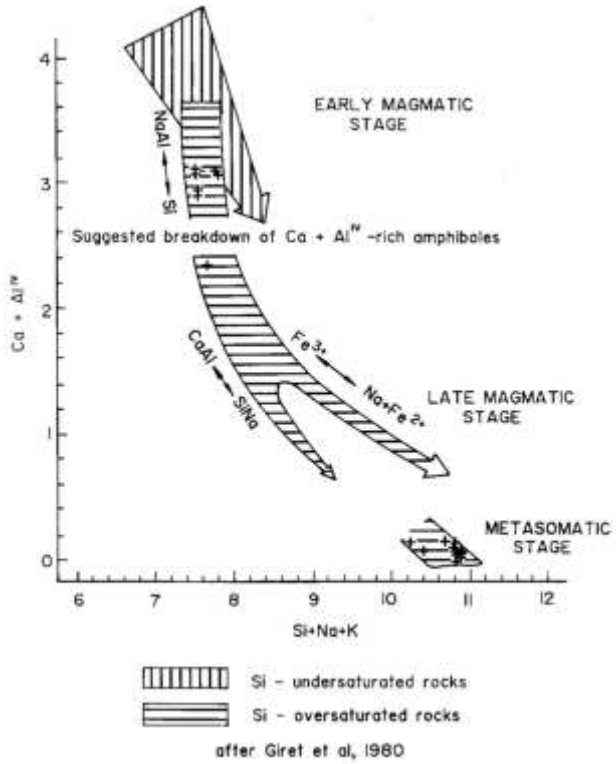

Fig. 59: Compositional trend of amphibole from Brandberg granites in the Ca+Al^{IV} versus Si+Na+K diagram.

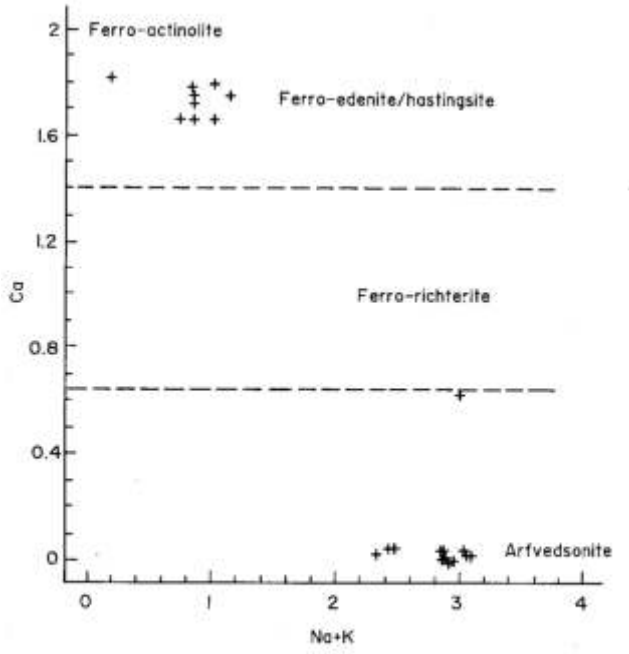

Fig. 60: Compositional trend of amphibole from Brandberg granites in the Ca/(Na+K) diagram.

Al^{IV} and enriched in Si+Na+K and Fe_t, reflecting $Fe^{3+}/(Fe^{3+} + Al^{IV})$ endmember-ratios towards 1 and $Mg/(Mg+Fe^{2+})$-ratios trending towards 0. Parallel with increasing agpaitic coefficients of their host granite, F and Zn have increasingly entered the amphibole lattice, reaching highest concentration in metasomatites (F >3 wt per cent, ZnO >4 wt per cent).

The $Ca+Al^{IV}/Si+Na+K$ diagram (Fig. 59) has been widely used to illustrate chemical variation trends for the amphibole group (Giret *et al.* 1980; Bonin, 1982).

The group of calcic amphiboles of the ferro-actinolite-ferro-edenite series is characterised by $Ca+Al^{IV}$ -contents >2.5 and Si+Na+K contents <8 whereas sodic-calcic- and sodic amphiboles show values <2.5 and >8 respectively. The gap existing between the two groups has been interpreted to represent the critical stage when the agpaitic coefficient of the host rock trends towards I, causing the breakdown of calcic amphibole in high alkaline/peralkaline environments (Giret *et al.* 1980). These authors therefore argue for the existence of two solid solution series where the first, Si-poor group (Si=6.00-7 .01) is suggested to represent the magmatic range of amphibole composition in non-agpaitic rocks. The second, Si-rich group (Si=6.76-8.00) covering the series of sodic amphiboles is believed to have crystallised during late-magmatic or subsolidus-stages and therefore is not strictly magmatic in origin (Giret *et al.* 1980). Arfvedsonites from the Amis Complex are believed to have crystallised in the subsolidus under the influence of a fluid-phase, rich in trace elements and fluorine. According to the international nomenclature scheme (Rock and Leake, 1984), sodic amphibole from Brandberg is zincian fluor-arfvedsonite paragenetically related with stanniferous aegirine and astrophyllite, rich in lithophile trace elements. Textural characteristics like the highly interstitial to poikilitic nature of arfvedsonite strongly point to a hydrothermal origin for these assemblages. Similar post-magmatic occurrences are reported from Nigerian arfvedsonite-aegirine granites (Bennett *et al.* 1984; Ike *et al.* 1985).

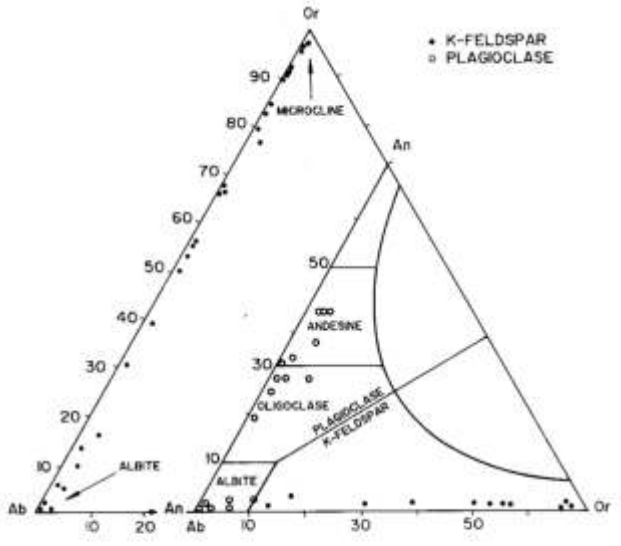

Fig. 61: Compositional range of feldspars in Brandberg granitoids in the Or-Ab-An and An-Ab-Or - diagram.

7.2.9 Feldspar

The compositional trend of feldspar in Brandberg granitoids ranges from plagioclase and alkali feldspar in subvolcanic rocks, towards endmember albite or microcline in subsolidus altered granitoids (Fig. 61). Resorbed, highly embayed plagioclase phenocrysts from the Naib and Gomatsarab quartz monzonites are commonly zoned. The cores of the crystals consist of andesine (Ab_{53-58} An_{36-43}) or oligoclase-andesine (Ab_{66-68} An_{30-31}) with rims of oligoclase (Ab_{69-72} An_{28-29}). In quartz monzonites, K-exchanged oligoclase-andesines are not uncommon, with potassium contents up to 4 per cent and increasing FeO concentrations. In metaluminous hornblende-bearing granites and fayalite granites, the plagioclases are characterised by an anorthite-rich core enveloped by an irregular zone of antiperthite-perthite which is occasionally overgrown by orthoclase to orthoclase-microperthite. Subsolidus exsolution in transolvus granites has produced perthites and microcline-microperthites in the compositional range Or_{56} - Or_{90}. Turbid microcline with tartan twinning (Or_{85-90}), which occurs in potash altered, metaluminous hornblende granites, successively grades into slightly reddish micro cline (Or_{91-97}) when the agpaitic coefficient of the host trends towards one.

Subsolidus granites typically contain two feldspars which have crystallised under ordered conditions. Tartan twinned microcline (Or_{83-92}) and late albite (Ab_{90-98}) occurs together with Li-mica, fluorspar and occasionally topaz, replacing feldspar in peraluminous granites. In peralkaline types, microcline-perthite and microcline are partly replaced by Na-albite (Na_2O >10 wt per cent, Ab_{92-99} in albitites).

K-exchanged, flesh- to deep-red feldspars associated with the deposition of sphalerite, cassiterite and fluorspar dominantly occur along prominent alteration zones of "reddened wallrock".

Representative analysis of feldspar from a sphalerite mineralised vein in basement granite is given in table 2.5 (1-4) of the appendix. Red, turbid and typically untwined maximum-microcline from the central portion of the vein shows Or-contents >Or_{98}. Less K-exchanged, turbid microcline-microperthite (Or_{56-62}) envelopes the reddened zone.

The entire compositional range of feldspar from Brandberg granitoids (Fig. 61) indicates that early subvolcanic rocks contain plagioclase and alkali feldspar which, in hydrothermally altered granite, are either Na- or K-exchanged. Depending on the intensity, composition and duration of subsolidus rock-fluid interaction processes the feldspars trend towards endmember composition.

A selection of feldspar analyses from various rock types is given in the appendix (table 2.5).

8. Hydrothermal alteration and style of mineralisation

8.1 Introduction

Tischendorf (1977) and Stemprok and Sulcek (1969) have shown that post-magmatic alteration processes associated with specialised granitic intrusions have only affected plutons that have crystallised and fractured and that alteration and deposition of ore minerals is caused by silicate melts and aqueous fluids enriched in Na, K, Li, B, Fe, H, F, and Cl. Terms like greisenisation, silification, chloritisation, fluoritisation etc. have been used to describe these processes. Alteration processes associated with alkaline anorogenic granites are known to occur in many alkaline provinces in the world. Mineralising processes which led to the deposition of economic important ore deposits of the Nigerian type, have been poorly understood in the past (Taylor 1979). More recently, Bowden and Kinnaird (1984) and Kinnaird *et al.* (1985a) showed that alteration and ore deposition in alkaline granites of the Nigerian Alkaline Province are late- to post-magmatic in origin. Based on some characteristic mineralogical and chemical changes which originated during hydrothermal rock-fluid interaction processes, they classified sodic metasomatism, potassic metasomatism, acid metasomatism, silica metasomatism and argillic alteration. In the Russian literature terms like albitisation and microclinisation have been used to describe Na for K and K for Na exchange processes (Shcherba, 1970; Korzhinskii, 1970). The alteration sequence model proposed by Smirnov (1976) illustrates that albitisation, microclinisation and greisenisation occur together and are sequentially emplaced in and around a rare-metal specialised intrusion.

Metasomatic processes associated with Brandberg granites, with a few exceptions, are similar to those reported from Nigerian ring complexes by Bowden and Kinnaird (1984a), Kinnaird (1984) and Kinnaird *et al.* (1985a). A sequence of post-magmatic fluid-rock interaction processes under subsolidus conditions is believed to be responsible for the change of the primary chemical and mineralogical composition of the granites.

8.2 Sodic metasomatism

Na for K exchange processes which led to the development of albite and associated sub solidus mineral assemblages have predominantly affected arfvedsonite-aegirine granite, biotite granite and to a lesser extent, subsolvus hornblende-biotite granites. Sodic metasomatised, peraluminous rocks are cream or light coloured, rich in albite, with dominantly porphyritic, saccharoidal textures and occur as irregular bodies in the cupola zone of the biotite granites or as lenticular, sheeted or layered bodies and ring-shaped dykes. Irregular masses of albitised biotite granite are found in the Hungurob Mulde, the Bushman Valley area, north of the Wasserfallfläche and south of Königstein. Lenticular and ring-shaped albite-rich zones and dykes occur in the lower Hungurob Ravine, southwest of the Horn and along the contact between the first and second ring of hornblende granite towards the northwest of the massif (Fig. 3). Microscopic studies and microprobe analyses of alkali feldspar, plagioclase, pyroxene, amphibole and mica comprise distinctive mineralogical, optical and prominent chemical changes during Na-metasomatism (chapter 7.2) similar to those described by (Kinnaird, 1985; Kinnaird *et al.*, 1985, 1985a; Charoy, 1982; Rose and Burt, 1979; Tischendorf 1977).

Depending on the alkalinity, different mineral assemblages and chemical trends have developed during Na for K exchange processes. Feldspars show the most drastic changes. With initial Na-metasomatism, the exchange of K-ions by Na-ions in primary perthites and microcline-perthites from biotite granites led to the development of patch perthite which progressively became replaced by chessboard albite. With increasing rock-fluid interaction most of the former alkali feldspar is replaced by ordered albite (Ab_{90-99}). During feldspar alteration the original medium-grained, grey biotite granite has been changed to a leucocratic, fine-grained albite-rich granite. Apical parts and cupola zones of biotite granite in the central part of the Brandberg Complex, and ring dykes along the contact of the hornblende granites are locally converted into albite-rich biotite granite or saccharoidal albitites.

The process of albitisation is less intense in hornblende bearing granites of the outer zone of the Brandberg Complex. These granites often comprise granophyric or myrmekitic textures. Perthite locally is replaced by chessboard albite or occasionally by small grains of ordered albite. Simultaneously with feldspar the composition of mica has been changed during sodic metasomatism. Dark-brown to red, strongly pleochroic biotite of annitic composition firstly interacts with the fluids by forming a pale-green reaction rim. With increasing metasomatism the former Ti/Mg-rich biotite is replaced by yellowish-green siderophyllite. In albitised biotite granites of the cupola, siderophyllite occasionally is rimmed by colourless zinnwaldite (Fig. 19). In contrast to albitised biotite granites from Nigeria (Kinnaird *et al.* 1985) no columbite is found in similar Brandberg rocks and cassiterite is the only rare ore mineral which may be present beside monazite, zircon and xenotime.

The process of albitisation of hornblende granites and biotite granites seems to be limited to cupola zones, which have obviously acted as trap for the fluids and along steeply dipping contacts between the different granite intrusions or along other pre-existing channel ways like ring dykes. Albitisation never reaches an advanced stage in hornblende bearing granites but slight Na-metasomatism may occur disseminated or patchily.

The peralkaline arfvedsonite-aegirine granites of the Amis Complex (chapter 9) comprise the most effective subsolidus changes during Na-metasomatism. Textural variations produced by the albitisation process range from porphyritic to equigranular saccharoidal with the typical "snowball" texture (Fig. 62).

In both provinces the process of sodic metasomatism produced light coloured, saccharoidal arfvedsonite albitites. Originally perthitic feldspar and microcline have been converted to albite, which forms small laths that surround or enclose quartz and microcline, or microcline-perthite (Fig.

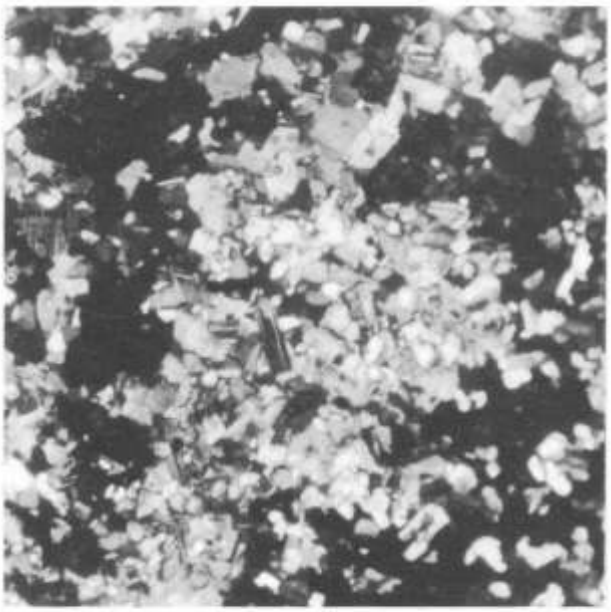

Fig. 62: Photomicrograph of albitised peralkaline granite with "snowball texture", Amis Complex (magnification x 41, XPL); description in text).

62). Arlvedsonite and aegirine are highly interstitial or poikilitic indicating late-stage crystallisation. At lower temperatures and increasing alkalinity arlvedsonite is progressively replaced by dark green aegirine. Depending on temporary changes in the peralkalinity of the fluids the process has occasionally been reversed. Microprobe analyses of sodic amphibole and aegirine (see appendix, table 2.3 and 2.4) reveal that extremely peralkaline metasomatising fluids were infiltrated at the bottom of the Amis Com-plex and penetrated through the overlaying network of alkali feldspar, quartz and late albite. During crystallisation of the sodic mineral assemblages the elevated levels of rare metals in the fluids led to some remarkable substitutions in arlvedsonite, astrophyllite and aegirine. Dark blue arfvedsonite has substituted appreciable amounts of Zn in the lattice (2.5-4.4 wt per cent ZnO), astrophyllite contains 0.21 wt per cent SnO_2, 5.10 wt per cent Zno and 0.89 wt per cent Nb_2O_5, and even late-stage aegirine holds up to 0.50 wt per cent SnO_2 in the lattice. The Na- silicate minerals are accompanied by dispersed, Nb-rich pyrochlore, zircon, monazite, yttrio- fluorite and cryolite, reflecting the high level of trace elements introduced by sodic alteration processes. The development of secondary, annitic biotite replacing arlvedsonite under subsolidus conditions is limited to late peralkaline dykes (brandbergites). Ernst (1962) has shown that at low temperatures arlvedsonite coexists with annite which is more stable than ferrous amphibole end-members. During cooling to lower temperatures arlvedsonite-riebeckite may react with perthite to form annite/stil-pnomelane under subsolidus conditions as proposed by Wones and Gilbert (1982).

Depending on the alkalinity and mineralogical composition of the original granite the process of sodic metasomatism has transformed peraluminous biotite granite into siderophyllite/ zinnwaldite - albite - quartz - microcline perthite rocks and in peralkaline environments has produced arlvedsonite - aegirine - albite - quartz - microcline assemblages with pyrochlore. Based on their study of Nigerian A -type granites, Bowden and Kinnaird (1984) classified the two contrasting styles, according to the associated mineralisation, into a columbite and pyrochlore type. Smirnov (1976) subdivided albite-rich mineral assemblages produced by sodic alteration processes of alkaline granite into biotite -quartz - albite - microcline types and aegirine - albite - quartz - microcline assemblages with zircon, monazite and yttrium minerals. Both types of Smirnov (1976) are present at Brandberg.

Geochemically, the process of sodic metasomatism is characterised by an increase in the major oxides, Na and Fe, combined with a decrease in K (chapter 7). Trace elements like Rb, Nb, Hf, Th, Zr, Zn and Sn display enrichment trends, especially in peralkaline granite. Peraluminous granites affected by sodic alteration generally show the same trace element variation with the main difference that Zn and Y follow a depletion trend in the subsolidus biotite granites (Fig. 44) indicating the important role of the peralkaline phase in leaching and concentrating Zn.

8.3 Potassic metasomatism

The process of potassic metasomatism or microclinisation is recorded from a number of important tin deposits in Cornwall, Bohemia, China and Nigeria. In the Nigerian type of tin deposit, potash alteration is characterised by partial to complete replacement of sodium by potassium in the feldspars of the biotite granites, the development of intermediate to maximum microcline, growth of annitic biotite and siderophyllite and chloritisation of the original mica and occurs as wallrock alteration along fractures, as pockets or below the volcanic cover (Bowden and Kinnaird 1984). In the Brandberg Complex, the K for Na exchange processes play the most significant role and can be recognised in the field by more or less intense reddening of the feldspars depending on the duration and intensity of fluid-rock interaction. The reddening of alkali feldspars during microclinisation processes can be explained by the release of iron during metasomatism to form haematite giving these assemblages its colour ("reddened wall rock" ; Bowden and Jones 1978). K for Na exchange processes have mainly affected biotite granite and country rock and to a lesser extent hornblende bearing varieties and peralkaline granites. The most characteristic feature of potassium metasomatised granite is the generation of ordered, red microcline. In their study of the Ririwai Complex in Nigeria, Kinnaird *et al.* (1985) showed that the new generated feldspar is more fully ordered, lacking the typical cross-hatch twinning and compositionally range from ordered to maximum microcline. Potassium metasomatism in Brandberg is selectively pervasive in peraluminous biotite granites. Plagioclase phenocrysts and groundmass plagioclases are replaced by turbid, red microcline and annitic biotite which is destabilised to green siderophyllite and magnetite. In some of the biotite granites the process continued to a more advanced stage where the rest-biotite is completely replaced by siderophyllite or chlorite and the feldspars have broken down to topaz

Fig. 63: Photomicrograph of zoned allanite (al), cassiterite (cass), quartz (qz) and alkali feldspar (kfsp) in potash altered biotite granite, Wasserfallfläche (magnification x 41, XPL).

Fig. 64: Reddened wallrock of maximum microcline (mic) bordering an alteration vein (v) in basement granite, Gomatsarab.

- Li mica - sericite assemblages, occasionally with epidote.

In hornblende granites ferroedenite has broken down to magnetite together with secondary zircon. In transolvus granite containing biotite and edenite, Ti/Mg-rich biotite is randomly replaced by annite-siderophyllite. Chevkinite, monazite and fluorite are common accessories. Both subfacies show a characteristic pinkish-red colour and are medium to fine grained. The wide variability of their texture and mineralogical composition reflects the intensity of subsolidus alteration processes and the consequent destruction of primary mineral assemblages.

Microclinisation processes have also affected granite porphyries which often are deep flesh red in colour. Phenocryst and groundmass feldspars consist of intensely haematised intermediate to ordered microcline.

Fine disseminated cassiterite and zoned allanite (Fig. 63) have occasionally been found in flesh-red, miarolic portions in the roof-zone of biotite granite but often the oxide ore-minerals were generated during later H^+-metasomatism which affected already altered granite.

Red coloured microcline assemblages bordering veins are widespread in potash altered environments and often playa significant role in the deposition of economically important oxide/sulphide ores in lodes (e.g. Ririwai lode, Nigeria; Kinnaird *et al.*, 1985). Vein and fissure controlled metasomatic processes have been recognised in biotite granite and country rock composed of Pan African, post-tectonic two-mica granite. Alteration zones are easily recognised by conspicuous brick-red microcline-zones (Fig. 64) along fractures or bordering a central quartz stringer.

Highly alkaline, potassium-rich aqueous solutions which migrated along fissures led to drastic changes in the chemical composition of feldspar in the Pan African granite. Microprobe analyses of feldspars from red alteration halos indicate apparent losses of sodium and significant increases in potassium. Former albites and perthites are transferred to microcline micro-perthite and microcline of endmember composition (Or_{98}). The intense reddening and loss of the typical twinning is due to micro-haematisation processes during metasomatism. Oxide/sulphide ore assemblages which occasionally occur together with microclinisation processes are believed to be associated with later H^+-metasomatism, silicification- and chloritisation processes which are superimposed on already microclinised rock.

Geochemical changes during potassium metasomatism are characterised by an increase in K combined with decreasing values for Na and most of the trace elements. Rb, Sn and Zn follow an enrichment trend during potassic alteration processes.

8.4 H^+-metasomatism (greisenisation)

Stemprok (1987) and Taylor (1979) have concluded that greisenisation is the most common metasomatic process accompanying tin and rare-metal specialised granitoids. In the past the term greisen has been used in many different senses to describe the decomposition of feldspar and mica and the formation of new micaceous mineral assemblages. Stemprok (1987) and Janecka and Stemprok (1967) defined the term greisenisation as a granite related, post-magmatic metasomatic process in the course of which biotite and feldspars became unstable to form quartz, mica, topaz assemblages accompanied by the deposition of ore minerals. Depending on the composition of the original rock type

and the chemical composition of the greisenising fluids the final mineral parageneses may differ. Greisenisation is known to be genetically linked with other metasomatic processes like silicification, tourmalinisation, fluoritisation, sericitisation and chloritisation (Taylor 1979; Stemprok 1987). The most important greisen-type tin deposits associated with alkaline granites of the intra-plate type occur in Nigeria (Taylor 1979). More recently Bowden and Jones (1978), Kinnaird (1984, 1985) and Kinnaird *et al.* (1985a) concluded that complex metasomatic processes, similar to those know from S- and I -type granite-related deposits, are responsible for the deposition of oxides and sulphides. Greisen-type alterations in Brandberg predominantly occur pervasively as irregular zones in the cupola of potash/sodic metasomatised granite and as fracture and fissure controlled alterations. Mineral assemblages produced during greisenisation processes are extremely complex depending on the intensity and duration of auto-metasomatic rock-fluid interaction and the mineralogical and chemical rock composition. Acid metasomatism is dominantly superimposed on earlier potash/sodic metasomatised biotite granites. In microclinised/albitised, porphyritic perthite granite the mineral assemblages are comparable with those reported from Nigerian equivalents (Kinnaird, 1984, 1985 and Kinnaird *et al.* 1985). Perthitic feldspars and plagioclase are partly replaced by micaceous aggregates of yellowish green Li-siderophyllite/protolithionite or occasionally by colourless zinnwaldite together with rounded topaz and minor fluorite. Deposition of fine grained disseminated cassiterite occurs sporadically in irregular zones associated with chloritised, micaceous aggregates which have been generated when the process continued to lower temperatures: If the process of H^+-metasomatism has affected granophyric or graphic intergrown, microclinised alkali granite the feldspar components have broken down to Li-siderophyllite/chlorite aggregates accompanied by the deposition of cassiterite which occasionally replaces the mica (Fig. 65). Greisenisation superimposed on quartz-microcline assemblages, which originated during early potash metasomatism in cupola zones of biotite granite, has produced quartz - Li-siderophyllite - feldspar assemblages with minor fluorite, topaz and cassiterite.

Vein controlled mineralisation produced by a combination of potash and H^+-metasomatism is best developed in altered country rock along the north-eastern contact of the complex. The fracture systems trend north-northeast and consist of a series of parallel quartz and greisen veins set in up to 10m wide zones of altered, greenish-grey, late Precambrian two-mica granite, separated by zones of reddened microcline wallrock.

The composite greisen-type quartz veins carry abundant sphalerite with minor cassiterite accompanied by micaceous zones of chlorite, siderite, quartz, epidote and occasionally topaz (Fig. 66). The granitic country rock adjacent to greisen veins shows a rapid transition from fresh muscovite - biotite - perthite granite through pinkish grey mica - sericite granite, continuously grading into a red microcline -chlorite rock with quartz-mica greisen (Fig. 67). Greisenisation processes are generally superimposed on early potash altered fracture zones along which the original feldspars has been broken down to red microcline (Fig. 67). Microprobe analyses of feldspar indicate that albite and

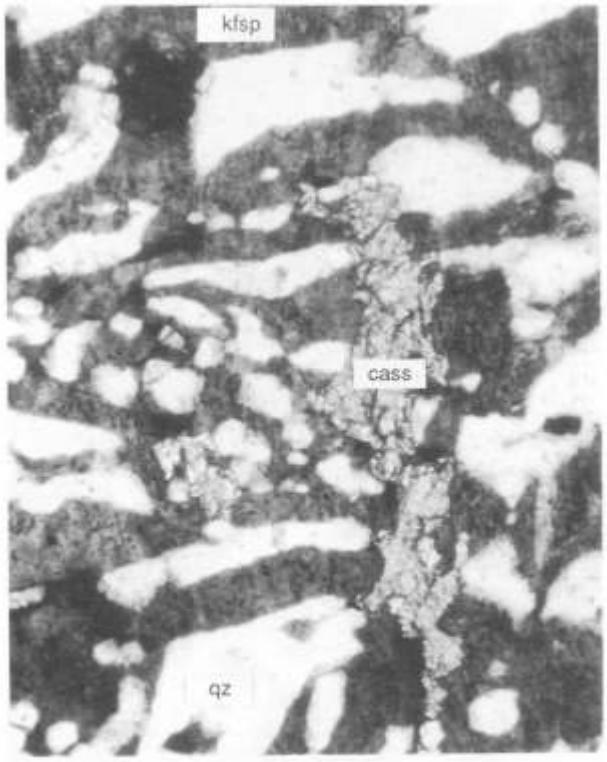

Fig. 65: Photomicrograph of late cassiterite (cass) having replaced biotite in graphic granite (qz and kfsp). Greisenised leuco-granite, Katarakt/Hungurob Ravine (magnification x 41, XPL).

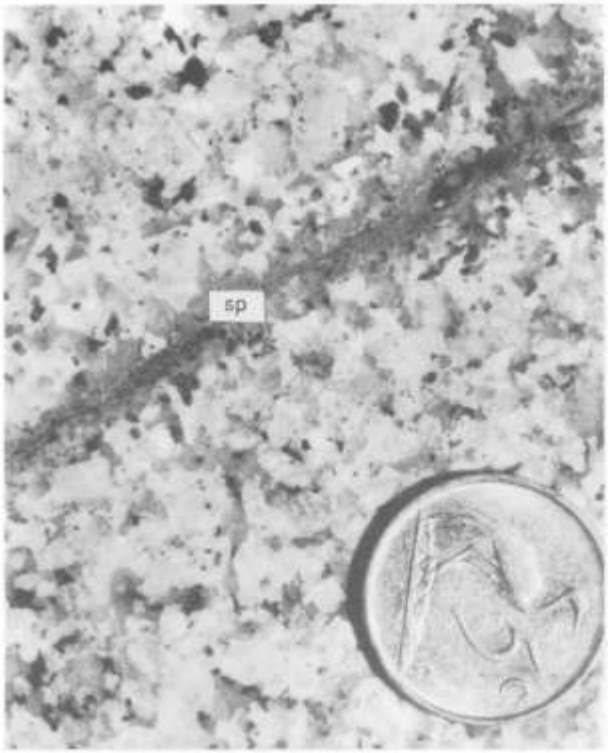

Fig. 66: Sphalerite vein (sp) in Pan African granite, produced by a combination of microclinisation and greisenisation processes, north of the Schaf Ravine.

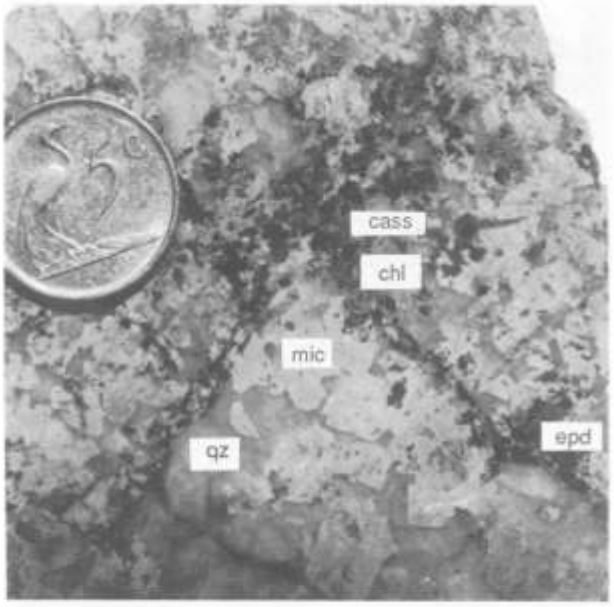

Fig. 67: Microclinised and greisenised granite consisting of quartz (qz), microcline (mic), chlorite (chl), epidote (epd) and fine disseminated cassiterite (cass).

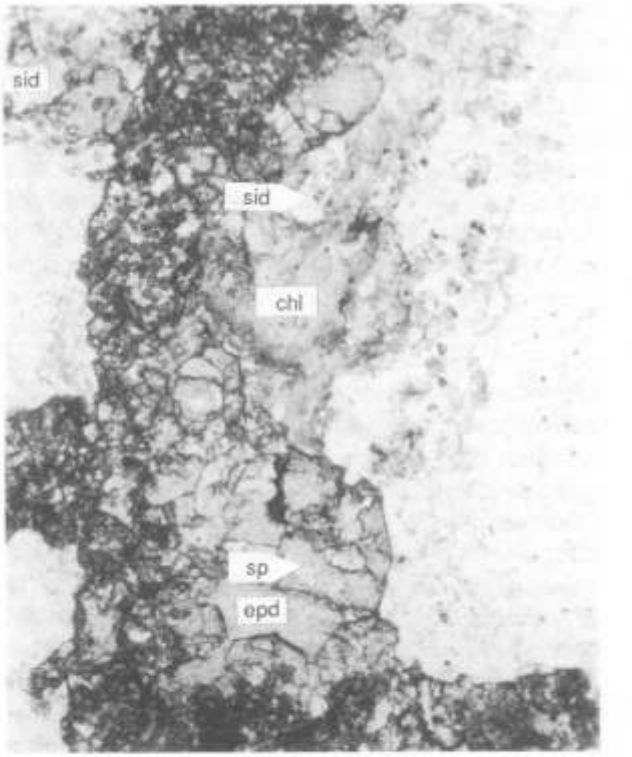

Fig. 68: Photomicrograph showing the central area of a sphalerite mineralised alteration vein in country rock. Sphalerite (sp), chlorite (chl) and epidote (epd) are cemented in siderite (sid), (magnification x 120, PPL).

perthite from fresh Pan African granite were subsequently transformed into microcline-microperthite and microcline. Deep red, turbid microclines adjacent to greisen veins are of endmember composition (Or_{98}).

This early process was accompanied by the deposition of zircon, allanite, monazite and cassiterite. With initial greisenisation, feldspars were decomposed to micaceous aggregates of possibly Li-siderophyllite and minor topaz. The dominant ore mineral which generated at this late stage consists of pale brown sphalerite cemented in abundant siderite which is concentrated in the central part of the vein (Fig. 68).

When the process of chloritisation continued to lower temperatures it is accompanied by the deposition of epidote.

Geochemically, the process of greisenisation is complex and very variable depending on the composition of the primary rock type and earlier metasomatic processes. In Brandberg, greisen-type alteration is generally superimposed on earlier potassium metasomatised granites and obviously the potash trace element pattern is reflected. Greisenisation is accompanied by an increase in Fe and Si and the decrease of Al caused by the breakdown of the feldspar minerals to mica. The trace element variation displays a general increase in Rb, Y, Zn, Sn, Th, W, Ta and Li, indicated by the development of lithionite/zinnwaldite mica, and depletion in Ba and Sr (chapter 7) which is indicated by the shift of altered samples, away from the magmatic trend (Figs 42, 43, 47 and 48).

8.5 Boron metasomatism (tourmalinisation)

Individual tin provinces are known to be enriched in boron or fluorine or both (Pollard *et al.* 1987) which may result in the formation of tourmaline-rich, leucocratic rocks. In Namibia, tourmaline-rich igneous rocks are predominantly associated with Pan African granites and pegmatites but occurrences of tourmaline nests or spots are reported from Erongo (Fig. 1), a Mesozoic ring complex 120 km SE of Brandberg (Gevers and Frommurze, 1929). Boron metasomatic processes in the Brandberg occur as tourmaline-rich nodules and spots in leucocratic biotite granite, as vein- and fracture controlled alteration zones in potash altered granite and in the kinas of the complex (killas=altered hornfelsic sediments in the contact with a granite intrusion).

Tourmaline nodules are known from many boron-rich granitic environments and essentially consist of quartz and bluish-green schorl replacing potassium feldspar (Nemec 1975). Roundish quartz-tourmaline segregations which are commonly rimmed by a light coloured halo, occur in the roof zone of a ring shaped sheet of albitised biotite granite in the Hungurob Ravine (Fig. 20). Essentially they consist of bluish-green, pleochroic schorl having replaced all mafic minerals and partly replacing potassium feldspar together with small laths of albite, quartz and accessory fluorite, monazite and zircon. Tourmaline most commonly displays variable pleochroic colour zonation. Yellowish-green cores usually grade into bluish outer zones and rims. The light colored halos around the tourmaline aggregates correspond to the mineralogical composition of the host granite but lack the mafic components. Along the transitional zone between granite and the halo, annitic biotite has broken down to colourless or slightly yellowish siderophyllite/zinnwaldite.

Despite the uncertainties concerning the origin of tourmaline segregations in aplogranites, tourmaline is thought to be either an integral part of the magmatic rock or of metasomatic origin (Taylor, 1979). In their study of tin liquidating glasses

in the $CaO\text{-}B_2O_3\text{-}2SiO_2$ system, Durasova and Barsukov (1973) however proved the presence of an immiscible boron-rich phase. To some extent their results can explain the possibility for tin and boron to be extracted from silicate melts by liquidation processes. On the other hand, tourmaline replacement units are believed to be a result of complex metasomatic processes. In his study of tourmaline spots in leucocratic granites, Nemec (1975) came to the conclusion that boron-rich fluids were introduced into the host rock and tourmaline grew at the expense of biotite and feldspar. The necessary concentration of iron needed for the precipitation of tourmaline was leached from the mafic minerals causing the breakdown of biotite, which produced the distinctive light coloured halos around the tourmaline spots (Nemec, 1975). The conversion of primary annitic biotite to siderophyllite along the outer margin of the halos possibly originated by the release of potassium during growth of schorl at the expense of alkali feldspar. Potash and sodic metasomatic processes generally seem to be genetically related with tourmalinisation. Isolated quartz-tourmaline segregations preferably occur in the roof facies of leucocratic, sodium-rich granites whereas in potassium altered environments, tourmalinisation is more of a pervasive nature forming stock- or dyke-like replacement units. Tourmaline typically forms radial arranged rosette-like aggregates in quartz-alkali feldspar rocks (Figs 21 and 22) similar to luxullianite. At the type locality, luxullianite is interpreted as a combined product of potash and boron metasomatism (Lister, 1978). Allman-Ward (1985) pointed out that at St. Austell, SW England, boron-rich aqueous fluids were channelled upwards along fractures located to one side of the granite cupola. He speculated that boron and silica-rich aqueous fluids separated at depth from a residual magma. Fluid over pressure fractured the already consolidated granite carapace to allow the distribution of the tourmalinising fluids. The mechanical energy produced by boron metasomatism seems to be an important control factor for the structural evolution (Pollard *et al.* 1987). Whether boron is a primary constituent of the magma or has been leached by aqueous fluids from boron-rich, exhalative Damaran metasediments (tourmalinites) or tourmaline-rich, orogenic granites is unclear. Leaching experiments of Hochstein and McKee (1986) showed that some boron can be leached from sediments at temperatures as low as 50°C and might have been released before any hydrothermal alteration occurred.

The tourmalinised killas of Karoo sediments were first recognised by Cloos and Chudoba (1931) and described as "kontakt pneumatolytisch" locally tourmaline bearing hornfelses and conglomerates. Rocks of the contact aureole consist of pelitic and quartzo-feldspathic andalusite hornfelses, quartz-pyrophyllite bearing pelites, epidotised and granitised volcanics and tourmalinised quartz-conglomerate. Metasomatic changes are most intense in the conglomerate horizon. Quartz has recrystallised as a granoblastic mosaic whereas the former matrix and feldspar-components are replaced by fine grained aggregates of colourless mica, topaz and quartz (Fig. 69).

Primary biotite in more arkosic varieties has broken down to yellowish protolithionite or chlorite. Bluish, strongly pleochroic tourmaline replaces mica or relict feldspar giving the rock a blasto-porphyritic texture. Frequently the conglomerate contains perfectly rounded, black pebbles of a tourmaline-rich metasediment. Stratabound tourmalinites are reported from the Damaran, which is known to be a boron-rich province (Badenhorst, 1989). The nearest outcrop of tourmalinite occurs at Uis, 30 km E of Brandberg (Diehl, 1986). In contrast to the yellowish-brown, unzoned tourmaline from the pebbles, tourmaline which originated from boron-rich fluids channelled out of the granite into conglomerates and gritstones is blue in colour. Along the outer rim of the tourmalinite pebbles the yellowish-brown tourmaline is overgrown by a later, blue variety.

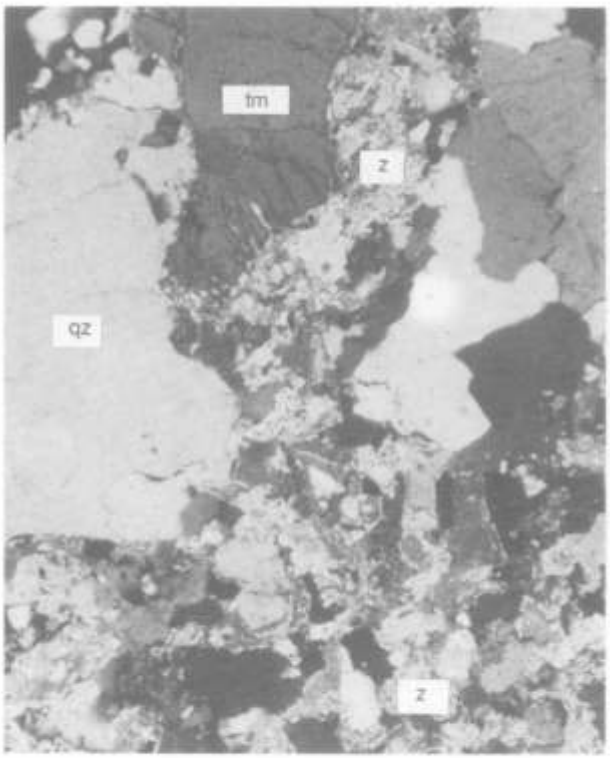

Fig. 69: Photomicrograph of tourmalinised conglomerate, Amis Complex showing zinnwalditic mica (z) together with granoblastic quartz (qz) and interstitially crystallised tourmaline (tm), (magnification x 41, XPL).

Boron metasomatism of Karoo sediments is most intense in the vicinity of the Amis Complex forming a tourmaline-rich aureole around peralkaline granite indicating a loss of the boron-rich phase associated with the intrusion. Boron-rich, aqueous fluids presumably have been released during an early stage in the history of the Amis Complex. In the complex itself tourmaline nodules only occur in a horizon of peraluminous biotite granite below the roof zone where boron has obviously been trapped in a more rapidly cooling unit (chapter 9).

London *et al.* (1988) showed that early vesiculation of aqueous fluids in a peraluminous system would remove boron. They concluded that the loss of boron would lead to higher liquidus and solidus temperatures decreasing water solubility and larger crystal-liquid partition coefficients resulting in an early precipitation of trace element bearing

phases (London *et al.* 1988) which should be interpreted as late- or post-magmatic.

Tourmaline is not a mineral of the peralkaline granite series of the complex but the occurrence of arfvedsonite-albite-fluorite nodules (lindinosite) indicates that genetically similar metasomatic segregation processes took place in peralkaline environments (chapter 9).

8.6 Pyrophyllite alteration

Pyrophyllite bearing, altered silt- and mudstones occur as irregular zones which envelope the tourmalinised sediments around the Amis Complex. The alteration often has produced lense-like patches or a mosaic of light coloured, angular zones in deep reddish-brown Karoo pelites which in places easily could be mistaken for brecciation (Fig. 70). The attractive rock has found use as an ornamental stone ("Brandberg pyrophyllite") and locally is mined on a small scale. Microscopically, the altered sediments consist of quartz and fine grained, granular, occasionally radiating, fibrous crystals of pyrophyllite (determined by XRD), haematite and accessory tourmaline and zircon. The light and dark areas only differ in the proportion of haematite and pyrophyllite indicating that iron has been remobilised and removed from the light coloured alteration zones.

Zaykoy *et al.* (1988) have pointed out that the formation of pyrophyllite during metasomatism is a regular process in an acid media at 300-450°C with a SiO_2:Al_2O_3-ratio >2.36. Since pyrophyllite alteration of Karoo pelites is limited to an area around the Amis Complex, a metasomatic origin of the quartz-pyrophyllite rocks can be assumed.

Fig. 70: Pyrophyllite bearing alteration zones (light coloured) in silt- and mudstones, south of the Amis Valley.

8.7 Silification

Late-stage release of silica which led to the deposition of quartz in veins and veinlets or as fillings in vuggy microclinised cupola granite (Fig. 18) occurs dominantly in deuterically altered granites of the complex and in adjacent Pan African granite. The generation of quartz-veinlets and stringers often accompanies or follows hydrothermal alteration processes occasionally producing vein-controlled oxide/sulphide ore assemblages dominated by pale brown sphalerite. Pervasive silification in microclinised granite is sporadically accompanied by the deposition of fine disseminated cassiterite.

Low temperature deposition of silica in the form of chalcedony is dominantly associated with fossil hot spring systems which occur along ring fractures and contacts of the individual ring-intrusions. Beside the known occurrence in the Numas Ravine (Pirajno, 1987), deposition of chalcedonic-jasperoidal material and argillic altered, hydrothermal breccia zones and dykes associated with fossil hot springs occurs in the Katarakt/upper Hungurob Ravine area and in the Basswaldrinne. All occurrences can be related to a late ring fracture along the contact between ferroedenite-augite and ferroedenite-biotite granite in the southern part of the complex.

9. The Amis Layered Complex

9.1 Geology

In the south-western periphery of the Brandberg Complex a predominantly agpaitic satellite intrusion has concordantly intruded into sediments, volcanics and breccia and post-dates the metaluminous and peraluminous intrusions of the main massif (Fig. 3).

The intrusion covers an area of 5 km^2 with a maximum thickness of ~350 m and dips 8-10° northeast, plunging 10-22° towards northwest, more or less corresponding to bedding and stratification of the sediments and volcanics. The occurrence of layered granite and "pneumatolytic" changes in arfvedsonite granite and country rock from the Amis Valley previously has been recognised by Cloos and Chudoba (1931). Silica oversaturated, agpaitic granites with well developed mineral layering occur as cyclic units of aegirine granite, aegirine-arfvedsonite granite and arfvedsonite granite, repeated rythmically in this order (Fig. 71). The top of each unit is composed of hornblende and/or biotite bearing granite. Certain types of mineral layers recur in specific cycles. Therefore, the Amis layered series can be subdivided into three cyclic units of mineral stratified, peralkaline granites overlain by alkaline horn-blende/biotite granites (Fig. 71). The base of a unit consists of aegirine-albite granite followed by a thin, zircon-rich layer overlain by aegirine-arfvedsonite granite.

The deuterically altered aegirine granite is characterised by the presence of perfect radial spherulites of aegirine (Fig. 72) set in a subsolidus originated matrix of ordered albite, chessboard albite and microcline. Alkali feldspar is partly replaced by euhedral albite, surrounding and partly enclosing anhedral quartz or untwined microcline. With increasing replacement of alkali feldspar by albite the rock grades into an aegirine-albitite with similar textural characteristics, described as "snowball texture" by Bowden and Kinnaird (1984) from Nigerian equivalents. Honey yellow, disseminated pyrochlore, up to 1 mm in size, is the characteristic Nb'- Ta ore-mineral in the albitites and albite-rich agpaites. Towards the top, the rock grades into a layer rich in quartz, albite and interstitial zircon, aegirine and arfvedsonite.

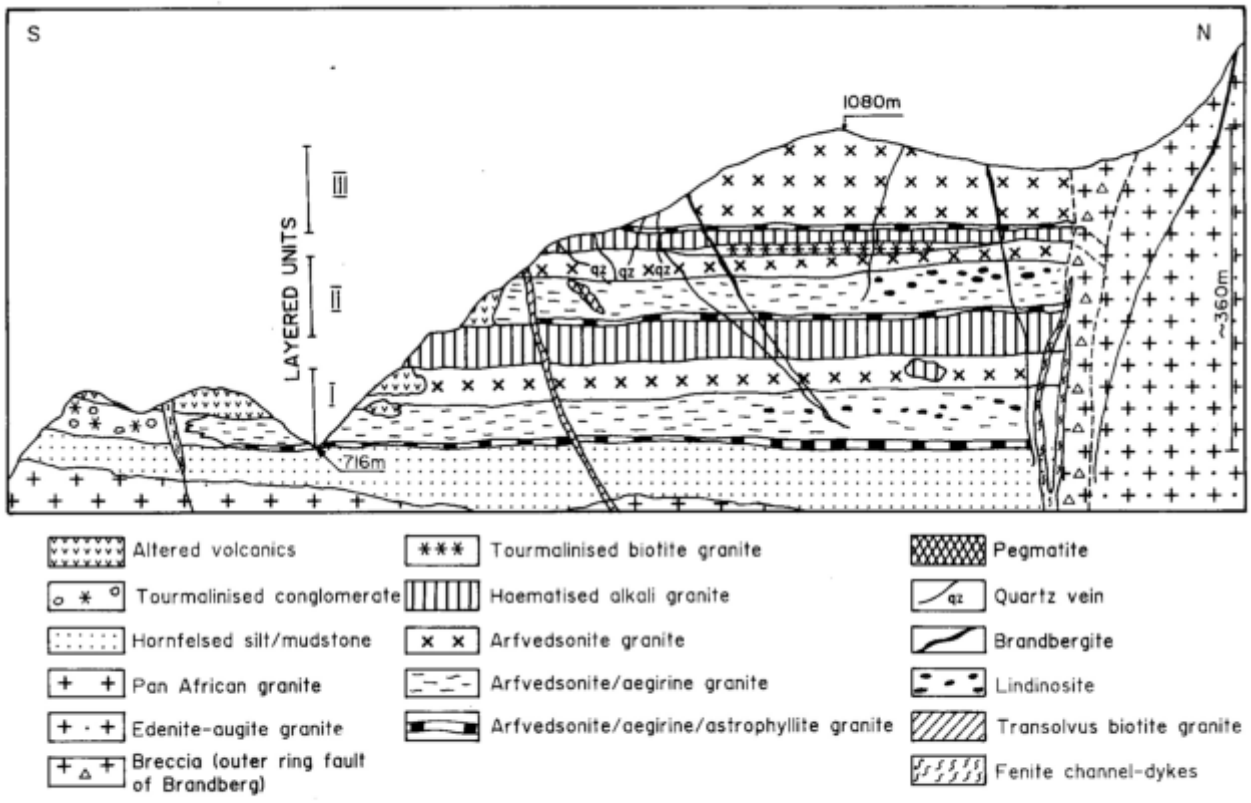

Fig. 71: Schematic profile of the Amis Layered Complex.

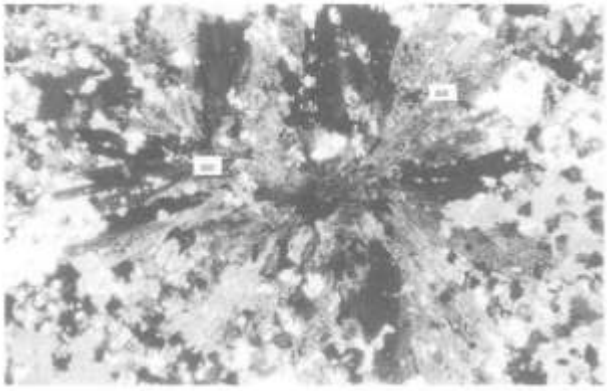

Fig. 72: Photomicrograph of radiate growing aegirine needles (ae) in fenitised peralkaline granite of layered unit 1, Amis Complex (magnification x 15, XPL).

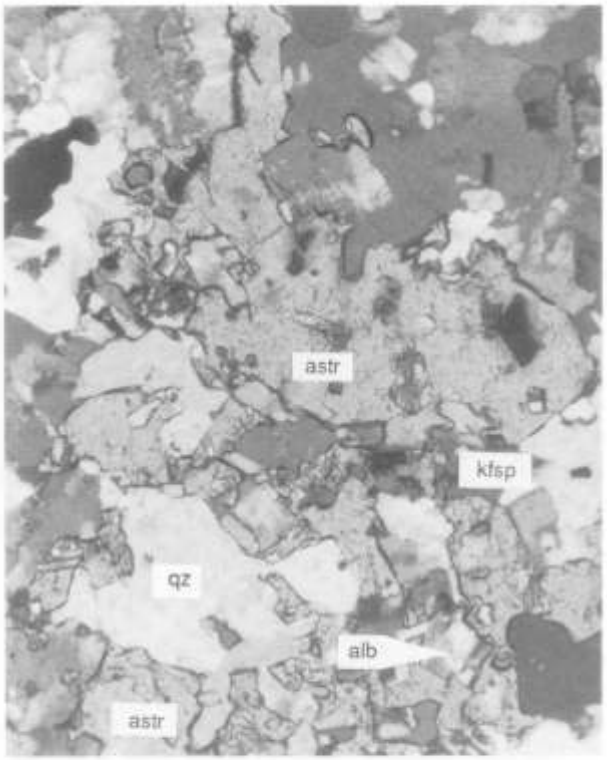

Fig. 73: Photomicrograph of poikilitic astrophyllite (astr), quartz (qz), albite (alb) and (kfsp) in fenitised peralkaline granite, Amis Complex (magnification x 41, XPL).

The following stratified horizon of arfvedsonite-astrophyllite granite is composed of interstitial aegirine replacing arfvedsonite, poikilitic, golden yellow astrophyllite (Ti-silicate), and interstitial, unzoned zircon set in an albite-microcline-quartz matrix (Fig. 73). The thickness of the basal layers decreases from unit 1 (60 cm) to unit 2 (20 cm) and unit 3 (4 cm).

The basal layers progressively grade into massive aegirine-granite, up to 20 m in thickness, containing lenticular, interstitial aegirine laths, zoned zircon and anhedral, interstitial quartz, set in a network of microcline-perthite and microcline partly replaced by albite. This layer gradually passes upwards into a stratified body of aegirine-arfvedsonite granite, up to 30 m thick. Aegirine progressively replaces arfvedsonite from the bottom towards the top of the layer which can result in a complete replacement of arfvedsonite. Frequently the layer of aegirine-arfvedsonite

granite therefore is suppressed. The aegirine granite of unit 1 additionally contains large (l cm), perfectly zoned crystals of zircon and specks of zinc-rich pyrophanite. Accessory pyrochlore occurs in aegirine- albite granite of unit 1 and 2 showing patches of granophyric intergrown alkali feldspar and quartz.

The aegirine-arfvedsonite granites are overlain by arfvedsonite-microcline granite and arfvedsonite-albitite with perfectly developed inch-scale layering (Fig. 74).

Fig. 74: Mineral layering in arfvedsonite granite of unit 1, Amis Complex.

Fig. 75: Mineral layering in arfvedsonite/aegirine granite of layered unit 1, Amis Complex, central part.

Fig. 76: Central part of the Amis Layered Complex (looking north) with a prominent cliff of haematised amphibole granite.

The transitional zone between the two horizons is marked by a 10 cm thick, pegmatitic zone of quartz-microcline-perthite-arfvedsonite granite, overlain by medium grained, aegirine-arfvedsonite granite which successively becomes finer grained after 5 - 8 cm. This horizon is up to 40 m thick and characterised by well developed, dark-blue mineral layers of arfvedsonite in a network of microcline and quartz with intercalated, rhythmically repeated, light coloured arfvedsonite albitites (Fig. 75). The thickness of the individual layers varies from a few millimeters to several meters. The dark zones consist of an interlocking network of microcline, in which quartz and arfvedsonite have crystallised interstitially. Albite laths, partly replacing microcline are surrounding anhedral quartz which give the rock the characteristic "snowball-texture". Interstitial zircon and fluorite are the dominant accessories. The leucocratic albitite layers consist of euhedral albite with interstitial quartz and minor arfvedsonite.

The top layer of a cyclic unit consists of altered amphibole/biotite granite which is more resistant to weathering and therefore forms a prominent cliff (Fig. 76). The equigranular, haematised alkali granite of unit 1 consists of microcline, microcline-perthite, perthite, orthoclase, quartz and deep red haematite. Alkali feldspar is partly replaced by albite or chessboard albite and is full of tiny haematite inclusions. All ferromagnesian minerals are replaced by deep-red haematite which has occasionally preserved the cleavage pattern of amphibole. Accessory minerals include zircon, fluorite and pyrochlore.

The top layer of unit 2 is less alkaline and consists of granophyric edenite/biotite granite. The feldspars are composed of orthoclase, perthite, microcline-perthite and plagioclase. Quartz, for the most part is micrographically intergrown with alkali feldspar. Ferroedenite occurs as ragged crystals partly replaced by clustered, yellowish-green biotite. Biotite of the first generation is of annitic composition forming euhedral, reddish-brown crystals whereas secondary biotite consists of green siderophyllite. Accessory minerals include apatite, fluorite, zircon and locally abundant, zoned allanite. Blocks of the hornblende-biotite granite, up to several meters in size, occur as enclaves in the underlaying peralkaline granites. The enclaves are enveloped by a characteristic, deep reddish-brown, fine grained reaction halo consisting of quartz and untwined, turbid microcline. Magnetite has replaced the mafic components and is often surrounded by secondary biotite. The reaction rim is rich in metamict zircon, allanite, fluorite, monazite and pyrochlore.

In contrast to unit 1, the hornblende granite of unit 2 is underlain by leucocratic, fine grained, tourmaline bearing biotite granite. In the eastern part of the Amis Complex the lenticular body is up to 12 m thick and consists of quartz, orthoclase, perthite, microcline-perthite which partly is re-

Fig. 77: Central part of the Amis Layered Complex (looking east) showing layered units 1, 2 and 3.

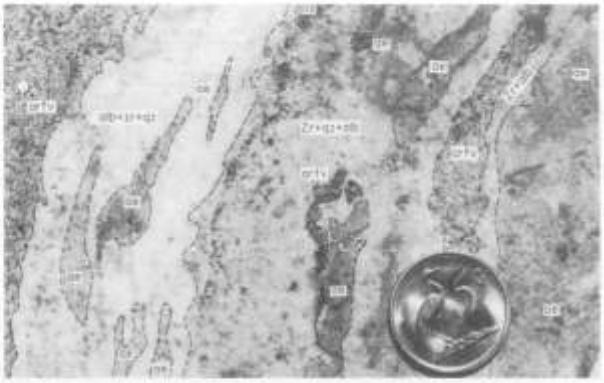

Fig. 78: Massive fenite consisting of schlieren of aegirine (ae), arfvedsonite (arfv), zircon (Zr), albite (alb) and quartz (qz), Amis East.

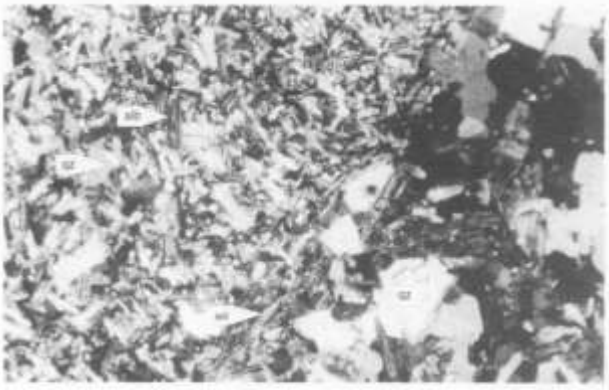

Fig. 79: Photomicrograph of a fenite channel (magnification x 15, XPL) showing needles of aegirine (ae), laths of albite (alb) and quartz (qz).

placed by albite and plagioclase and greenish-brown, ragged siderophyllite. Characteristic tourmaline nodules, resembling those of the Hungurob ring dyke (Fig. 20) are up to 10 cm in diameter and contain interstitial, bluish-green schorl, often replacing biotite, perthite, quartz, albite and accessory zircon and apatite. The tourmalinised biotite granite horizon thins out towards the northwest with decreasing tourmaline content.

In the extreme western part, tourmaline-free, albitised biotite granite is composed of turbid alkali feldspar, albite, euhedral quartz and highly altered, clustered granules of biotite and green Fe-spinel. Brown, skeletal biotite is partly replaced by colorless mica which occurs together with deep green, xenomorphic crystals of hercynite, partly altered to possibly hoegbomite. A similar assemblage was described from the northern contact zone of the complex (Fig. 30).

9.2 Fenites and fenitisation

Fenites are known to be mainly associated with carbonatite complexes and the term has been applied to describe metasomatic rocks of varied chemical compositions associated with alkaline intrusions (McKie, 1966). The process of fenitisation, characterised by sodium-ferric, metasomatic changes does not necessarily imply the presence of a carbonatite magma since occurrences of fenites have been reported to occur in association with silica-oversaturated alkaline intrusions (Bowden, 1985). The separation of a residual fluid phase from granites rich in alkalies and incompatible elements is the most likely process to produce fluids which are responsible for the development of sodium-metasomatites similar to the fenite aureole about carbonatite centres.

In the vicinity of the Amis Complex highly peralkaline, channel-like dykes cross-cut Mesozoic granite and country rock. The dykes consist of characteristic schlieren and bands of massive aegirine - and arlvedsonite-albite rock, separated by massive bands of unzoned, interstitial zircon and pyrochlore set in a matrix of albite and quartz. Albite laths have almost completely replaced the former perthite and microcline-perthite surrounding or overgrowing euhedral quartz. Aegirine and arlvedsonite needles are mostly orientated parallel to the channelling direction, giving the rock a texture resembling flow-banding (Figs 78 and 79).

Penetrating the lower part of the peralkaline granite series the massive fenite-schlieren dissolve and successively grade into dispersed, fiamme-shaped clusters of aegirine and arlvedsonite (Fig. 80). The ring fracture associated with the Amis Complex obviously acted as a channel way for metasomatising fluids and hence, irregular zones of fenitised country rock sporadically occur along the ring fracture (Fig. 81). The process of fenitisation has affected all rock types present along the ring-fault including sedimentary , volcanic and plutonic rocks.

A zoned fenite dyke cross-cutting volcanics has been found in the eastern part of the Amis Valley. The dyke is up to 20 cm wide consisting of a central zone of albitised alkali feldspar and quartz with abundant interstitial zircon and two, mineralogically different border zones. One wall zone contains distinctive clusters of radial arranged aegirine needles, in contrast to the opposite wall which contains haematised arlvedsonite aggregates, both set a in quartz-albite groundmass (Fig. 82).

9.3 Origin of layering and genesis of the different rock types

The Amis Layered Complex offers an unique example to study metasomatic processes in oversaturated, agpaitic environments and the role of alkali-oversaturated, rare-metal

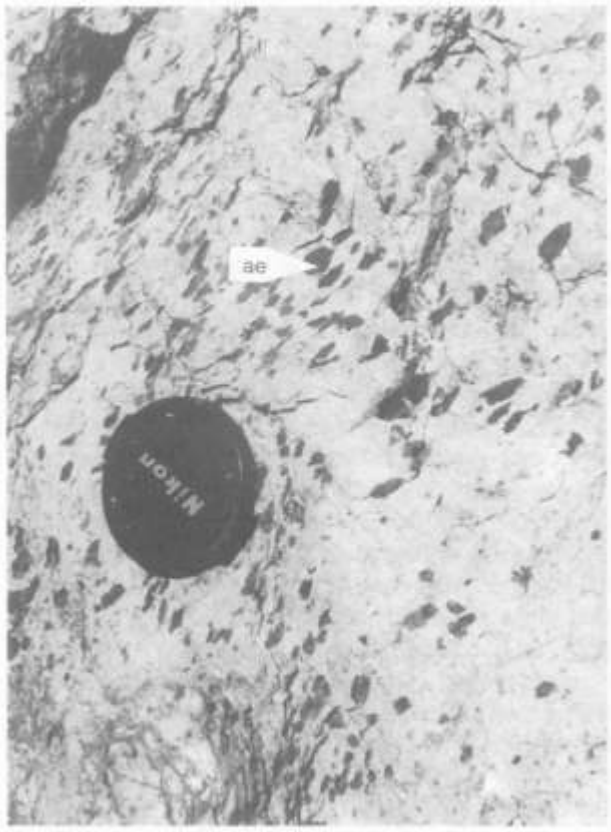

Fig. 80: Lower part of layered unit 1 showing fiamme shaped clusters of aegirine (ae), penetrating and fenitising the layered suite, Amis West.

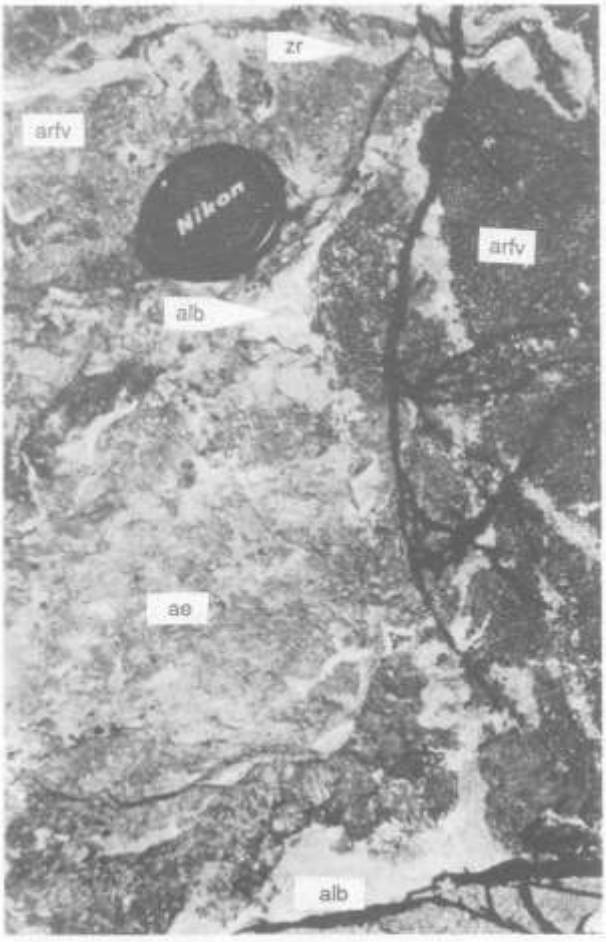

Fig. 81: Fenitised Karoo volcanics along the Amis ring fracture, consisting of schlieren of aegirine (ae), arfvedsontie (arfv), albite (alb) and zircon (z) with disseminated pyrochlore mineralisation.

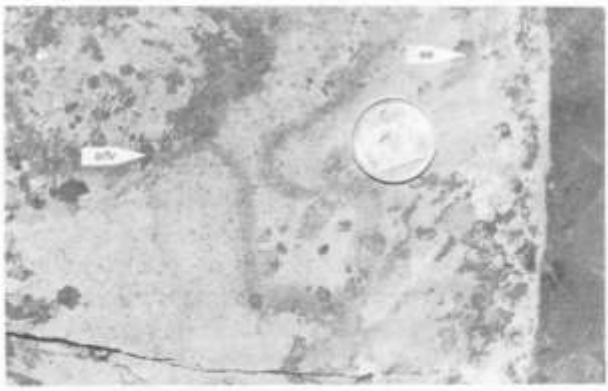

Fig. 82: Zoned fenite dyke cutting volcanics, Amis Complex, eastern part (explanation in text).

enriched hydrothermal fluids in the formation of a mineral stratified peralkaline complex. Bennett *et al.* (1984) reported the occurrence of layered arfvedsonite granite from the Birji complex, Nigeria. They concluded that the layering was not produced by gravitational accumulation but by selective crystallisation controlled by diffusion.

Before discussing the origin of the layering, the genetic and geological implication of the term has to be defined. In his paper on the terminology of layered intrusions Irvine (1981) redefined the name "cumulus" as an "igneous rock characterised by a framework of touching crystals and mineral grains that were concentrated through fractional crystallisation" which implies that "crystal settling is a possible but not essential process in the origin of layered rocks" (Irvine, 1980). Physio-dynamical experiments and chemo-petrological studies of Chen and Turner (1980), McBirney and Noyes (1979), Irvine (1980) and Wilson and Larson (1985) explore the idea that mineral layering is produced by the phenomena of "double diffusive fractional crystallisation". This process involves heat and mass transfer by diffusion and convection (Turner and Chen, 1974). Growth of the crystals is controlled by the formation of horizontal layers which have generated by the action of numerous small convection cells (Irvine, 1980). In the past the terminology for layered intrusion has been mainly applied to cumulates which originated by crystal settling (basic to ultrabasic intrusions in a strict sense) but also has been successfully used to describe mineral stratified, Si-undersaturated agpaitic rocks of the Ilimaussaq intrusion (Larsen and Sörensen, 1987). The use of the cumulate terminology gets confusing when processes like "post-cumulus metasomatism" or "post-magmatic infiltration metasomatism" become evident (Irvine, 1980, 1981), features which obviously characterise Si-oversaturated, agpaitic rocks of the Amis Complex. The mineral-stratification in the peralkaline granites is believed

not to be magmatic in a strict sense but, due to die limited availability of suitable expressions to describe stratification of such sequences, the terminology which has been applied to layered intrusions is used in a more loose sense.

In the Amis Complex mineral layering occurs in rocks which are characterised by a network of touching alkali feldspars. During post-magmatic, sodic metasomatism the original K-feldspar has been partly or completely replaced by albite. Early crystallised rocks from the top cooling unit have preserved the original, interlocking network of perthite and microcline which in some way resembles that of cumulates of layered intrusions but with the important difference that the interlocking framework of feldspar has not originated by a process of crystal settling. Quartz occupies the interstitial space between the feldspars together with highly interstitial or poikilitic arfvedsonite and/or aegirine. To some extent, the interstitial assemblage exhibits distinctive characteristics of a post-cumulate. The percentage of the ferromagnesian constituents changes from 25- 30 per cent in the melanocratic to 5-12 per cent in the leucocratic layers, whereas the proportions are reversed for quartz but constant for feldspar. Both arfvedsonite and aegirine show endmember-composition (chapter 7.2) and aegirine commonly replaces arfvedsonite, preferentially in albite-rich zones. The crystallisation of the sodic minerals is accompanied by changes in the feldspar composition, which resulted in the replacement of the feldspar-network by albite depending on the duration and intensity of the process. Such reactions of a "cumulate" with upward migrating "intercumulus liquid" have been described as infiltration metasomatism (Irvine, 1980). In the case of the Amis Complex it is obvious that highly peralkaline fluids - possibly in multiple pulses - have been channeled into a laccolithic intrusion with three early cooling units separated by a crystallising network of alkali feldspar. The infiltrated fluids, similar to fenitising fluids, rapidly increased the alkalinity of the system and could therefore explain the intense metasomatic changes but not the process of layering. Bennett *et al.* (1984) have reported very similar, layered arfvedsonite granite from the Shira Complex in Nigeria and concluded that "oscillating crystallisation of interstitial quartz and arfvedsonite, controlled by diffusion processes in a rapidly cooling body" is the most likely process which produced mineral layers in the Birji-granite. Such an oscillation has not been recognised in layered rocks of the Amis Complex. Arfvedsonite poikilitically encloses quartz and albite and therefore has crystal-lised later than quartz and even post-dates the albitisation event. Other speculations on the origin of layering in agpaitic rocks of the Ilimaussaq intrusion are given in Sörensen (1969) and Larsen and Sörensen (1987). They concluded that the layered agpaitic rocks at Ilimaussaq form the top zone of a stratified basalt-syenite magma chamber at depth. The earliest agpaitic rocks crystallised downwards from the roof with an upward accumulation of residuals (Larsen and Sörensen, 1987). Similarly for the Amis Complex it is difficult to state if any chemical or thermodynamical diffusion was involved. The most likely process to produce layering in Amis could be the development of an early double-diffusive convection system which was controlled by sheet-like intrusions of alkaline, but not necessarily peralkaline, magma. The assumption that the earliest pulses of magma could originally have been peraluminous in composition is based on the fact that the top of each cyclic unit consists of non-agpaitic rock types. The occurrence of peraluminous biotite granite carrying tourmaline nodules confirms the presence of boron in the original magma, and obviously boron has been trapped in the rapidly cooling roof of the intrusion. An early loss of boron from such a peraluminous magma would furthermore explain the tourmalinised killas around the entire intrusion. If such a double diffusive system, which already had developed a "cumulate" (network of feldspar) with convection cells and interstitially crystallising quartz abruptly is infiltrated by a highly peralkaline, possibly residual fluid system, laminae of interstitial "postcumulus" could have developed (Fig. 83). The crystallisation of arfvedsonite (aegirine) in layers could therefore be explained by a metasomatic front of an agpaitic fluid progressively entering such a convective system and changing the chemical conditions. With increasing alkalinity at low temperatures the crystallising amphibole becomes progressively more sodic, trending towards arfvedsonite of endmember composition which at even lower temperatures was replaced by "hydrothermal aegirine". Although the model of infiltration metasomatism (Irvine, 1980) involves infiltration of a melt into a cumulate, it has been shown by Boudreau (1988) that an infiltration of fluids can produce analogous features in layered intrusions.

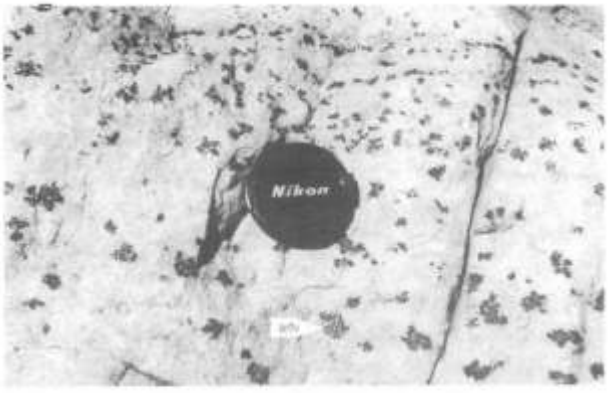

Fig. 83: Laminae of sieve-like crystallised arvedsontie (arfv) in albitised peralkaline granite of layered unit 1, Amis Complex, central part.

Such residual, alkali-oversaturated fluids, rich in lithophile elements are therefore believed to be responsible for the late crystallisation of the ferric-sodic, interstitial minerals and albitisation processes. At the bottom of each unit the rare metal-rich fluids are over-saturated in alkalis and produced arfvedsonite-aegirine-astrophyllite metasomatites with characteristic minerals such as zincian fluor-arfvedsonite, stanniferous aegirine, astrophyllite rich in Zn, Nb and Sn, pyrochlore and REE-and zirconium minerals. In such mineral assemblages quartz to some extent has recrystallised and is characterised by the presence of abundant fluid inclusions, whereas the entire framework of alkali feldspar has col-

lapsed and been replaced by albite. The late crystallising arfvedsonite accommodated zinc and aegirine incorporated tin available from the liquid. It is obvious that aegirine has crystallised down to lowest temperatures (rosette like or fiamme-shaped aggregates, Fig. 80) which in the vicinity of the feeder channel resulted in the entire replacement of arfvedsonite. Nb, Zn and Sn-rich astrophyllite is the characteristic mineral of such alkali-saturated fenite-fronts which first is coexistent with arfvedsonite and later was replaced by aegirine which contains similar concentration of "inherited" tin in the lattice (see appendix, table 2.4).

Advanced stages with complete replacement of arfvedsonite by aegirine occur only in the lower most part of a cyclic unit. Such destabilisation of sodic amphibole is controlled by severe post-magmatic oxidation (Bonin, 1982). The equilibrium between a residual fluid-phase and the rock may therefore have been disturbed during the infiltration of extremely fluorine and rare-metal enriched fluids via ring fractures, which causes disequilibrium conditions and metasomatic replacement processes. Thus, the development of late aegirine-astrophyllite-pyrochlore assemblages is very similar to replacement processes associated with carbonatite-centres, known as fenitisation. Late replacement of aegirine by zincian fluor-arfvedsonite only occurs at lower temperatures when equilibrium conditions were re-established. Under the described conditions, crystallisation of arfvedsonite is obviously extended into the hydrothermal field and has produced mesocratic, nodular replacement aggregates of arfvedsonite, albite and fluorite (lindinosites) which occur in the central portion of the complex above the feeder channels of the fenitising fluids. If the fluid-phase could escape via fractures, fenite-rocks previously described as brandbergites (Chudoba, 1930) could develop. The experimental work of Ernst (1962, 1968) on amphiboles and their stability has shown that riebeckite-arfvedsonite solid solutions are stable at temperatures below 595°C at 1 kb pH_2O and fO_2 defined by bunsenite-nickel buffer.

Any tectonic movement at this evolutionary stage would allow such critical "fenitising" fluids to escape along fractures and the subsequent generation of fenite dykes. Such metasomatic replacement dykes associated with the Amis Complex previously have been described as brandbergite (Chudoba, 1930) and hence are interpreted as fenite dykes which generated when highly peralkaline (fenitising) fluids could escape from the system.

9.4 Lindinosite

Lindinosite is a melanocratic, sodic amphibole bearing rock (Lacroix, 1923) and occurs as "enclaves" in alkaline granites (Quin, 1962). Lindinosite nodules, up to 5 cm in diameter, occur in medium grained arfvedsonite granite in the central part of the Amis Complex.

The nodules can be described as an albite-quartz-fluorite rock with deep blue, arfvedsonitic amphibole as the prominent, highly interstitial mafic mineral. Micro-perthite and microcline are replaced by fine laths of albite which together with quartz host sieve-like, poikilitic arfvedsonite (Fig. 84).

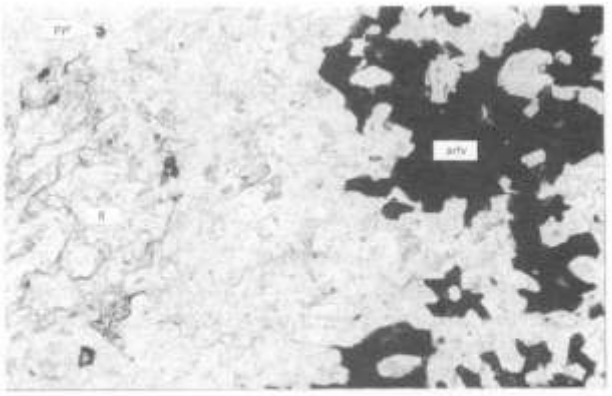

Fig. 84: Photomicrograph of lindinosite showing sieve-like crystallised arfvedsonite (arfv), and abundant fluorite (fl) in a quartz-albite matrix (magnification x 43, PPL).

Fig. 85: Brandbergite dyke cross cutting hornblende-biotite granite , Amis Complex.

Fluorite (up to 3 vol per cent) is the dominant accessory which beside greyish, unzoned zircon occupies the interstitial space between the albite laths. Petrographically lindinosite resembles albite-rich brandbergite but carries abundant fluorite. The nodular mode of occurrence genetically links lindinosite with the tourmaline segregation in albite-biotite granites.

Bonin (1982) has pointed out that lindinosites should be interpreted as rocks of metasomatic origin rather than enclaves of chilled margins or as precursors of a peralkaline phase (Quin, 1962). The occurrence of brandbergite dykes and lindinosite nodules, far away from any contact seems to be linked with post-magmatic, metasomatic replacement processes. In the central area of the complex brandbergite dykes are absent, indicating that it was impossible for the peralkaline fluid-system to escape, which resulted in autometasomatic replacement processes and possibly the formation of nodular aggregates of a arfvedsonite - albite - fluorspar rock (lindinosite).

Rocks originally described as "branctbergite" (Chudoba, 1930) from Brandberg, Namibia, "lindinosite" (Lacroix, 1923) from Lindosa, Corsica, "rockallite" (Judd, 1897; Lacroix, 1923) from islet of Rockall, North Atlanic Ocean, and the peralkaline segregations "dahamite", "paisanite" and "lestiwarite" (Rosenbusch, 1910), are all very similar, mesocratic, porphyritic, peralkaline rocks which should be interpreted as late-stage or post-magmatic products of fenitisation associated with alkaline complexes.

9.5 Brandbergite

A number of highly peralkaline, aplitic dykes cross cut the layered rock series, country rock and hornblende granite (Fig. 85). The fine grained, dense rock is steel-blue or greyish-blue in colour and occurs as steeply dipping, 30-80 cm wide dykes without any preferential orientation.

A porphyritic type from the Amis Valley, containing feldspar, quartz, biotite and arfvedsonite was first discovered by Cloos in 1929. A mineralogical description and a wet chemical analysis has been published by Chudoba (1930) and he introduced the name "brandbergite", for the previously unknown rock type.

Brandbergites comprise a variety of textures ranging from anhedral, granular through porphyritic to granophyric. The dominant mafic mineral present in all types is deep-blue, ragged arfvedsonite which crystallised as the latest mineral component. Arfvedsonite forms sieve-like clusters giving the rock a porphyritic appearance or in other types is finely disseminated. In coarser grained brandbergite, arfvedsonite is coexistent with reddish-brown annite-lepidomelane. The feldspars show subsolidus growth and are composed of plagioclase, orthoclase, perthite, and microcline-perthite partly replaced by laths of albite.

Quartz has crystallised interstitially between the feldspar network or is granophyrically intergrown with alkali feldspar of the matrix. Extremely fine grained brandbergite lacking biotite, contains disseminated needles of arfvedsonite in a dominantly granophyric groundmass. In biotite bearing brandbergite replacement of arfvedsonite by late biotite is accompanied by intense albitisation. Quartz and alkali feldspar are surrounded by small albite laths resembling the subsolidus "snowball" texture of albitised peraluminous granites. Brandbergites carry abundant, euhedral and interstitial zircon, frequently abundant pyrochlore and fluorite, xenotime and magnetite.

A very distinctive type of brandbergite occurs in the Numas Ravine as small dykes or veins (2-6 cm wide) in the biotite-hornblende granite ring-dyke (Fig. 86). Radiate textured needles of aegirine surrounded by white halos of albite are set in a bluish-grey, fine grained matrix consisting of albite, quartz and arfvedsonite (Fig. 87).

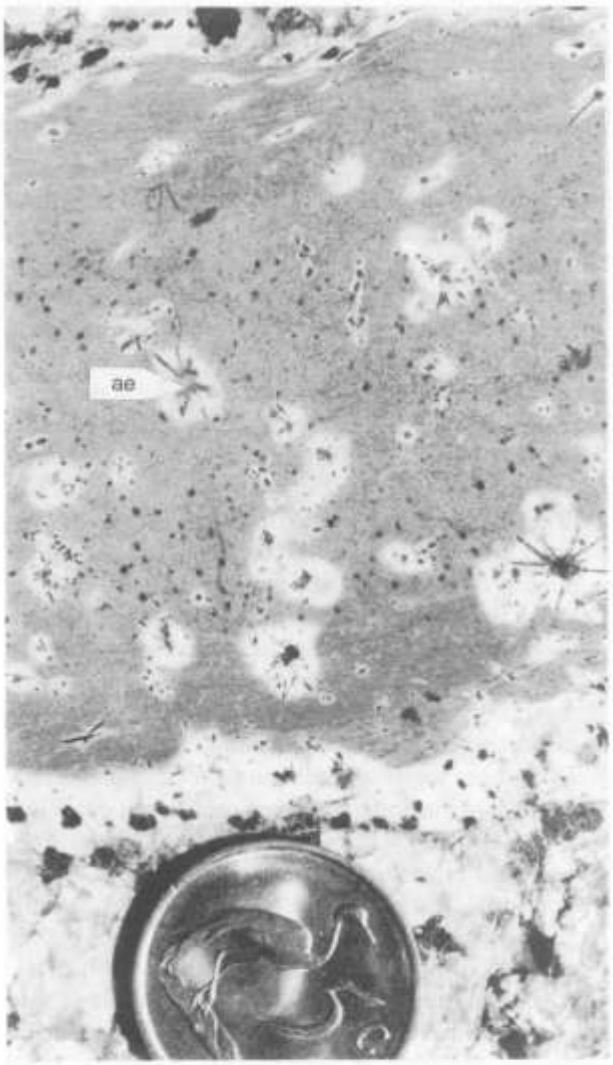

Fig. 86: Small dyke of brandbergite with radial arranged needles of aegirine (ae) and associated albite-rich (alb), "bleached halos", Numas Ravine.

The light colour of the halos is characterised by the absence of arfvedsonite whereas the proportions of quartz and albite stay unchanged. In the central portion of the vein albite is replaced by colourless to slightly greyish zinnwaldite, enclosing quartz (Fig. 88). Towards the margins of the vein the rock grades into a massive albitite up to 0.5 cm in width. Stepwise replacement of the host granite is marked by distinct metasomatic fronts of sodium-rich, agpaitic fluids. K-feldspar is replaced by albite along fissures and grain boundaries followed by the breakdown of edenitic hornblende to golden or yellowish-brown aggregates of biotite. Deep reddish-brown granitic biotite simultaneously is replaced by colourless to light green Li-siderophyllite. The next metasomatic front or pulse of fenitising fluids led to the destruction of the mafic assemblages by the generation of arfvedsonite and the complete replacement of alkali feldspar by albite. Increasing concentrations of zircon, lithium, rubidium and tin are indicated

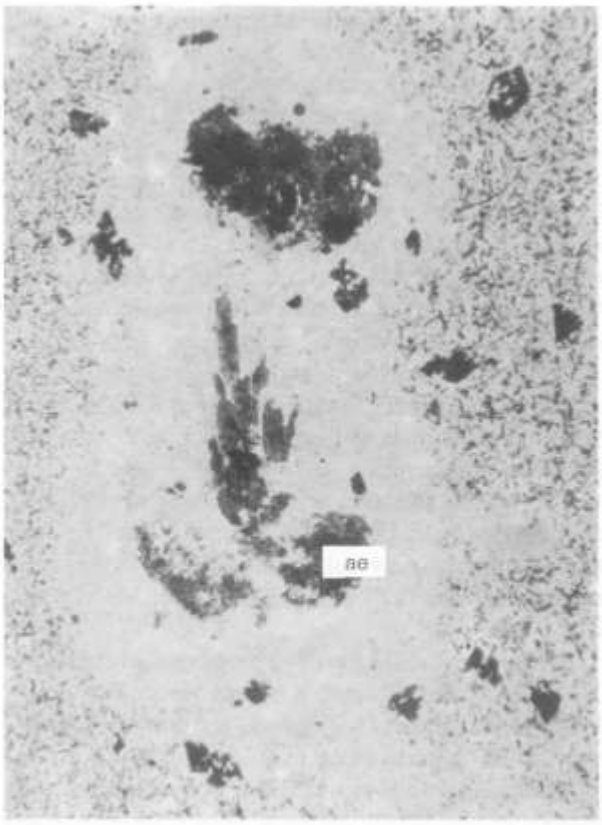

Fig. 87: Photomicrograph of brandbergite from the Numas Ravine showing radiate growth of aegirine (ae) with a well developed halo in quartz-albite-arfvedsonite matrix (magnification x 41, PPL).

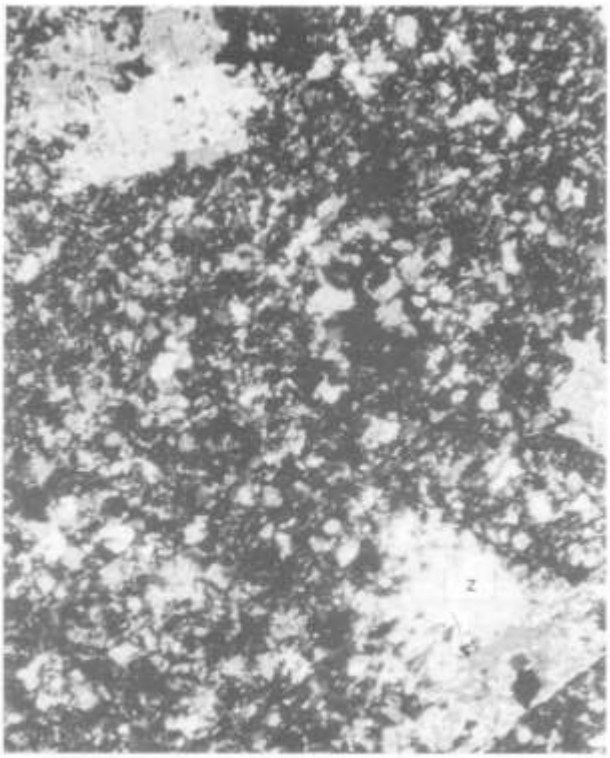

Fig. 88: Photomicrograph of brandbergite consisting of zinnwaldite crystals (z) set in an albite-quartz matrix (magnification x 41, XPL).

by the generation of zircon and big flakes of zinnwaldite enclosing quartz (Fig. 88).

The latest metasomatic front is characterised by the destruction and overgrowth of arfvedsonite by Fe-rich, stannian aegirine. The necessary leaching of iron to form iron-rich sodic pyroxene is believed to be responsible for the generation of the previously described "bleached halos" around the radiate growing needles of aegirine (Figs 86 and 87). All these metasomatic features and replacement processes classify brandbergites as metasomatic replacement rocks with distinctive features of fenite-dykes.

10. Conclusions

The Brandberg Alkaline Complex demonstrates an excellent example of granitic, anorogenic magmatism associated with Mesozoic, intra-plate volcanic activity. Geological, mineralogical and geochemical studies reveal that Brandberg granites carry characteristic features of the HHP-alkali granite series with a compositional range from metaluminous through peraluminous, to peralkaline subsolidus types.

Post-magmatic deuteric alteration in the sub solidus indicates the significant role of residual fluid phases and hydrothermal replacement processes associated with multiple boiling in high uranium/thorium-granites. Auto-metasomatic re-equilibration of these fluids and infiltration metasomatic processes (fenitisation) are responsible for the development of potash and sodium feldspar, trioctahedral mica of the siderophyllite - zinnwaldite series in peraluminous granite and sodic pyroxene and amphibole in peralkaline types.

The Brandberg Complex has mineralogical and geochemical similarities with Mesozoic alkali-complexes elsewhere in Africa, and the pattern of mineralisation has some similarities with the Nigerian Sn-Zn type of deposit.

In both provinces the deposition of ore minerals can be related to late/post-magmatic alteration processes like albitisation, microclinisation and greisenisation which are described by Bowden and Kinnaird (1984, 1984a, 1988) and Kinnaird (1985) to be responsible for the deposition of economic and subeconomic quantities of cassiterite, columbite, sphalerite and other rare metals in the Nigerian Younger Granite Province.

Geochemically, the various metasomatic processes are characterised by distinct changes in the pattern of both, major oxides and trace element. Variations in the major oxide chemistry are best displayed using multi-cationic parameters (Debon and Lefort, 1988) which clearly discriminate between a magmatic alkali-oversaturated trend and hydrothermal trends depending on the chemical com-position of the metasomatising fluids. The trace element pattern clearly indicates that during hydrothermal re-equilibration processes there is a general enrichment trend in HFS- and LIL-elements which in peralkaline environments has produced pyrochlore-REE type mineralisation and in peraluminous conditions led to disseminated and vein-controlled cassiterite - sphalerite mineralisation.

In the Brandberg Complex deuteric alteration processes and associated deposition of- subeconomic quantities of oxide/sulphide minerals started with K for Na exchange processes followed by albitisation, fenitisation combined with Na for K exchange processes and vein controlled greisen-type alteration. The sequence of alteration types in Nigeria where the process of potash metasomatism generally is superimposed on sodic types (Kinnaird 1985; Kinnaird *et al.* 1986) is somewhat unique. The economic importance of the Mesozoic Sn-Zn deposits in Nigeria is possibly based on the relatively early occurrence of peralkaline magmatism. Such early agpaitic fluid-phases may be regarded as the most likely process for the leaching of lithophile elements and subsequent mineralisation. The absence of tourmaline in the Younger Granites of Nigeria (Kinnaird *et al.* 1985) could therefore be explained by an early loss of the boron-phase in a peralkaline environment whereas in Brandberg the occurrence of peralkaline rocks postdates the intrusion of peraluminous types. A similar, early loss of the boron-rich phase has been recognised around the peralkaline Amis Complex in the south western periphery of the Brandberg massif which in this case led to the tourmalinisation of the country rock (killas).

The occurrence of tourmaline in Brandberg and other granitic complexes of the province (Erongo, Spitzkoppe and Otjihorongo) is generally not a widespread process but reflects significant differences in the sequential order of the metasomatic events in both provinces.

Factors which may control the presence or absence of mineralisation in a province are discussed in Taylor (1976) and theories on the origin of tin range from crustal- to mantle-derived. Mineralisation in anorogenic granites have mainly been reported from alkaline complexes intrusive into Pan African orogenic belts like in Nigeria, Brazil and Namibia which are known as tin-rich provinces and where tin-mineralisation has occurred at different geological times. Anorogenic magmatism is therefore regarded as an important process in leaching tin and lithophile elements from crustal rocks and/or metasediments. The presence of HHP-elements, which are responsible for multiple boiling and the generation of hydrothermal convection, is the most important factor for the leaching, concentration and deposition of ore minerals. Therefore, it can be concluded that hydrothermal processes associated with Mesozoic intraplate magmatism in Sn-Zn-rich provinces like the Damaran , can remobilise economic important trace elements and accumulate sufficient quantities of ore to produce a mineral deposit.

11. Aknowledgements

This study is based on a project of the Geological Survey of Namibia which provided the framework for a Dr. rer. nat. dissertation carried out at the Institut für Geowissenschaften, Mineralogie, Johannes Gutenberg Universität Mainz, West Germany. The writer would like to express his thanks to Dr. R. Miller and Mr. D. Newman of the Geological Survey in Windhoek, Profs Drs H. von Platen and M. Fürst, Johannes Gutenberg Universität Mainz, West Germany and Prof. Dr. P. Bowden, University of St. Andrews, Scotland for their support, supervision and encouragement making this study possible.

A special word of thanks goes to the various laboratories which provided the analytical facilities and geochemical analyses.

The Department of Geochemistry, University of Cape Town is thanked for the "free data", the use of the microprobe, assistance and advice. Namely: Profs Drs T. Erlank and A. Duncan, Dr. A. Le Roux and Mr. D. Rickard; Prof. A. Duncan and Dr. S. Milner kindly provided additional analyses of quartz-monzonitic rocks.

The geochemical laboratory of the Geological Survey of South Africa (Drs C. Frick, F. Walraven and Mrs. M. du Preez) provided most of the whole rock analyses and is thanked most sincerely.

The Institut für Geowissenschaften, Mineralogie, Johannes Gutenberg Universität, Mainz is thanked for making available their analytical facilities. Thanks for assistance and advice goes to Dr. B. Schulz-Dobrick and Mr. M. Hemmer.

The writer would like to thank the laboratory staff of the Geological Survey of Namibia, namely Messrs G. Brooker-Smith, I.M. Hlahane, G. Tjikukutu and Mrs. F. Kandelo, who carried out most of the sample preparation for XRD and XRF analyses and provided over 300 thin sections and polished sections during this study. Miss. P. Badenhorst and Mr. S. Cloete of the drawing office did most of the final drawings. To all of them a word of thanks.

Messrs E. Hoa-Hoab and M. Garoeb of the Geological Survey, Windhoek are thanked for their assistance in the field and for accompanying the writer on many climbing tours in the Brandberg massif.

A special word of thanks goes to Dr. J.A. Kinnaird and Prof. P. Bowden for their encouragement and stimulating discussions in the field.

The writer would like to express his thanks to Profs H. von Platen and P. Bowden, Dr. J.A. Kinnaird and Mr. D. Newman for reviewing the text and their critical comments.

The Satellite Application Centre, MIKOMTEK, CSIR kindly granted permission to publish the satellite image of Brandberg (SCENE ID: 2237-08165, produced by SAC, MIKOMTEK).

12. References

Afifi, A.M. and Essene, E.J. 1988. MINFILE: A microcomputer program for storage and manipulation of chemical data on minerals. *Am Miner*., **73**, 446-448.

Allman-Ward, P. 1985. Distribution of uranium and thorium in the western lobe of the St.Austell granite and the effects of alteration processes. *In*: *High heat production (HHP) granites, hydrothermal circulation and ore genesis*. The Institution of Mining and Metallurgy, 437-458.

Badenhorst, F. 1989. A note on stratiform tourmalinites in the late Precambrian Kuiseb Formation, Damara Sequence. *Communs Geol. Surv. S.W. Africa/Namibia*, **4**, 67-70.

Batchelor, A. and Bowden, P. 1985. Petrogenic interpretation of granitoid rock series using multicationic parameters. *Chem. Geol*., **48**, 43-55.

Bennett, J.N., Turner, D.C., Ike, E.C. and Bowden, P. 1984. The geology of some northern Nigerian anorogenic ring complexes. *Overseas Geol. & Miner. Resour.*, **61**, 65pp.

Black, R., Morton, W.H., Rex, D.C. and Shackleton, R.M. 1972. Sur la découverte en Afar (Ethiopie) d'un granite hyperalcalin miocène: Ie massif de Limmo. *C.R. Acad. Sci. Fr.*, **274**, 1453-1456.

Black, R., Lameyre, J. and Bonin, B. 1985. The structural setting of alkaline complexes. *J. Afr. Earth Sci.*, **3**, 1/2, 5-16.

Bonin, B. 1982. Les granites des complexes annulaires. B.R.G.M. *Manuels et Méthodes.*, **4**, 183pp.

Bonin, B. and Giret, A. 1985. Clinopyroxene compositional trends in oversaturated and undersaturated alkaline ring complexes. *J. Afr. Earth Sci.*, **3**, 175-183.

Boudreau, A.E. 1988. Investigations of the Stillwater Complex. IV. The role of volatiles in the petrogenesis of the J - M Reef, Minneapolis adit section. *Can. Miner.*, **26**, 193-208.

Bowden, P. 1966. Zirconium in younger granites of northern Nigeria. *Geochim. Cosmochim. Acta.*, **25**, 985-993.

Bowden, P. 1985. The geochemistry and mineralisation of alkaline ring complexes in Africa (a review). *J. Afr. Earth Sci.*, 3, 17-39.

Bowden, P. and Whitley, J.E. 1974. Rare-earth patterns in peralkaline and associated granites. *Lithos,* **3**, 15-21.

Bowden, P. and Turner, D.C. 1974. Peralkaline and associated ring-complexes in the Nigeria-Niger Province, West Africa. *In*: Sörensen, H. (Ed.) *The Alkaline Rocks*, 330-351, John Wiley, London.

Bowden, P., Van Breemen, O., Hutchinson, J. and Turner, D.C. 1976. Paleozoic and Mesozoic age trends for some ring complexes in Niger and Nigeria. *Nature,* **259**, 297-299.

Bowden, P. and Jones, J.A. 1978. Mineralisation in the younger granite province of Nigeria. *Metallisation Associated with Acid Magmatism*, **3**, 179-190.

Bowden, P. and Kinnaird, J.A. 1978. Younger granites of Nigeria - a zinc-rich tin province. *Trans. I.M.M.* (section B), B66-B69.

Bowden, P. and Karche, J.P. 1984. Mid plate A-type magmatism in the Niger-Nigeria anorogenic province: Age variations and implications. *In*: Klerks, J. and Michot, J. (Eds), *African Geology*, 167-177.

Bowden, P. and Kinnaird, J.A. 1984. Geology and mineralisation of the Nigerian anorogenic ring complexes. *Geol. Jb.*, **B 56**, 3-65.

Bowden, P. and Kinnaird, J.A. 1984a. The petrology and geochemistry of alkaline granites from Nigeria. *Physics of the Earth and Planetary Interiors.*, **35**, 199-211.

Bowen, N.I. 1945. Phase equilibria bearing on the origin and differentiation of alkaline rocks. *Am. J. Sc. Dayly Vol.*, **243A**, 75-89.

Burger, A.J., Von Knorring, O. and Clifford, T.N. 1965. Mineralogical and radiometric studies of monazite and sphene occurrences in the Namib desert, South West Africa. *Min. Mag.*, **35**(271), 519-528.

Cerny, P. 1982. Anatomy and classification of granitic pegmatites. *In*: Cerny, P. (Ed.), *Petrogenesis of granite pegmatites in science and industry*. Short Course Handb. Mineralog. Assoc. Canada, **8**, 1-39.

Charoy, B. 1982. Tourmalinisation in Cornwall, England. *In*: *Mineralisation associated with acid metasomatism*, 63-70, John Wiley & Sons Ltd.

Chayes, F. 1955. Alkali feldspar as a by-product of the biotite-chlorite transformation. *J. Geol.*, **73**, 75-82.

Chen, C.F. and Turner, J.S. 1980. Crystallisation in a Double-Diffusive System. *J. geophys. Res.*, **85**, 2573-2593.

Chudoba, K. 1930. "Brandbergit", ein aplitisches Gestein aus dem Brandberg (SW-Afrika). *Zentbl. Miner. Geol. Paläont. Abt. A*, 389-395.

Cloos, H. 1911. Geologische Beobachtungen in Südafrika. II. Geologie des Erongo im Hererolande (Vorläufige Mitteilungen). *Beitr. geol. Erforsch. dt. Schutzgeb.*, **3**, 84 pp.

Cloos. H. 1919. Der Erongo. Ein vulkanisches Massiv im Tafelgebirge des Hererolandes und seine Bedeutung für die Raumfrage plutonischer Massen. *Beitr. geol. Erforsch. dt. Schutzgeb.*, **17**, 238 pp.

Cloos, H. 1929. Alter und Verband der jungen Granite in Südwestafrika. *C. r. 15th int geol. Congr. South Africa.*, **2**, 437.

Cloos, H. and Chudboa, K. 1931. Der Brandberg. Bau, Bildung und Gestalt der jungen Plutone in Südwestafrika. *Neues Jb. Miner. Geol. Paläont. BeilBd.*, **66B**., 1-130.

Deans, T. 1966. Economic geology of African Carbonatites. *In*: Tuttle, O.F. and Gittins, J. (Eds), *Carbonatites*, 385-413, J. Wiley & Sons.

Debon, F. and Lefort, P. 1988. A cationic classification of common plutonic rocks and their magmatic associations: principles, method and applications. *Bull. Mineral.*, **111**, 493-510.

Deer, W.A., Howie, R.A. and Zussmann, J. 1962. *Rock Forming Minerals II: Sheet Silicates*. Longman, London, 270pp.

De La Roche, H. 1964. Sur l'expression graphique des relations entre la composition chimique et la composition minéralogique quantitative des roches cristallines - Présentation d'un diagramme destiné à l'étude chimico-minéralogique des massifs granitique et granodioritiques - Application aux Vosges cristallines. *Sci. Terre*, **9**(3), 293-337.

De La Roche, H., Leterrier, J., Grand Claude, P. and Marchal M. 1980. A classification of volcanic and plutonic rocks using R1-R2 diagrams and major element analyses - its relationship with current literature. *Chem. Geol.*, **29**, 183-210.

Diehl, M. 1986. Preliminary report on the Cape Cross-Vis pegmatite field. *Communs geol. Surv. S.W. Africa/Namibia*, **2**, 39-45.

Dietrich, R.V. 1968. Behaviour of zirconium in certain artificial magmas under diverse P.T. conditions. *Lithos,* **1**, 20-29.

Durasova, N.A. and Barsukov, V.L. 1973. The behaviour of tin in liquating boron-bearing silicate melts. *Geochem. Int.*, **10**, 920-922.

El Bouseily, A.M. and El Sokkary, A.A. 1975. The relation between Rb, Ba, and Sr in granitic rocks. *Chem. Geol.*, **16**, 207-219.

Ernst, W.G. 1962. Synthesis, stability relations, and occurrences of riebeckite and riebeckite-arfvedsonite solid solutions. *J. Geol.*, **70**, 689-736.

Ernst, W.G. 1968. *Amphiboles, Crystal Chemistry, Phase Relations and Occurence*. Springer-Verlag, New York, 125pp.

Foster, M.D. 1962. Interpretation of the composition and classification of the chlorites. *U.S. Geol. Surv., Prof Pap.*, **414**-A, 33pp.

Frey, M. 1987. Very low-grade metamorphism of clastic sedimentary rocks. *In*: Frey, M. (Ed.), *Low temperature metamorphism,* 9-57. Blackie, Glasgow and London, 351 pp.

Gevers,T.W. and Frommurze, H.F. 1929. The geology of north western Damaraland, in South-West Africa. *Trans. geol. Soc. S. Afr.*, **32**, 31-55.

Ginsburg, A.I., Timofeyev, I.N. and Feldman, L.G. 1979. Principals of geology of granitic pegmatites. *Nedra Moskow*, 296 pp.; (in Russian).

Giret, A., Bonin, B. and Leger, J.M. 1980. Amphibole compositional trends in oversaturated and undersaturated alkaline plutonic ring complexes. *Can. Miner.*, **18**, 481-495.

Giret, A. and Lameyre, J. 1985. Inverted alkaline-tholeiitic sequences related to lithospheric thickness in the evolution of continental rifts and oceanic islands. *J. Afr. Earth Sci.*, **3**,

261-268.

Haughton, S.H., Frommurze, H.F., Gevers, T.W., Schwellnus, C.M. and Rossouw, P.J. 1939. *The Geology and mineral deposits of the Onzaruru area South West Africa. Expl. Sheet 71 (Omaruru. S.W.A.*), Geol. Surv. S. Afr., 151pp. *Abstracted in 1939 in S. Afr. Min. Engng. J.*, **50** (12426), 677-678.

Hochstein, M.P. and McKee, G.A.M.C. 1986. Boron in thermal spring systems in the Greater Auckland area, (New Zealand). *Proc. 8th. NZ. Geothermal Workshop*, 219-223.

Hogarth, D.D. 1977. Classification and nomenclature of the pyrochlore group. *Am. Miner.*, **62**, 403-410.

Hogarth, D.D., Chao, G.Y. and Townesend, M.G. 1987. Potassium- and flourine-rich amphiboles from the Gatineau area. *Quebec*. *Can. Miner.*, **25**, 739-753.

Hodgson, F.D.I. 1972. *The geology of the Brandberg-Aba Huab area South West Africa*. D.Sc. thesis Univ. Orange Free State, 174pp.

Hodgson, F.D.I. 1973. Petrography and evolution of the Brandberg intrusion, South West Africa. *In*: Lister, L.A., (Ed.), *Symposium on granites, gneisses and related rocks*. Spec. Publ. geol. Soc. S. Afr., **10**, 339-343.

Ike, E.E., Bowden, P. and Martin, R.F. 1985. Amphibole in the porphyries of the Tibchi an orogenic ring complex, Nigeria: Product of deuteric adjustments. *Can. Miner.*, **23**, 447-456.

Imeokparia, E.G. 1982. Tin content of biotites from the Afu Younger Granite complex, central Nigeria. *Econ. Geol.*, **77**, 1710-1724.

Imeokparia, E.G. 1983. Geochemical aspects of the evolution and mineralisation of the Amo Younger Granite complex (northern Nigeria). *Chem. Geol.*, **40**, 293-312.

Imeokparia, E.G. 1986. Geochemical evolution of the metaluminous and peraluminous granites of Ganawuri granite complex, northern Nigeria. *J. Afr. Earth Sci.*, **5/2**, 193-200.

Irvine, T.N. 1980. Magmatic infiltration metasomatism, double-diffusive fractional crystallisation and adcumulus growth in the Muskox intrusion and other layered intrusions. *In*: Hargraves, R.B.(Ed.), *Physics of Magmatic Processes*, 325-384.

Irvine, T.N. 1981. Terminology for layered intrusions. *J. Petrology*, **23**, 127-162.

Janecka, J. and Stemprok, M. 1967. Endogenous tin mineralisation in the Bohemian Massif. *A technical conference on tin*. London Intern. Tin Council, **1**, 245-265.

Judd, J.W. 1897. On the petrology of Rockall. *Trans. Roy Irish Acad.*, **31**, 48-58.

Kinnaird, J.A. 1984. Contrasting styles of Sn-Nb- Ta-Zn mineralisation in Nigeria. *J. Afr. Earth Sci.*, **2**, 81-90.

Kinnaird, J.A. 1985. Hydrothermal alteration and mineralisation of the alkaline anorogenic ring complexes of Nigeria. *J. Afr. Earth Sci*., **3** (1/2), 229-251.

Kinnaird, J.A., Bowden, P., Ixter, R.A. and Odling, N.W.A. 1985. Mineralogy, geochemistry and mineralisation of the Ririwai complex, northern Nigeria. *J. Afr. Earth Sci.*, **3** (1/2), 185-222.

Kinnaird, J.A., Batchelor, R.A., Whitley, J.E. and Mackenzie, A.B. 1985a. Geochemistry, mineralization and hydrothermal alteration of the Nigerian high heat producing granites. *In*: *High heat production (HHP) granites, hydrothermal circulation and ore genesis*. The Institution of Mining and Metallurgy, 169-195.

Korzhinskii, D.S. 1970. *Theory of metasomatic zoning*. Oxford Clarendon Press, 162pp.

Lacroix, A. 1923. Sur la signification des granites alcalins très riches en soude. *C.R. Acad. Sci. Fr*., **177**, 417-422.

Lameyre, R.B.J. and Bonin, B. 1985. The structural setting of alkaline complexes. *J. Afr. Earth Sci.*, **3**(1/2), 5-16.

Larsen, E.S. 1938. Some new variation diagrams for groups of igneous rocks. *J. Geol.*, **46**, 505-520.

Larsen, L.M. and Sorenson, H. 1987. The Ilimaussag intrusion - progressive crystallization and formation of layering in an agpaitic magma. *In*: Fitton, J.G. and Upton, B.J. (Eds), *Alkaline Igneous rocks*. Geol. Soc. Spec. Publ., **30**, 473-488.

Leake, B.A. 1965. The relationship between tetrahedral aluminium and the maximum possible octahedral aluminium in natural calciferous and sub-calciferous amphiboles. *Am. Mineral.*, **50**, 843-851.

Leake, B.A. 1978. Nomenclature of amphiboles. *Am. Miner.*, **63**, 1023-1052.

Linning, K. 1968. *Die Stollingskompeks Kaap Kruis, Suidwes-Afrika*. M.Sc. thesis, Univ. Pretoria, 108pp.

Lister, C.J. 1978. " Luxullianite in situ within the St. Austell granite, Cornwall". *Mineral. Mag.*, **42**, 295-297.

Loiselle, M.C. and Wones, D.R. 1979. Characteristics and origin of anorogenic granites. *Geol. Soc. Am., Abs. Prog*., **11**, 468 pp.

London, D.L., Hervig, R.L. and Morgan, G.B.,VI. 1988. Melt vapor solubilities and elemental partitioning in peraluminous granite-pegmatite systems: experimental results with Macusani glass at 200 MPa. *Contrib. Mineral. Petrol*., **99**, 360-373.

Marsh, J.S. 1973. Relations between transform directions and alkaline igneous rock lineaments in Africa and South America. *Earth Planet Sci. Lett.*, **18**, 317-323.

McBirney, A.R. and Noyes, R.M. 1979. Crystallisation and layering of the Skaergaard intrusion. *J. Petrology*, **20**, 487-554.

McKie, D. 1966. Fenitisation. *In*: Tuttle, O.F. and Gittins, J. (Eds), *Carbonatites*, 261-294. John Wiley & Sons.

Milner. S.C. 1988. *The Geology and Geochemistry of the Etendeka Formation Quartz Latites, Namibia*. Ph. D. thesis, Univ. of Cape Town, 263pp.

Nemec, D. 1975. Genesis of tourmaline spots in leucocratic granites. *N. Jb. Miner. Mh*., **7**, 308-317.

Neumann, E.R. 1976. Compositional relation among pyroxenes, amphiboles and other mafic phases in the Oslo Region plutonic rocks. *Lithos,* **9/2**, 85-109.

Parker, R.L. and Fleischer, M. 1968. Geochemistry of Niobium and Tantalum. *Geol. Surv. Prof. Paper*, **612**, 43pp.

Pirajno, F. 1987. A fossil hot spring system in the Brandberg Complex, Damara Province, SWA/Namibia. *S. Afr. J. Geol.*, **90**, 509-513.

Pollard, P.J., Pichavant, M. and Charoy, B. 1987. Contrasting evolution of flourine- and boron-rich systems. *Mineral. Deposita*, **22**, 315-321.

Prins, P. 1981. The geochemical evolution of the alkaline and carbonatite complexes of the Damaraland Igneous Province, South West Africa. *Annals Univ. Stellenbosch, Series A1 (Geology*), **3**, 145-278.

Quin, J.-P. 1962. La lindinosite (granite mésocrate à riebeckite) du massif d'Evisa (Corse). *Bull. Soc. Grol. Fr.*, **4**, 380-383.

Radain, A.A.M., Fyfe, W.S. and Kerrich, R. 1981. Origin of peralkaline granites of Saudi Arabia. *Contrib. Mineral. Petrol*., **78**, 358-366.

Rock, N.M.S. and Leake, B.E. 1984. The International Mineralogical Association amphibole nomenclature scheme: computerisation and its consequences. *Miner. Mag.*, **48**, 211-227.

Robinson, P. 1980. The composition space of terrestrial pyroxenes - Internal and external limits. *In*: Prewitt, C.T. (Ed.), *Pyroxenes*, Rew. Miner., **7**, 419-494, Geol. Soc. Am.

Robinson, P., Spear, F.S., Schumacher, J.C., Laird, J., Klein, C.,

Evans, B.W. and Doolan. B.L. 1982. Phase relation of metamorphic amphiboles: Natural occurrences and theory. *In*: Veblen, D.R. and Ribbe, P.H. (Eds), *Amphiholes: Petrology and Experimental Phase Relations*, **9B**, 1-227, Mineral. Soc. Am.

Rose, A.W. and Burt, D.M. 1979. Hydrothermal alteration. *In*: Barnes. H.L. (Ed.) *Geochemistry of Hydrothermal Ore Deposits*, 173-235. New York (Wiley).

Rosenbusch. H. 1910. *Elemente der Gesteinslehre*. 3th. ed. Schweitzerbart, Stuttgart, 692pp.

Schlag. C. and Willgallis, A. 1988. Short Communication. Similarities in tin mineralisation associated with the Brandberg granite of SWA/Namibia and granites in northern Nigeria. *J. Afr. Earth Sci*., **7/1**, 307-310.

Shcherba, G.N. 1970. Greisens. *Int. geol. Rev.*, **12**, 114-150.

Siedner. G. and Miller, J.A. 1968. K/Ar age determinations on basaltic rocks from South-West Africa and their bearing on continental drift. *Earth planet. Sci. Lett.*, **4**(6), 451-458.

Siedner, G. and Mitchell, J.G. 1976. Episodic Mesozoic volcanism in Namibia and Brazil: A K/Ar isochron study bearing on the opening of the South Atlantic. *Earth planet. Sci. Lett*., **30**(2), 292-302.

Simpson, P.R., Brown, G.C., Plant, J. and Ostle, D. 1979. Uranium mineralisation and granite magmatism in the British Isles. *Phil. Trans. R. Soc., London*, **A291**, 385-412.

Smirnov, V.L 1976. *Geology of mineral deposits*. Moskow, MIR publications, 520pp.

Sörensen, H. 1969. Rhythmic layering in peralkaline intrusions. *Lithos,* **2**, 261-283.

Speer, J.A. 1984. Micas in igneous rocks. *In*: Bailey, S.W. (Ed.), *Micas. Reviews in mineralogy*, **13**, Mineral. Soc. Am., 299-356.

Stemprok, M. 1987. Greisenisation (a review). *Geol. Rundsh*., **76/1**, 169-175.

Stemprok, M. and Sulcek, Z. 1969. Geological profile through an ore bearing lithium granite. *Econ. Geol.*, **64**, 392-404.

Stone, M. and Exley, C.S. 1985. High heat production granites of SW-England and their associated mineralisation: a review. *In*: *High heat production (HHP) granites, hydrothermal circulation and ore genesis*. The Institution of Mining and Metallurgy, 571-593.

Taylor, R.G. 1979. *Geology of tin deposits*. Amsterdam Elsevier, 543pp.

Teale, G.S. and Lottermoser, B.G. 1987. Palaeozoic granites of the Umberatana region, South Australia: the role of volatiles in the crystallisation of some alkaline-peralkaline granites. *Geol. Rdsch*., **76/3**, 857-868.

Tischendorf, G. 1977. Geochemical and petrographic characteristics of silicic magmatic rocks with rare element mineralisation. *In*: Stemprok, M., Bumol, L. and Tischendorf, G. (Eds),. *Metallisation Associated with Acid Magmatism*. (MAWAM). Geol. Surv. Prague, **2**, 41-96.

Tröger, W.E. 1969. *Optische Bestimmung der gesteinsbildenden Minerale*. 2th. ed., Schweizerbart, Stuttgart, 823pp.

Turner, J.S. and Chen, C.F. 1974. Two-dimentional effects in double-diffusive convection. *J. Fluid Mechanics*, **63**, 577-592.

Tuttle, O.F. and Bowen, N.L. 1958. Origin of granite in the light of experimental studies in the system $NaAlSi_3O_5$ - SiO_2 - H_2O. *Geol. Soc. Amer. Mem*., **74**, 153 pp.

Van Breemen, O. and Bowden, P. 1973. Sequential age trends for some Nigerian Mesozoic granites. *Nature,* **242**, 9-11.

Von Knorring, O. 1985. A note on tin-tantalum pegmatites in the Damara Orogen and alkali rocks associated with the Brandberg Complex. *Communs geol. Surv. S.W. Africa/Namibia*, **2**, 63-64.

Wilson, J.R. and Larsen, B. 1985. Two dimensional study of a layered intrusion - the Hyllingen Series, Norway. *Geol. Mag.*, **122**, 97-121.

Wones, D.R. and Eugster, H.P. 1965. Stability of biotite: experiment, theory, and applications. *Am. Mineral*., **50**, 1228-1272.

Wones, D.R. and Gilbert, M.C. 1982. Amphiboles in the igneous environment. *In*: Veblen, D.R. and Ribbe, P,H. (Eds), *Amphiboles: Petrology and Experimental Phase Relations*, 355-390, Mineral. Soc. Am.

Zaykov, V.V, Udachin. V.N. and Sinyakovskaya IV. 1988. Pyrophyllite deposits. *Int. Geol. Rev*., **30**, 90-103.

Zuleger, E. 1987. *Geochemische und petrographische Untersuchungen am Messum und Cape Cross Ringkomplex in Namibia*. Diploma thesis, Univ. Giessen, 92 pp.

13. Appendix

The following tables give the composition of Brandberg granitoids and of associated mineral phases.

In addition, a few whole rock analyses (Schlag and Willgallis(1988) [CH] and Von Knorring [VK], open file report, Geological Survey SWA/Namibia) have been used in the geochemical variation diagrams to complete the list of geochemical data on Brandberg granites.

Analytical methods:

Mineral analyses have been carried out at the Department of Geochemistry, University of Cape Town using a Cameca Camebax wavelenghts-dispersion, 4-spectrometer microprobe operating at 15 kV, with a probe current of 40nA and 20nA for flourine-bearing minerals and a counting time of 10sec per measurement. A mixture of natural standards and pure metal standards for Ta and Nb were used.

Structural formulas and estimations of Fe^{3+}/Fe^{2+} have been caluclated using the microcomputer program MINFILE (Afifi and Essene, 1988).

Major whole rock and trace elemental analyses were carried out by the Geological Survey of South Africa, Pretoria, the Institut für Geowissenschaften, Mineralogie Johannes Gutenberg Universität Mainz, the Department of Geochemistry, University of Cape Town and the Geological Survey of Namibia, using XRF, AAS and ICP-techniques available at the different laboratories.

Sn, Li and B are determined by AAS (Perkin-Elmer 402, Geological Survey, Windhoek and ICP (Mineralogie Mainz).

Major oxide concentrations are given in weight per cent, trace elements in ppm.

Fe_2O_3 = total iron as Fe_2O_3
FeO = determined volumetrically
H_2O = loss at 110^o
LOI = loss at 1000^o
NA = not analysed
\- = below LLD

TABLE 1: Analyses and CIPW Norms of Brandberg Granites

	MD12	MD195	MD50	MD51	MD53	MD54		MD107	MD211	MD213	MD215	MD237
SiO_2	60.69	61.61	69.31	65.28	69.20	67.64	SiO_2	70.20	66.59	68.85	68.82	69.82
TiO_2	0.91	1.36	0.66	0.94	0.66	0.67	TiO_2	0.57	0.89	0.61	0.61	0.54
Al_2O_3	13.79	13.62	13.52	14.45	14.08	14.32	Al_2O_3	12.84	13.43	12.83	12.77	12.75
Fe_2O_3	4.96	3.71	3.98	2.82	2.12	2.38	Fe_2O_3	5.50	7.02	5.68	5.68	5.13
FeO	4.95	4.30	1.74	3.97	2.42	3.39	MnO	0.10	0.11	0.11	0.10	0.09
MnO	0.18	0.19	0.14	0.15	0.24	0.19	MgO	0.31	0.78	0.36	0.33	0.30
MgO	0.86	1.03	0.22	0.69	0.24	0.28	CaO	1.64	2.71	1.75	1.68	1.59
CaO	3.52	3.54	1.51	2.45	1.23	1.52	Na_2O	3.34	3.47	3.37	3.61	3.53
Na_2	03.95	3.82	3.84	3.97	4.06	4.00	K_2O	5.13	4.31	4.78	4.85	4.87
K_2O	4.28	4.85	4.23	4.53	4.84	4.93	P_2O_5	0.10	0.26	0.12	0.12	0.10
P_2O_5	0.56	0.46	0.11	0.24	0.11	0.13	H_2O^-	0.08	0.17	0.18	0.19	0.16
CO_2	0.23	0.20	0.31	0.26	0.26	0.33	LOI	0.25	0.28	1.36	1.17	1.44
H_2O^+	0.95	1.02	0.22	0.47	0.5?	0.45						
H_2O^-	0.22	0.27	0.03	0.05	0.05	0.05						
TOTAL	100.05	99.98	99.82	100.27	100.79	100.21	TOTAL	100.06	100.02	100.00	99.93	100.32
Li	41	40	20	15	-	15	Zn	108	101	117	99	95
Zn	155	194	230	120	143	157	Rb	196	155	150	158	181
Rb	125	133	171	151	155	168	Sr	138	208	156	147	118
Sr	209	218	147	212	163	161	Y	72	67	69	70	69
Y	70	77	62	57	61	63	Nb	48	40	46	47	47
Nb	55	56	40	33	41	41	Zr	422	377	410	410	409
Ta	<5	<5	2	4	4	4	Pb	18	18	19	24	18
Sn	3	3	NA	NA	NA	NA	Th	23	19	22	22	24
Zr	373	400	385	352	388	387	U	5	4	4	6	5
Pb	16	16	22	42	20	25	Ba	955	914	929	942	911
Th	12	15	23	21	22	21						
U	3	4	6	4	5	5						
Ba	811	797	NA	NA	NA	NA						
F	NA	NA	700	950	1100	1100						
Q	14.00	13.78	28.33	18.40	24.56	21.26	Q	27.93	24.33	27.39	26.13	27.58
Co	-	-	0.84	-	0.77	0.53	C	-	-	-	-	-
Z	0.07	0.08	0.08	0.07	0.08	0.08	Z	0.08	0.08	0.08	0.08	0.08
Or	25.29	28.66	25.00	26.77	28.60	29.13	O	30.31	25.47	28.25	28.66	28.78
Ab	33.42	32.32	32.49	33.59	34.35	33.85	A	28.26	29.36	28.52	30.55	29.87
An	7.26	5.69	4.86	8.23	3.79	5.10	An	4.89	8.34	5.76	4.32	4.56
Di%Wo	2.22	3.27	-	0.33	-	-	Di%Wo	0.52	0.41	0.28	0.73	0.57
Di%En	0.81	1.51	-	0.11	-	-	Di%En	0.45	0.36	0.24	0.63	0.49
Di%Fs	1.45	1.73	-	0.23	-	-	Hy%En	0.33	1.59	0.65	0.19	0.25
Hy%En	1.33	1.06	0.55	1.61	0.60	0.70	Il	0.21	0.24	0.24	0.24	0.19
Hy%Fs	2.37	1.21	-	3.45	1.05	3.51	Hm	5.50	7.02	5.68	5.68	5.13
Mt	7.19	5.38	4.15	4.10	4.36	3.45	Sp	1.12	1.88	1.19	1.22	1.08
Il	1.73	2.58	1.25	1.79	1.25	1.27	Ap	0.24	0.62	0.28	0.28	0.24
Hm	-	-	1.12	-	-	-						
Ap	1.33	1.09	0.26	0.57	0.26	0.31						
Cc	0.52	0.45	0.71	0.59	0.59	0.59						
TOTAL	98.99	98.81	99.64	99.84	100.28	99.78	TOTAL	99.84	99.69	98.57	98.68	98.83
agp. index	0.81	0.85	0.80	0.79	0.84	0.83	agp. index	0.86	0.77	0.84	0.88	0.87

TABLE 1: Analyses and CIPW Norms of Brandberg Granites (continued)

	MD101	MD 87	MD 94	MD 92	MD153	MD125		MD126	MD100	MD124	MD 90	MD118	MD140
SiO_2	73.84	75.95	71.76	72.43	74.00	75.95	SiO_2	74.23	74.31	75.51	74.81	81.21	72.39
TiO_2	0.26	0.08	0.29	0.26	0.32	0.16	TiO_2	0.15	0.29	0.15	0.25	0.26	0.26
Al_2O_3	12.49	12.53	14.34	14.17	12.15	12.41	Al_2O_3	13.75	12.01	12.04	12.72	11.65	10.60
Fe_2O_3	2.30	1.20	1.99	1.82	2.72	0.96	Fe_2O_3	0.96	2.41	1.52	1.50	1.18	5.81
MnO	0.07	0.04	0.03	0.05	0.07	0.01	MnO	0.02	0.06	0.04	0.02	0.01	0.04
MgO	0.24	0.15	0.67	0.57	0.23	0.14	MgO	0.31	0.22	0.16	0.19	0.11	0.22
CaO	0.82	0.51	1.39	1.22	0.89	0.58	CaO	1.19	0.78	0.63	0.33	0.15	0.40
Na_2O	3.86	4.23	3.60	2.98	3.12	3.31	Na_2O	4.24	3.48	3.89	3.12	0.10	3.38
K_2O	5.31	4.52	4.92	5.29	5.48	5.23	K_2O	4.79	5.51	5.27	5.36	0.12	4.80
P_2O_5	0.04	0.02	0.12	0.17	0.04	0.02	P_2O_5	0.09	0.03	0.02	0.03	0.03	0.03
LOI	0.65	0.50	1.25	0.84	0.58	0.57	LOI	0.59	0.51	0.45	0.97	4.46	0.78
TOTAL	99.88	99.73	100.35	99.80	99.59	99.34	TOTAL	100.32	99.62	99.67	99.31	99.28	98.72
Li	NA	NA	NA	NA	NA	NA	Li	NA	NA	NA	NA	NA	NA
Zn	73	33	59	62	70	51	Zn	30	80	57	22	12	546
Rb	300	643	225	232	265	360	Rb	183	258	381	266	10	732
Sr	47	3133	91	47	22		Sr	116	37	13	40	37	12
Y	68	69	66	46	87	50	Y	50	75	88	45	51	200
Nb	60	99	54	53	53	48	Nb	84	56	58	63	63	300
Ta	NA	NA	NA	NA	4	5	Ta	5	NA	6	NA	7	18
Sn	7	8	10	4	8	9	Sn	2	6	7	7	14	NA
W	NA	NA	NA	NA	1	7	W	4	NA	5	NA	7	14
Zr294	155	207	181	339	193		Zr	120	379	191	256	356	1184
Pb	NA	NA	NA	NA	25	27	Pb	41	NA	32	NA	17	43
Th	NA	NA	NA	NA	44	51	Th	39	NA	50	NA	45	37
U	NA	NA	NA	NA	9	16	U	28	ND	11	ND	7	37
Ba	395	-	719	408	353	154	Ba	463	465	56	350	-	15
Ga	NA	NA	NA	NA	26	29	Ga	21	NA	30	NA	31	44
Q	29.62	32.90	28.26	31.81	32.96	35.26	Q	28.65	31.62	31.89	35.19	75.41	33.71
Co	-	-	0.78	1.69	-	0.28	Co	-	-	-	1.23	9.47	-
Z	0.06	0.03	0.04	0.04	0.07	0.04	Z	0.02	0.08	0.04	0.05	0.07	0.25
Or	31.38	26.71	29.07	31.26	32.38	30.91	Or	28.31	32.56	31.14	31.67	1.00	28.36
Ab	32.66	35.79	30.46	25.22	26.40	28.01	Ab	35.88	29.45	32.59	26.40	11.25	27.80
An	1.07	1.86	6.30	5.05	2.96	2.79	An	4.34	0.88	-	1.52	0.66	-
Di%Wo	0.69	0.18	-	-	0.18	-	Wo	-	0.25	0.64	-	-	-
Di%En	0.60	0.15	-	-	0.16	-	Di%Wo	0.28	0.63	0.46	-	-	0.44
Hy%En	-	0.22	1.67	1.42	0.42	0.35	Di%En	0.24	0.55	0.40	-	-	0.38
Il	0.15	0.09	0.06	0.11	0.15	0.02	Hy%En	0.53	-	-	0.47	0.37	0.17
Hm	2.30	1.20	1.99	1.82	2.72	0.02	Il	0.04	0.13	0.09	0.04	0.02	0.09
Sp	0.44	0.09	-	-	0.59	-	Hm	0.96	2.41	1.42	1.50	1.24	5.54
Ru	-	-	0.26	0.20	-	0.15	Sp	0.31	0.55	0.26	-	-	0.53
Ap	0.09	0.05	0.28	0.40	0.09	0.05	Ru	-	-	-	0.23	0.26	-
							Ap	0.21	0.07	0.05	0.07	0.07	0.07
TOTAL	99.29	99.26	99.18	99.02	99.09	98.81	TOTAL	99.78	99.18	99.26	98.38	99.83	89.11
agp.index	0.97	0.95	0.78	0.75	0.91	0.89	agp.index	0.88	0.97	1.00	0.86	0.20	1.02

TABLE 1: Analyses and CIPW Norms of Brandberg Granites (continued)

	MD 1	MD 2	MD 5	MD 7	MD1 0	MD 4
SiO_2	80.79	71.35	72.48	71.60	70.15	73.24
TiO_2	-	0.11	0.12	-	0.11	-
Al_2O_3	8.25	10.00	11.72	10.50	9.96	10.04
Fe_2O_3	1.26	5.84	1.09	3.87	5.44	3.02
FeO	1.01	1.78	1.85	2.39	2.72	2.49
MnO	-	0.11	-	0.66	0.08	-
MgO	-	-	0.05	-	-	0.02
CaO	-	0.44	0.90	0.10	0.15	0.25
Na_2O	3.93	4.69	5.89	4.90	4.89	4.91
K_2O	3.77	4.88	5.94	5.16	5.01	4.63
P_2O_5	0.12	0.12	0.16	0.13	0.11	0.12
CO_2	0.05	0.08	0.23	0.07	0.08	0.18
H_2O^+	0.15	0.40	0.33	0.19	0.35	0.25
H_2O^-	0.06	0.10	0.11	0.07	0.05	0.09
TOTAL	99.39	99.90	99.87	99.64	99.10	99.24
Li	136	416	190	358	539	437
Zn	316	1008	91	941	961	814
Rb	757	679	260	1189	897	1265
Sr	4	8	23	7	10	5
Y	214	438	92	455	461	562
Nb	216	351	64	335	456	150
Ta	5	7	3	11	15	4
Sn	51	247	6	145	163	52
Zr	1269	1380	311	632	2913	594
Pb	45	25	32	90	88	18
Th	54	37	32	104	35	29
U	17	31	4	19	45	4
Ba	3	-	525	4	3	5
Q	47.92	27.57	24.22	25.65	24.27	30.38
Z	0.25	0.28	0.06	0.13	0.59	0.12
Or	22.28	28.84	35.10	30.49	29.61	27.36
Ab	21.45	24.27	27.21	25.28	23.34	25.87
Ac	3.65	13.58	3.15	11.20	15.74	8.74
Ns	1.79	-	4.43	0.81	0.04	1.34
D%Wo	-	0.37	0.87	-	-	-
Di%En	-	-	0.04	-	-	-
Di%Fs	-	0.42	0.94	-	-	-
Hy%En	-	-	0.09	-	-	0.05
Hy%Fs	1.85	1.92	2.26	5.62	4.96	4.58
Mt	-	1.66	-	-	-	-
Il	-	0.21	0.23	-	0.21	-
Ap	-	0.28	0.38	0.18	0.26	0.28
Cc	-	0.18	0.52	-	0.01	0.16
TOTAL	99.19	99.58	99.50	99.36	99.03	98.88
agp. index	1.28	1.30	1.37	1.30	1.35	1.30

	MD 38	MD 39	MD 40	MD 41	MD 42	MD 44
SiO_2	73.06	73.12	72.08	68.20	75.79	80.50
TiO_2	0.34	0.28	0.21	0.18	0.23	0.22
Al_2O_3	10.61	11.21	12.28	11.50	9.38	11.12
Fe_2O_3	2.88	3.11	2.72	1.44	5.98	0.42
FeO	1.61	1.44	2.43	2.42	-	-
MnO	0.12	0.13	0.09	0.20	0.11	0.03
MgO	-	-	-	2.10	-	0.10
CaO	-	-	-	0.08	-	-
Na_2O	6.95	5.04	6.23	8.51	3.12	7.34
K_2O	3.40	4.62	3.13	4.95	4.80	0.08
P_2O_5	0.01	0.01	0.04	0.32	0.02	0.02
H_2O^+	0.20	0.20	0.24	0.21	0.82	0.17
H_2O^-	0.02	0.02	0.03	0.03	0.28	0.01
CO_2	0.15	0.22	0.62	0.15	0.11	0.15
TOTAL	99.35	99.41	100.10	100.30	100.64	100.11
Li	690	460	570	540	320	-
Zn	1229	1120	754	776	982	36
Rb	898	1481	580	1034	666	8
Sr	10	10	5	11	12	32
Y	591	552	25	169	271	33
Nb	856	711	53	89	413	26
Ta	44	39	-	5	42	8
Zr	5867	3361	494	797	2598	77
Pb	9	10	35	18	23	165
Th	182	42	17	30	47	29
W	25	11	-	4	12	10
U	151	111	3	8	66	3
Ga	32	42	55	46	36	16
Ba	NA	NA	NA	NA	NA	NA
F	1800	3000	1650	3100	900	500
B	85	85	55	35	40	45
Q	28.06	27.42	23.70	16.03	40.22	39.94
Z	1.18	0.67	0.10	0.16	0.52	0.02
Or	20.09	27.30	18.50	29.25	28.36	0.47
Ab	35.65	31.94	45.74	31.59	21.52	56.75
Ac	8.33	9.00	6.15	4.17	4.30	1.22
Ns	3.19	0.11	-	8.33	-	0.93
Hy%En	-	-	-	5.23	-	0.25
Hy%Fs	2.62	2.42	3.79	4.52	-	-
Mt	-	-	0.86	-	-	-
Il	0.65	0.53	0.40	0.34	0.24	0.06
Hm	-	-	-	-	4.50	-
Ru	-	-	-	-	0.11	0.14
Ap	-	-	-	0.15	-	-
TOTAL	99.76	99.41	99.24	99.77	99.76	99.77
agp. index	1.42	1.18	1.11	1.68	1.10	1.09

TABLE 1: Analyses and CIPW Norms of Brandberg Granites (continued)

	MD 6	MD 9	MD 13	MD 3	MD 21	MD 8
SiO_2	75.30	72.89	75.72	70.38	70.53	69.71
TiO_2	0.07	0.21	0.19	0.25	0.27	-
Al_2O_3	10.68	9.33	8.59	12.83	12.59	16.32
Fe_2O_3	1.49	4.00	5.00	2.77	3.82	0.34
FeO	2.67	0.91	-	1.98	0.80	1.15
MnO	-	1.28	-	0.08	0.05	0.11
MgO	-	-	0.02	0.03	0.06	0.18
CaO	0.06	0.06	-	1.48	1.24	0.61
Na_2O	4.97	6.02	4.53	3.80	3.94	3.85
K_2O	3.52	2.33	2.35	5.64	5.82	6.66
P_2O_5	0.16	0.19	0.15	0.18	0.18	0.38
CO_2	0.10	0.13	0.12	0.07	0.10	0.10
H_2O^+	0.37	0.23	0.28	0.32	0.35	0.30
H_2O^-	0.12	0.07	0.16	0.11	0.05	0.10
TOTAL	99.51	97.65	97.11	99.92	99.80	99.81
Li	320	186	720	190	180	550
Zn	501	1860	405	146	126	119
Rb	613	939	675	219	206	252
Sr	8	7	4	76	85	4
Y	247	1474	618	86	92	56
Nb	739	967	2037	61	57	48
Ta	28	10	97			
Sn	464	1185	1298	7	7	15
Zr	4437	7719	11387	439	433	99
Pb	26	191	305	27	24	38
Th	114	361	155	24	21	15
U	89	81	314	4	4	3
Ba	3	6	5	809	899	281
Q	32.61	31.36	41.25	24.57	25.01	20.63
Co	-	-	-	-	-	2.78
Z	0.89	1.55	2.29	0.09	0.09	0.02
Or	20.80	13.77	13.89	33.33	34.39	39.36
Ab	35.34	35.02	31.10	32.15	32.36	32.58
An	-	-	-	1.29	-	-
Ac	4.31	11.57	6.37	-	0.87	-
Ns	0.42	0.65	-	-	-	-
Wo	-	-	-	0.89	2.14	-
Di%Wo	-	-	-	1.04	-	-
Di%Fs	-	-	-	1.08	-	-
Hy%En	-	-	0.05	0.07	-	0.45
Hy%Fs	4.79	3.72	-	-	-	2.04
Mt	-	-	-	4.02	1.96	0.49
Il	0.13	0.40	-	0.47	0.51	-
Hm	-	-	2.80	-	2.17	-
Ru	-	-	0.19	-	-	-
Ap	0.11	0.11	-	0.43	0.43	0.90
Cc	-	-	-	0.16	0.02	0.20
TOTAL	99.41	98.15	97.94	99.59	99.94	99.45
agp.index	1.12	1.33	1.16	0.96	0.82	1.00

	VK18O	VK181	VK182	VK183	CS184	CS185
SiO_2	69.26	70.79	70.21	75.96	69.58	69.90
TiO_2	0.54	0.47	0.45	0.45	0.44	0.49
Al_2O_3	13.19	12.99	13.04	13.08	13.23	13.10
Fe_2O_3	4.74	4.39	4.15	1.84	3.98	4.45
MnO	0.15	0.14	0.13	0.03	0.11	0.12
MgO	0.38	0.24	0.17	-	0.33	0.26
CaO	1.70	1.55	1.51	0.13	1.43	1.53
Na_2O	4.04	3.85	3.95	0.39	3.75	3.74
K_2O	5.03	5.01	5.10	4.07	5.09	5.12
P_2O_5	0.10	0.09	0.08	0.09	0.09	0.09
LOI	0.55	0.60	0.45	3.43	0.45	0.60
TOTAL	99.69	100.12	99.26	99.48	98.48	99.40
Li	NA	NA	NA	NA	NA	NA
Zn	108	137	100	20	91	125
Rb	208	209	200	172	238	259
Sr	119	113	128	44	110	115
Y	75	73	69	67	58	77
Nb	63	54	53	62	39	44
Sn	NA	NA	NA	NA	18	1020
Zr	416	424	445	469	361	460
Pb	32	26	27	16	28	45
Th	23	26	28	28	21	21
U	3	4	4	4	-	-
Ba	849	825	757	596	842	797
La	61	62	80	81	NA	NA
Ce	124	135	153	150	101	141
Q	23.54	26.53	25.07	58.00	25.41	25.75
Co	-	-	-	7.96		
Z	0.09	0.09	0.09	0.09	0.07	0.09
Or	29.72	29.61	30.14	24.05	30.08	30.26
Ab	34.19	32.58	33.42	3.30	31.73	31.65
An	3.00	3.37	3.77	0.19	4.23	3.84
Wo	0.45	0.50	0.49	-	-	0.14
Di%Wo	1.10	0.69	0.49	-	0.62	0.75
Di%En	0.95	0.60	0.42	-	0.54 0.65	
Hy%En	-	-	-	-	0.28	-
Il	0.32	0.30	0.28	0.06	0.30	0.26
Hm	4.74	4.39	4.15	1.8	3.98	4.45
Sp	0.91	0.77	0.74	-	0.69	0.87
Ru	-	-	-	0.42	-	-
Ap	0.42	0.21	0.19	0.21	0.21	0.21
TOTAL	99.23	99.64	99.25	96.12	98.14	98.92
agp.index	0.92	0.90	0.90	0.38	0.88	0.89

TABLE 1: Analyses and CIPW Norms of Brandberg Granites (continued)

	VK189	VK190	VK191	VK192	VK193	VK194
SiO_2	72.91	72.97	71.28	75.71	73.85	73.64
TiO_2	0.25	0.22	0.09	0.08	0.25	0.42
Al_2O_3	10.50	9.86	12.94	11.50	9.94	9.60
Fe_2O_3	5.32	5.12	2.40	1.70	4.82	4.72
MnO	0.10	0.12	0.06	0.05	0.11	0.09
MgO	0.01	0.10	0.03	0.02	0.01	0.09
CaO	0.07	0.26	0.08	0.23	0.10	0.07
Na_2O	5.11	5.07	5.26	4.85	6.07	7.70
K_2O	4.50	3.92	5.64	4.18	2.98	0.10
P_2O_5	0.04	0.02	0.02	0.07	0.04	0.05
LOI	0.35	0.60	0.34	0.45	0.24	0.70
TOTAL	99.16	98.26	98.14	98.84	98.41	97.18
Li	NA	NA	NA	NA	NA	NA
Zn	700	1002	436	259	1167	257
Rb	1024	1261	1636	966	687	600
Sr	12	31	7	11	3	8
Y	287	579	472	453	361	2173
Nb	294	1313	382	285	966	1547
Zr	1192	4207	3717	1741	6083	8867
Pb	200	126	161	98	153	934
Th	141	66	146	56	203	703
U	19	119	40	24	73	120
Ba	9	-	6	2	4	-
La	81	286	158	368	97	314
Ce	217	735	388	620	360	847
Q	29.13	31.01	21.20	32.39	31.16	31.77
Z	0.24	0.84	0.75	0.35	1.22	1.78
Or	26.59	23.16	33.33	24.70	17.61	0.59
Ab	28.96	28.89	35.16	35.88	34.02	48.82
Ac	12.58	12.34	6.94	4.45	13.49	13.66
Ns	-	-	0.34	-	0.35	0.19
Di%Wo	-	0.29	0.08	0.20	-	-
Di%En	-	0.25	0.07	0.05	-	-
Hy%En	0.02	-	-	-	0.02	0.22
Il	0.22	0.26	0.13	0.11	0.24	0.21
Hm	0.97	0.85	-	0.13	-	-
Sp	0.06	0.20	0.05	0.05	0.17	0.02
Ru	0.11	-	-	-	0.06	0.31
Ap	0.09	0.05	0.05	0.17	0.09	0.12
TOTAL	98.87	98.14	98.10	98.48	98.43	97.69
agp.index	1.26	1.28	1.14	1.09	1.34	1.3

TABLE 2: Microprobe Analyses
TABLE 2.1: Mica

	1	2	3	4	5	6
SiO_2	35.85	35.47	35.89	35.39	27.93	42.20
TiO_2	1.89	0.93	1.28	1.86	-	2.74
Al_2O_3	21.11	22.20	21.33	19.87	20.78	16.63
FeO	19.61	20.60	20.89	21.63	22.91	17.61
MnO	0.23	0.26	0.33	0.36	0.59	0.32
MgO	8.62	7.20	7.66	8.00	17.49	9.14
CaO	-	-	-	-	-	-
Na_2O	0.16	0.10	0.14	0.14	0.04	0.05
K_2O	9.14	9.41	9.13	9.35	-	8.73
F	1.94	1.78	1.47	1.70	0.56	1.26
less O = F	0.82	0.75	0.62	0.72	0.24	0.53
TOTAL	97.73	97.20	97.50	97.58	90.06	98.13
Structural formula calculated on the basis of 22 oxygens						
Si	5.354	5.350	5.388	5.365	4.429	6.101
Al^{IV}	2.646	2.650	2.612	2.635	3.571	1.899
Sum	8.000	8.000	8.000	8.000	8.000	8.000
Ti	0.312	0.104	0.145	0.210	-	0.298
Al^{VI}	1.071	1.297	1.163	0.916	0.314	0.935
Fe	2.449	2.599	2.623	2.742	3.038	2.130
Mn	0.029	0.033	0.042	0.046	0.079	0.039
Mg	1.919	1.618	1.714	1.807	4.134	1.969
Sum	5.681	5.652	5.686	5.723	7.566	5.372
Ca	-	-	-	-	-	-
Na	0.046	0.029	0.041	0.041	0.012	0.014
K	1.742	1.811	1.749	1.808	0.113	1.610
Sum^{Alk}	1.788	1.840	1.789	1.849	0.126	1.624
Mg/Mg+Fe	0.4392	0.3838	0.3952	0.3973	0.5763	0.4803
Fe/Fe+Mg	0.5606	0.6163	0.6047	0.6322	0.4235	0.5611

1 MD 8 (core)
2 MD 8 (rim)
3 MD 8
4 MD 8
5 MD 92 (core)
6 MD 92 (rim)

	7	8	9	10	11	12
SiO_2	37.45	37.47	36.84	36.56	37.15	47.42
TiO_2	3.42	1.74	3.67	3.07	3.06	0.42
Al_2O_3	17.21	11.54	12.79	14.50	14.48	19.95
FeO	19.86	34.37	30.50	29.82	31.35	14.74
MnO	0.49	0.63	0.51	0.73	1.00	-
MgO	9.84	3.73	5.38	3.18	3.12	0.34
CaO	0.04	tr	-	0.05	-	0.28
Na_2O	0.08	0.05	0.13	0.14	0.06	0.25
K_2O	9.38	8.17	8.36	8.64	8.47	8.81
F	1.23	0.45	0.75	1.27	1.45	0.46
less O=F	0.52	0.19	0.32	0.53	0.61	0.19
TOTAL	98.48	97.96	98.79	97.43	99.66	92.92.
Structural formula calculated on the basis of 22 oxygens						
Si	5.557	5.971	5.739	5.771	5.768	6.967
Al^{IV}	2.443	2.029	2.261	2.229	2.232	1.033
Sum	8.000	8.000	8.000	8.000	8.000	8.000
Ti	0.382	0.209	0.430	0.364	0.357	0.046
Al^{VI}	0.567	0.139	0.087	0.469	0.419	2.422
Fe	2.464	4.580	3.973	3.937	4.071	1.811
Mn	0.062	0.085	0.067	0.098	0.132	-
Mg	2.176	0.886	1.249	0.748	0.722	0.074
Sum	5.651	5.899	5.807	5.616	5.701	4.354
Ca	0.006	-	-	0.008	-	0.044
Na	0.023	0.015	0.039	0.043	0.018	0.071
K	1.776	1.661	1.661	1.740	1.678	1.651
Sum_{Alk}	1.805	1.676	1.701	1.791	1.696	1.767
Mg/Mg+Fe	0.4689	0.1621	0.2392	0.1597	0.1506	0.0395
Fe/Fe+Mg	0.5310	0.8379	0.7608	0.8403	0.8493	0.9605

7 MD 92
8 MD 5
9 MD 5
10 MD 125 (core)
11 MD 125 (core)
12 MD 125 (rim)

TABLE 2.1: Mica (continued)

	13	14	15	16	17	18
SiO_2	36.97	37.52	33.13	35.74	36.73	37.70
TiO_2	2.96	2.64	3.08	4.71	4.41	3.74
Al_2O_3	14.41	14.17	18.35	17.41	16.51	13.15
FeO	31.37	30.54	22.69	21.64	20.11	20.52
MnO	0.63	0.71	0.59	0.51	0.38	1.14
MgO	3.11	3.85	10.83	8.80	10.10	10.58
CaO	0.05	-	0.05	-	0.05	-
Na_2O	0.06	0.11	0.05	0.11	0.12	0.08
K_2O	8.64	8.31	5.52	8.75	8.82	9.37
F	1.27	1.57	0.59	0.84	1.10	1.74
less O=F	0.53	0.66	0.25	0.35	0.46	0.73
TOTAL	98.94	98.76	94.63	98.16	97.87	97.40
Structural formula calculated on the basis of 22 oxygens						
Si_{IV}	5.772	5.839	5.112	5.360	5.487	5.751
Al^{IV}	2.228	2.161	2.888	2.640	2.513	2.249
Sum	8.000	8.000	8.000	8.000	8.000	8.000
Ti_{VI}	0.350	0.309	0.357	0.531	0.495	0.429
Al^{VI}	0.424	0.439	0.450	0.439	0.394	0.115
Fe	4.096	3.975	2.928	2.714	2.512	2.618
Mn	0.083	0.094	0.077	0.065	0.048	0.147
Mg	0.724	0.893	2.490	1.967	2.248	2.409
Sum	5.676	5.710	6.303	5.716	5.698	5.714
Ca	0.008	-	0.008	-	0.008	-
Na	0.018	0.033	0.015	0.032	0.035	0.024
K	1.717	1.650	1.087	1.674	1.681	1.823
Sum^{Alk}	1.743	1.683	1.110	1.706	1.724	1.847
Mg/Mg+Fe	0.1501	0.1834	0.4596	0.4202	0.4723	0.4788
Fe/Fe+Mg	0.8497	0.8165	0.5404	0.5797	0.5277	0.5212

13 MD 125 (core)
14 MD 125 (rim)
15 MD 92
16 MD 92
17 MD 92
18 MD 101

	19	20	21	22	23	24
SiO_2	38.54	38.61	38.19	34.41	26.52	25.96
TiO_2	3.53	3.61	3.61	3.40	-	-
Al_2O_3	12.85	13.46	13.63	13.03	20.27	20.02
FeO	20.85	21.35	20.67	37.68	32.38	32.53
MnO	1.89	0.99	0.75	0.43	0.65	0.75
MgO	10.28	10.73	10.26	1.18	11.36	11.13
CaO	-	-	-	0.05	-	-
Na_2O	0.07	0.08	0.04	-	-	0.04
K_2O	9.29	9.17	9.48	8.33	-	-
F	2.21	1.89	1.79	-	-	-
less O=F	0.93	0.80	0.75	-	-	-
TOTAL	98.58	98.67	98.67	97.67	91.18	90.42
Structural formula calculated on the basis of 22 oxygens						
Si_{IV}	5.829	5.776	5.786	5.567	4.372	4.333
Al^{IV}	2.171	2.224	2.214	2.433	3.628	3.667
Sum	8.000	8.000	8.000	8.000	8.000	8.000
Ti_{VI}	0.402	0.406	0.411	0.414	-	-
Al^{VI}	0.120	0.150	0.220	0.053	0.312	0.273
Fe	2.637	2.671	2.619	5.098	4.464	4.542
Mn	0.242	0.125	0.096	0.059	0.091	0.106
Mg	2.317	2.392	2.317	0.285	2.791	2.769
Sum	5.718	5.744	5.664	5.908	7.658	7.691
Ca	-	-	-	0.009	-	-
Na	0.021	0.023	0.012	-	-	0.013
K	1.792	1.750	1.832	1.719	-	-
Sum^{Alk}	1.813	1.773	1.844	1.728	-	0.013
Mg/Mg+Fe	0.4677	0.4725	0.4694	0.0529	0.3847	0.3788
Fe/Fe+Mg	0.5322	0.5275	0.5305	0.9471	0.6152	0.6212

19 MD 101
20 MD 101
21 MD 101
22 MD 160
23 MD 68 (chloritised)
24 MD 68 (chloritised)

TABLE 2.1: Mica (continued)

	25	26	27	28	29	30		31	32	33	34	35	36
SiO_2	27.73	26.81	39.78	38.08	39.46	36.36	SiO_2	37.06	36.07	24.92	25.47	35.70	36.73
TiO_2	-	-	1.65	1.10	1.75	1.16	TiO_2	2.77	2.22	-	0.11	4.68	3.94
Al_2O_3	19.73	20.42	7.29	7.84	7.94	21.09	Al_2O_3	15.54	20.68	21.21	22.11	14.04	13.14
FeO	30.61	32.44	35.75	37.28	33.31	19.50	FeO	21.53	10.03	33.85	34.02	17.57	21.68
MnO	0.60	0.63	1.39	1.52	1.28	0.36	MnO	0.16	0.25	0.37	0.02	-	0.97
MgO	12.5	11.98	0.98	0.51	0.93	8.02	MgO	10.02	8.63	9.14	9.15	13.49	9.71
CaO	-	-	-	-	0.07	-	CaO	-	-	-	-	0.06	-
Na_2O	0.05	-	-	-	0.07	0.13	Na_2O	0.15	0.15	-	-	0.16	0.06
K_2O	-	-	8.84	8.88	8.37	9.56	K_2O	9.34	9.40	0.03	-	9.19	9.43
F	-	-	3.57	3.06	3.10	2.12	F	2.51	2.25	-	-	0.25	1.49
less O=F	-	-	1.50	1.29	1.31	0.89	less O=F	1.06	0.95	-	-	0.21	0.63
TOTAL	90.71	92.28	97.59	96.98	94.94	97.41	TOTAL	98.02	98.73	89.52	90.88	94.93	96.52
Structural formula calculated on the basis of 22 oxygens							Structural formula calculated on the basis of 22 oxygens						
Si	4.511	4.361	6.575	6.416	6.607	5.471	Si	5.625	5.682	4.230	4.235	5.448	5.686
Al^{IV}	3.489	3.639	1.425	1.584	1.393	2.529	Al^{IV}	2.375	2.318	3.770	3.765	2.552	2.314
Sum	8.000	8.000	8.000	8.000	8.000	8.000	Sum	8.000	8.000	8.000	8.000	8.000	8.000
Ti	-	-	0.205	0.139	0.220	0.131	Ti	0.316	0.263	-	0.014	0.537	0.459
Al^{VI}	0.296	0.277	-	-	0.174	1.212	Al^{VI}	0.406	1.523	0.474	0.569	-	0.084
Fe	4.165	4.413	4.942	5.253	4.664	2.402	Fe	2.733	1.321	4.805	4.731	2.242	2.807
Mn	0.093	0.087	0.195	0.217	0.182	0.046	Mn	0.021	0.033	0.053	0.003	0.003	0.127
Mg	3.045	2.904	0.241	0.128	0.232	1.798	Mg	2.267	2.026	2.312	2.267	3.068	2.240
Sum	7.589	7.681	5.578	5.711	5.472	5.590	Sum	5.742	5.167	7.645	7.584	5.824	5.716
Ca	-	-	-	-	0.013	-	Ca	-	-	-	-	0.010	-
Na	0.016	-	-	-	0.023	0.038	Na	0.044	0.046	-	-	0.047	0.018
K	0.016	-	1.864	1.909	1.823	1.873	K	1.809	1.889	0.006	-	1.789	1.862
Sum^{Alk}	0.016	-	1.864	1.909	1.823	1.873	Sum^{Alk}	1.853	1.935	0.006	-	1.846	1.880
Mg/Mg+Fe	0.4224	0.3969	0.0466	0.0238	0.0474	0.4281	Mg/Mg+Fe	0.4534	0.6053	0.3249	0.3240	0.5777	0.4439
Fe/Fe+Mg	0.5774	0.6031	0.9535	0.9762	0.9526	0.5719	Fe/Fe+Mg	0.5466	0.3946	0.6751	0.6759	0.4222	0.5561

25 MD 68 (chloritised)
26 MD 68 (chloritised)
27 MD 6
28 MD 6
29 MD 6
30 MD 8

31 MD 8
32 MD 8
33 MD 47
34 MD 47
35 MD 166
36 MD 101

TABLE 2.1: Mica (continued)

	37	38	39	40	41	42
SiO_2	36.86	36.82	38.53	35.00	36.77	35.66
TiO_2	1.90	1.68	0.98	2.38	1.94	2.01
Al_2O_3	19.28	19.19	20.89	18.49	19.28	18.39
FeO	29.27	28.40	25.15	31.19	29.69	30.65
MnO	0.83	0.89	0.82	0.45	0.76	0.65
MgO	0.62	0.64	0.63	0.59	0.61	0.73
CaO	-	-	-	-	-	-
Na_2O	0.11	0.17	0.12	0.13	0.10	0.10
K_2O	8.95	9.18	9.07	8.98	8.93	9.13
F	2.28	2.47	3.02	2.34	2.69	2.44
less O=F	0.96	1.03	1.27	0.99	1.13	1.03
TOTAL	99.14	98.41	97.94	99.01	99.64	98.73
Structural formula calculated on the basis of 22 oxygens						
Si	5.687	5.721	5.885	5.521	5.668	5.601
Al^{IV}	2.312	2.279	2.115	2.479	2.332	2.399
Sum	8.000	8.000	8.000	8.000	8.000	8.000
Ti	0.220	0.198	0.113	0.282	0.225	0.237
Al^{VI}	1.194	1.237	1.646	0.959	1.171	1.007
Fe	3.777	3.691	3.212	4.114	3.827	4.026
Mn	0.108	0.117	0.106	0.060	0.099	0.086
Mg	0.143	0.148	0.143	0.139	0.140	0.171
Sum	5.442	5.389	5.221	5.554	5.463	5.528
Ca	-	-	-	-	-	-
Na	0.033	0.051	0.036	0.040	0.030	0.030
K	1.762	1.820	1.767	1.807	1.756	1.830
Sum^{Alk}	1.795	1.871	1.803	1.847	1.786	1.860
Mg/Mg+Fe	0.0364	0.0386	0.0427	0.0326	0.0353	0.0407
Fe/Fe+Mg	0.9635	0.9614	0.9573	0.9673	0.9467	0.9592

37 MD 111
38 MD 111 (core)
39 MD 111 (rim)
40 MD 111
41 MD 111
42 MD 111

TABLE 2.2: Astrophyllite

	1	2	3	4
SiO_2	34.95	34.66	34.95	36.80
TiO_2	10.81	10.86	10.25	10.48
Al_2O_3	0.10	0.13	0.09	0.18
FeO	25.85	26.16	25.83	25.70
MnO	6.09	6.19	6.11	6.39
MgO	-	0.38	-	0.06
CaO	0.14	1.15	0.08	0.12
Na_2O	2.77	2.70	2.69	3.02
K_2O	4.55	4.60	4.68	4.55
ZnO	5.03	5.18	5.02	5.16
SnO_2	0.31	0.12	0.19	0.21
Nb_2O_5	0.87	1.03	0.82	0.85
F	1.60	1.56	1.44	1.47
less O=F	0.67	0.66	0.61	0.62
TOTAL	92.40	94.06	91.54	94.36

TABLE 2.3: Amphibole
Sodic Amphibole

	1	2	3	4	5	6		7	8	9	10	11	12
SiO_2	52.34	53.00	51.90	52.66	52.22	53.03	SiO_2	52.45	52.39	52.50	49.85	50.44	50.43
TiO_2	1.17	1.14	1.77	1.26	0.88	1.45	TiO_2	0.87	1.14	0.81	0.97	0.75	1.09
Al_2O_3	0.45	0.43	0.51	0.66	0.72	0.48	Al_2O_3	0.66	0.65	0.66	0.60	0.49	0.59
FeO	26.79	26.08	27.15	28.48	26.21	26.16	FeO	25.86	27.05	26.20	32.94	32.54	32.10
MnO	1.55	1.47	1.46	1.24	1.73	1.56	MnO	1.61	1.55	1.62	0.71	0.66	0.83
MgO	0.11	0.25	0.07	-	0.25	0.17	MgO	0.33	0.08	0.27	0.72	0.55	0.36
CaO	-	-	-	0.07	-	-	CaO	-	0.05	-	0.12	0.06	0.09
Na_2O	8.78	8.78	8.80	9.01	8.74	8.51	Na_2O	8.61	8.82	8.93	7.01	6.57	7.24
K_2O	1.84	1.75	1.76	1.26	1.89	1.87	K_2O	1.87	1.30	1.90	1.51	1.46	1.39
ZnO	3.81	4.17	3.67	2.93	4.17	4.30	ZnO	4.36	3.62	4.37	0.96	0.91	0.87
F	2.51	3.16	2.94	2.68	3.31	2.76	F	3.01	2.96	2.97	1.81	1.41	1.71
less O=F	1.06	1.33	1.24	1.13	1.39	1.16	less O=F	1.27	1.25	1.25	0.76	0.59	0.72
TOTAL	98.83	98.90	98.79	99.12	98.73	99.22	TOTAL	98.36	98.36	98.98	96.46	95.25	95.98
Structural formula calculated on the basis of 15 cations							Structural formula calculated on the basis of 15 cations						
Si	7.97	8.05	7.90	7.96	7.94	8.04	Si	8.00	8.00	7.94	7.82	8.03	7.94
Al^{IV}	0.03	-	0.09	0.04	0.06	-	Al^{IV}	-	-	0.06	0.11	-	0.06
Fe^{3+}	-	-	0.01	-	-	-	Fe^{3+}	-	-	-	0.07	-	-
Sum T	8.00	8.05	8.00	8.00	8.00	8.04	Sum T	8.00	8.00	8.00	8.00	8.03	8.00
Al^{VI}	0.05	0.08	-	0.08	0.07	0.09	Al^{VI}	0.12	0.12	0.05	-	0.09	0.05
Fe^{3+}	2.26	2.09	2.24	2.16	2.33	1.96	Fe^{3+}	2.19	2.09	2.41	1.98	1.60	1.85
Ti	0.13	0.13	0.20	0.14	0.10	0.17	Ti	0.10	0.13	0.09	0.11	0.09	0.13
Mg	0.02	0.06	0.02	-	0.06	0.04	Mg	0.08	0.02	0.06	0.17	0.13	0.08
Fe^{2+}	1.15	1.22	1.21	1.44	1.01	1.36	Fe^{2+}	1.11	1.37	0.91	2.27	2.73	2.38
Zn	0.43	0.47	0.41	0.33	0.47	0.48	Zn	0.49	0.41	0.49	0.11	0.11	0.10
Mn	0.20	0.19	0.19	0.16	0.22	0.20	Mn	0.21	0.20	0.21	0.09	0.09	0.11
Ca	-	-	-	0.01	-	-	Ca	-	0.01	-	0.02	0.01	0.02
Sum C	4.25	4.23	4.26	4.32	4.26	4.29	Sum C	4.29	4.34	4.22	4.76	4.85	4.71
Fe^{2+}	-	-	-	-	-	-	Fe^{2+}	-	-	-	-	-	-
Zn	-	-	-	-	-	-	Zn	-	-	-	-	-	-
Mn	-	-	-	-	-	-	Mn	-	-	-	-	-	-
Ca	-	-	-	0.01	-	-	Ca	-	0.01	-	0.02	0.01	0.02
Na	2.00	2.00	2.00	1.99	2.00	2.00	Na	2.00	1.99	2.00	1.98	1.99	1.98
Sum B	2.00	2.00	2.00	2.00	2.00	2.00	Sum B	2.00	2.00	2.00	2.00	2.00	2.00
Na	0.59	0.58	0.60	0.65	0.58	0.50	Na	0.55	0.62	0.62	0.15	0.04	0.22
K	0.36	0.34	0.34	0.24	0.37	0.36	K	0.36	0.25	0.37	0.30	0.30	0.28
Sum A	0.95	0.92	0.94	0.89	0.94	0.86	Sum A	0.91	0.87	0.98	0.45	0.34	0.50

1- 4 MD 55 zincian arfvedsonite
5- 6 MD 9 zincian arfvedsonite

7- 9 MD 13a zincian arfvedsonite
10-12 MD 6 arfvedsonite

Sodic Amphibole (continued)

	13	14	15	16	17
SiO_2	52.04	51.06	49.85	51.37	51.69
TiO_2	1.14	1.34	1.16	1.25	1.37
Al_2O_3	0.31	0.67	0.97	0.43	0.36
FeO	30.87	31.90	30.48	31.67	31.15
MnO	0.57	0.64	0.56	0.57	0.60
MgO	0.43	0.27	0.36	0.30	0.27
CaO	0.06	0.11	1.90	0.09	0.07
Na_2O	9.26	9.51	9.49	9.55	9.30
K_2O	1.94	1.48	1.51	1.78	1.91
ZnO	0.84	0.90	0.55	0.51	0.88
F	2.42	2.46	3.50	2.49	2.37
less O=F	1.02	1.04	1.47	1.05	1.00
TOTAL	98.86	99.30	98.86	98.94	98.97
Structural formula calculated on the basis of 15 cations					
Si	7.81	7.64	7.49	7.69	7.76
Al^{IV}	0.05	0.12	0.17	0.08	0.06
Fe^{3+}	0.14	0.24	0.34	0.23	0.18
Sum T	8.00	8.00	8.00	8.00	8.00
Al^{VI}	0.06	0.13	0.18	0.08	0.07
Fe^{3+}	-	-	-	-	-
Ti	0.13	0.15	0.13	0.14	0.15
Mg	0.10	0.06	0.08	0.07	0.06
Fe^{2+}	1.13	1.05	0.59	1.00	1.12
Zn	0.09	0.10	0.06	0.06	0.10
Mn	0.07	0.08	0.07	0.07	0.08
Ca	0.01	0.02	0.31	0.01	0.01
Sum C	4.14	4.16	4.15	4.09	4.13
Fe^{2+}	-	-	-	-	-
Zn	-	-	-	-	-
Mn	-	-	-	-	-
Ca	0.01	0.02	0.31	0.01	0.01
Na	1.99	1.98	1.69	1.99	1.99
Sum B	2.00	2.00	2.00	2.00	2.00
Na	0.70	0.78	1.07	0.79	0.72
K	0.37	0.28	0.29	0.34	0.37
Sum A	1.07	1.06	1.36	1.13	1.09

13-14 MD 10 arfvedsonite
15-17 MD 156 arfvedsonite

TABLE 2.3: Amphibole
Sodic Amphibole

	1	2	3	4	5	6		7	8	9	10	11	12
SiO_2	52.34	53.00	51.90	52.66	52.22	53.03	SiO_2	52.45	52.39	52.50	49.85	50.44	50.43
TiO_2	1.17	1.14	1.77	1.26	0.88	1.45	TiO_2	0.87	1.14	0.81	0.97	0.75	1.09
Al_2O_3	0.45	0.43	0.51	0.66	0.72	0.48	Al_2O_3	0.66	0.65	0.66	0.60	0.49	0.59
FeO	26.79	26.08	27.15	28.48	26.21	26.16	FeO	25.86	27.05	26.20	32.94	32.54	32.10
MnO	1.55	1.47	1.46	1.24	1.73	1.56	MnO	1.61	1.55	1.62	0.71	0.66	0.83
MgO	0.11	0.25	0.07	-	0.25	0.17	MgO	0.33	0.08	0.27	0.72	0.55	0.36
CaO	-	-	-	0.07	-	-	CaO	-	0.05	-	0.12	0.06	0.09
Na_2O	8.78	8.78	8.80	9.01	8.74	8.51	Na_2O	8.61	8.82	8.93	7.01	6.57	7.24
K_2O	1.84	1.75	1.76	1.26	1.89	1.87	K_2O	1.87	1.30	1.90	1.51	1.46	1.39
ZnO	3.81	4.17	3.67	2.93	4.17	4.30	ZnO	4.36	3.62	4.37	0.96	0.91	0.87
F	2.51	3.16	2.94	2.68	3.31	2.76	F	3.01	2.96	2.97	1.81	1.41	1.71
less O=F	1.06	1.33	1.24	1.13	1.39	1.16	less O=F	1.27	1.25	1.25	0.76	0.59	0.72
TOTAL	98.83	98.90	98.79	99.12	98.73	99.22	TOTAL	98.36	98.36	98.98	96.46	95.25	95.98
Structural formula calculated on the basis of 15 cations							Structural formula calculated on the basis of 15 cations						
Si	7.97	8.05	7.90	7.96	7.94	8.04	Si	8.00	8.00	7.94	7.82	8.03	7.94
Al^{IV}	0.03	-	0.09	0.04	0.06	-	Al^{IV}	-	-	0.06	0.11	-	0.06
Fe^{3+}	-	-	0.01	-	-	-	Fe^{3+}	-	-	-	0.07	-	-
Sum T	8.00	8.05	8.00	8.00	8.00	8.04	Sum T	8.00	8.00	8.00	8.00	8.03	8.00
Al^{VI}	0.05	0.08	-	0.08	0.07	0.09	Al^{VI}	0.12	0.12	0.05	-	0.09	0.05
Fe^{3+}	2.26	2.09	2.24	2.16	2.33	1.96	Fe^{3+}	2.19	2.09	2.41	1.98	1.60	1.85
Ti	0.13	0.13	0.20	0.14	0.10	0.17	Ti	0.10	0.13	0.09	0.11	0.09	0.13
Mg	0.02	0.06	0.02	-	0.06	0.04	Mg	0.08	0.02	0.06	0.17	0.13	0.08
Fe^{2+}	1.15	1.22	1.21	1.44	1.01	1.36	Fe^{2+}	1.11	1.37	0.91	2.27	2.73	2.38
Zn	0.43	0.47	0.41	0.33	0.47	0.48	Zn	0.49	0.41	0.49	0.11	0.11	0.10
Mn	0.20	0.19	0.19	0.16	0.22	0.20	Mn	0.21	0.20	0.21	0.09	0.09	0.11
Ca	-	-	-	0.01	-	-	Ca	-	0.01	-	0.02	0.01	0.02
Sum C	4.25	4.23	4.26	4.32	4.26	4.29	Sum C	4.29	4.34	4.22	4.76	4.85	4.71
Fe^{2+}	-	-	-	-	-	-	Fe^{2+}	-	-	-	-	-	-
Zn	-	-	-	-	-	-	Zn	-	-	-	-	-	-
Mn	-	-	-	-	-	-	Mn	-	-	-	-	-	-
Ca	-	-	-	0.01	-	-	Ca	-	0.01	-	0.02	0.01	0.02
Na	2.00	2.00	2.00	1.99	2.00	2.00	Na	2.00	1.99	2.00	1.98	1.99	1.98
Sum B	2.00	2.00	2.00	2.00	2.00	2.00	Sum B	2.00	2.00	2.00	2.00	2.00	2.00
Na	0.59	0.58	0.60	0.65	0.58	0.50	Na	0.55	0.62	0.62	0.15	0.04	0.22
K	0.36	0.34	0.34	0.24	0.37	0.36	K	0.36	0.25	0.37	0.30	0.30	0.28
Sum A	0.95	0.92	0.94	0.89	0.94	0.86	Sum A	0.91	0.87	0.98	0.45	0.34	0.50

1- 4 MD 55 zincian arfvedsonite
5- 6 MD 9 zincian arfvedsonite

7- 9 MD 13a zincian arfvedsonite
10-12 MD 6 arfvedsonite

TABLE 2.4: Pyroxene

	1	2	3	4	5	6	7	8	9	10	11
SiO_2	43.35	44.79	44.02	46.01	47.92	49.4	50.45	50.15	52.99	53.00	52.85
TiO_2	0.94	0.79	0.47	0.26	0.22	0.58	0.42	0.63	0.49	1.65	1.96
Al_2O_3	6.92	6.46	7.56	5.18	2.93	0.81	0.89	0.79	0.27	0.20	0.22
FeO	30.83	27.08	30.40	33.10	27.84	21.09	20.25	21.31	31.44	29.89	29.79
MnO	0.96	0.56	0.64	0.73	0.68	0.82	0.51	0.81	0.10	0.12	0.14
MgO	2.56	6.86	7.08	2.70	5.48	8.50	8.45	7.86	-	-	-
CaO	12.06	10.55	7.61	11.35	11.11	18.73	18.77	18.23	-	-	0.05
Na_2O	1.29	1.48	0.58	0.81	0.52	0.32	0.25	0.27	12.76	12.91	12.95
K_2O	1.02	1.00	0.49	-	0.46	0.32					
TOTAL	99.93	99.57	98.85	100.14	97.16	100.25	99.99	100.05	98.05	97.77	97.96
Fe_2O_{3c}							0.37	0.24	29.90	27.80	27.88
FeO_c							19.92	21.09	4.54	4.88	4.71
Structural formula calculated on the basis of 4 cations							Structural formula calculated on the basis of 4 cations				
Si_{IV}	1.74	1.76	1.77	1.87	1.97	1.92	1.97	1.97	2.02	2.03	2.02
Al^{IV}	0.25	0.24	0.23	0.13	0.03	0.04	0.03	0.03	-	-	-
Sum T	2.00	2.00	2.00	2.00	2.00	1.96	2.00	2.00	2.02	2.03	2.02
$Al^{VI}+$	0.07	0.06	0.12	0.12	0.12	-	Al^{VI} 0.01	0.01	0.01	0.01	0.01
Ti	0.03	0.02	0.01	0.01	0.01	0.02	0.01	0.02	0.01	0.05	0.06
Fe^{3+}	0.28	0.30	0.15	0.06	-	0.13	0.01	0.01	0.86	0.80	0.80
Mg	0.15	0.40	0.42	0.16	0.34	0.49	0.49	0.46	-	-	-
Fe^{2+}	0.76	0.59	0.87	1.07	0.96	0.56	0.65	0.69	0.14	0.16	0.15
Mn	0.03	0.02	0.02	0.03	0.02	0.03	0.03	0.02	0.02	0.03	0.02
Ca	0.52	0.44	0.33	0.49	0.49	0.78	0.79	0.77	-	-	-
Na	0.10	0.11	0.05	0.06	0.04	0.02	0.02	0.02	0.94	0.96	0.96
K	0.05	0.05	0.03	-	0.02	0.02	-	-	-	-	-
Sum $M_{1/2}$	2.00	2.00	2.00	2.00	2.00	2.04	2.00	2.00	1.98	1.97	1.98

1 MD 54 sodian ferro-augite
2 MD BG2 sodian ferro-augite
3 MD BG2 ferro-hedenbergite/augite
4-5 MD 12 ferro-hedenbergite
6 MD 12 ferro-augite

7-8 MD 12 ferro-augite
9-11 MD 9a aegirine

TABLE 2.4: Pyroxene (continued)

	12	13	14	15	16	17
SiO_2	53.30	53.11	52.73	51.95	52.57	51.61
TiO_2	1.62	1.23	1.35	2.02	2.03	0.87
Al_2O_3	0.24	0.27	0.34	0.23	0.23	0.24
Fe_2O_3	29.74	21.81	29.28	29.37	29.20	30.77
MnO	0.17	0.14	-	0.19	0.14	0.10
Na_2O	13.85	13.74	12.95	13.07	12.96	13.19
K_2O	0.01	-	-	-	-	-
SnO_2	0.10	-	0.10	0.43	0.37	0.31
TOTAL	99.03	99.30	97.75	97.23	97.60	97.09
Fe_2O_{3c}	32.20	23.39	27.85	29.15	27.50	32.82
FeO_c	0.77	0.76	4.22	3.14	4.45	1.23

Structural formula calculated on the basis of 4 cations

Si	2.00	2.14	2.03	2.00	2.02	1.99
Al^{IV}	-	-	-	-	-	0.01
Sum T	2.00	2.14	2.03	2.00	2.02	2.00
Al^{VI}	0.01	0.01	0.02	0.01	0.01	-
Ti	0.05	0.04	0.04	0.06	0.06	0.03
Fe^{3+}	0.91	0.71	0.81	0.85	0.80	0.95
Mg	-	-	-	-	-	-
Fe^{2+}	0.02	0.03	0.14	0.10	0.14	0.04
Mn	0.01	-	-	0.01	-	-
Ca	-	-	-	-	-	-
Na	1.01	1.07	0.97	0.98	0.97	0.98
K	-	-	-	-	-	-
Sum $M_{1/2}$	2.00	1.86	1.97	2.00	1.98	2.00

12-14 MD 2 aegirine/stanniferous aegirine
15-17 MD 9 stanniferous aegirine

TABLE 2.5: Feldspars

	1	2	3	4	5	6	7	8	9	10
SiO_2	68.98	67.10	65.55	65.38	65.39	66.38	65.64	66.15	65.45	67.33
Al_2O_3	19.02	18.52	17.80	17.97	17.85	17.76	17.42	17.81	17.86	18.19
FeO	-	0.16	-	0.15	0.13	0.11	-	-	-	-
CaO	0.30	0.14	-	-	0.11	-	-	0.15	-	-
Na_2O	10.09	4.73	0.17	0.18	0.21	1.06	0.95	2.15	0.94	4.56
BaO	-	-	0.18	0.24	-	0.11	-	-	0.13	0.14
K_2O	1.08	9.27	15.70	15.18	15.52	13.74	14.55	13.19	14.74	9.19
TOTAL	99.47	99.92	99.40	99.09	99.21	99.70	98.56	99.45	99.12	99.41
Structural formula calculated on the basis of 32 oxygens										
Si	12.099	12.077	12.134	12.120	12.116	15.836	12.186	12.129	12.116	12.144
Al	3.932	3.928	3.883	3.925	3.898	3.836	3.810	3.849	3.895	3.866
TOTAL	16.031	16.005	16.017	16.045	16.114	19.672	15.996	15.978	16.011	16.010
Fe_2	-	0.025	-	0.024	0.020	0.016	-	-	-	-
Ca	0.056	0.027	-	-	0.022	-	-	0.029	-	-
Na	3.430	1.651	0.062	0.064	0.076	0.567	0.342	0.763	0.336	1.594
Ba	-	-	0.013	0.018	-	0.008	-	-	0.009	0.010
K	0.242	2.128	3.708	3.587	3.667	3.213	3.447	3.085	3.480	2.115
TOTAL	3.728	3.831	3.783	3.693	3.785	3.794	3.789	3.877	3.825	3.729
%An	1.50	0.71	0.09	0.01	0.58	-	0.20	0.75	0.09	1.01
%Ab	92.02	43.37	1.63	1.75	1.99	15.00	9.01	19.68	8.79	42.54
%Or	6.48	55.92	98.28	98.24	97.97	85.00	90.08	79.57	91.12	56.45

1 MD 142 albite
2 MD 142 microcline microperthite
3 MD 142 maximum microcline
4 MD 142 maximum microcline
5 MD 3 maximum microcline (untwinned)
6 MD 3 microcline (turbid)
7 MD 5 microcline (tartan twinned core)
8 MD 5 microcline microperthite
9 MD 5 maximum microcline microperthite
10 MD 125 orthoclase microperthite

TABLE 2.5: Feldspars (continued)

	11	12	13	14	15	16
SiO_2	61.57	62.11	62.42	62.63	61.53	61.93
Al_2O_3	23.30	23.61	22.73	22.96	23.32	23.26
FeO	0.22	0.33	1.01	0.44	0.30	0.21
CaO	5.79	6.22	4.93	5.69	6.12	5.59
Na_2O	7.18	7.25	7.65	7.65	7.43	7.47
BaO	0.31	0.15	0.16	0.16	0.19	0.15
K_2O	1.19	0.50	0.47	0.27	0.18	0.52
TOTAL	99.56	100.17	99.37	99.80	99.07	99.13
Structural formula calculated on the basis of 32 oxygens						
Si	11.033	11.020	11.164	11.136	11.030	11.082
Al	4.922	4.938	4.790	4.811	4.928	4.906
TOTAL	15.955	15.958	15.954	15.947	15.958	15.988
Fe_2	0.033	0.048	0.151	0.065	0.044	0.031
Ca	1.112	1.183	0.945	1.084	1.176	1.072
Na	2.493	2.497	2.663	2.638	2.580	2.593
Ba	0.022	0.011	0.011	0.011	0.014	0.011
K	0.272	0.114	0.107	0.060	0.042	0.120
TOTAL	3.932	3.853	3.877	3.858	3.856	3.827
%An	28.68	31.18	25.53	28.65	30.93	28.32
%Ab	64.31	65.82	71.59	69.75	67.96	68.50
%Or	7.01	3.00	2.88	1.60	1.11	3.18

11 MD 54 oligoclase (rim)
12 MD 54 oligoclase andesine (intermediate zone)
13 MD 54 oligoclase (intermediate zone)
14 MD 54 oligoclase (core)
15 MD 54 oligoclase andesine (core)
16 MD 54 oligoclase (rim)

	17	18	19	20	21	22
SiO_2	58.87	59.49	59.19	67.78	68.74	61.67
Al_2O_3	24.89	24.64	25.13	18.77	19.01	22.81
FeO	0.42	0.37	0.45	0.12	-	0.52
CaO	8.64	8.45	8.36	0.51	0.11	6.12
Na_2O	5.90	6.03	5.99	9.00	10.37	4.99
BaO	-	-	0.14	-	-	-
K_2O	0.73	0.54	0.61	2.66	0.16	4.11
TOTAL	99.43	99.52	99.87	98.84	98.39	100.22
Structural formula calculated on the basis of 32 oxygens						
Si	10.608	10.687	10.616	12.062	12.172	11.075
Al	5.286	5.217	5.312	3.937	3.952	4.828
TOTAL	15.894	15.904	15.928	15.999	16.079	15.903
Fe_2	0.062	0.056	0.067	0.001	-	0.078
Ca	1.664	1.626	1.607	0.097	0.022	1.178
Na	2.062	2.100	2.083	3.106	3.546	1.739
Ba	-	-	0.010	-	-	-
K	0.167	0.123	0.139	0.603	0.036	0.940
TOTAL	3.855	3.905	3.806	3.807	3.603	3.939
%An	42.74	42.25	41.98	2.54	0.603	0.54
%Ab	52.96	54.56	54.41	81.60	98.40	45.08
%Or	4.30	3.19	3.62	15.85	1.01	24.38

17 MD BG 2 andesine (rim)
18 MD BG 2 andesine (core)
19 MD BG 2 andesine (core)
20 MD 101 K-high albite
21 MD 111 albite
22 MD 12 K-high oligoclase andesine

TABLE 2.5: Feldspars (continued)

	23	24	25	26	27	28
SiO_2	68.34	69.16	68.98	69.27	66.26	60.81
Al_2O_3	18.85	18.51	19.30	19.12	20.88	24.08
FeO	0.35	0.28	0.11	-	0.15	0.24
CaO	0.42	0.21	0.62	0.29	2.77	7.22
Na_2O	9.63	10.46	9.91	10.64	9.23	6.46
BaO	-	-	-	-	-	-
K_2O	1.64	0.16	0.99	0.04	0.26	1.03
TOTAL	99.26	98.78	99.91	99.36	99.55	99.84
Structural formula calculated on the basis of 32 oxygens						
Si	12.066	12.176	12.056	12.111	11.672	10.866
Al	3.922	3.852	3.975	3.940	4.334	5.070
TOTAL	15.988	16.028	16.041	16.051	16.006	15.936
Fe_2	0.056	0.041	0.016	-	0.022	0.036
Ca	0.080	0.040	0.115	0.055	0.523	1.382
Na	3.295	3.572	3.358	3.608	3.191	2.237
Ba	-	-	-	-	-	-
K	0.370	0.035	0.220	0.010	0.058	0.234
TOTAL	3.801	3.688	3.709	3.673	3.794	3.889
%An	2.13	1.09	3.12	1.50	14.02	35.87
%Ab	87.98	97.96	90.93	98.24	84.42	58.06
%Or	9.89	0.95	5.95	0.26	1.56	6.08

23 MD 100 K-high albite
24 MD 154 albite
25 MD 101 albite
26 MD 101 albite
27 MD 160 oligoclase (greenish color)
28 MD 12 andesine

	29	30	31	32	33	34
SiO_2	66.06	66.78	65.53	66.75	66.11	66.62
Al_2O_3	18.07	18.45	18.50	18.35	18.07	19.58
FeO	-	-	0.12	0.08	-	0.95
CaO	0.10	0.23	0.36	0.17	0.22	0.42
Na_2O	1.70	5.36	6.57	4.97	3.35	8.92
BaO	-	-	-	-	0.13	0.13
K_2O	13.70	8.38	6.68	8.81	11.38	2.15
TOTAL	99.63	99.20	97.76	99.13	99.26	98.77
Structural formula calculated on the basis of 32 oxygens						
Si	12.019	12.071	11.988	12.090	12.086	11.896
Al	3.904	3.930	3.989	3.917	3.894	4.122
TOTAL	16.013	16.001	15.977	16.007	15.980	16.018
Fe_2	-	-	0.018	0.013	-	-
Ca	0.603	0.044	0.020	0.033	0.043	0.080
Na	0.603	1.878	2.330	1.746	1.188	3.088
Ba	-	-	-	-	0.009	0.009
K	3.203	1.933	1.558	1.746	2.654	0.490
TOTAL	3.825	3.855	3.976	3.538	3.894	3.667
%An	0.50	1.14	1.77	0.87	1.11	2.20
%Ab	15.77	48.72	58.86	45.77	30.57	84.42
%Or	83.73	50.14	39.36	53.36	68.32	13.38

29 MD 92 microcline
30 MD 92 microcline microperthite
31 MD 3 "anorthoclase"
32 MD 101 orthoclase microperthite
33 MD 160 microcline microperthite
34 MD 160 peristerite